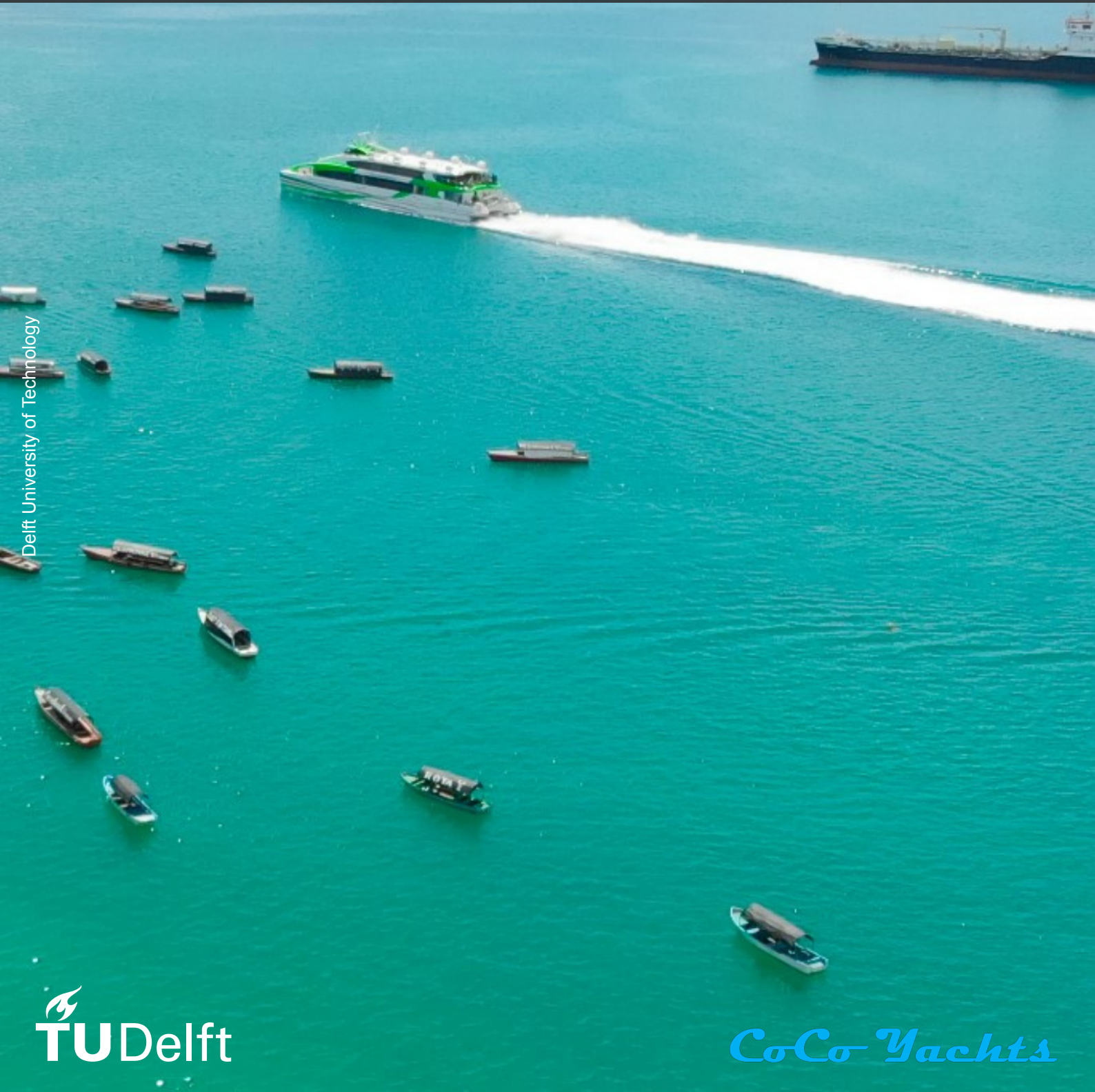


# Design and Feasibility of a 30- To 40-Knot Emission-Free Ferry

Marine Technology MSc Thesis

Patryk Doornebos



Delft University of Technology



# Design and Feasibility of a 30- To 40-Knot Emission-Free Ferry

by

Patryk Doornebos

to obtain the degree of Master of Science  
in Marine Technology in the specialisation of Ship Design  
at the Delft University of Technology,  
to be defended publicly on Wednesday, July 27, 2022, at 13:00.

Student number:	4724569
Thesis number:	MT.21/22.039.M
Project duration:	November 10, 2021 – July 27, 2022
Thesis committee:	Dr. A. A. Kana, TU Delft, supervisor, chair
	Dr. ir. L. van Biert, TU Delft
	Dr. ir. I. Akkerman, TU Delft
	Dr. ir. M. Hoogreef, TU Delft
	Ir. M. Francis, CoCo Yachts, supervisor

An electronic version of this thesis is available at <http://repository.tudelft.nl/>.



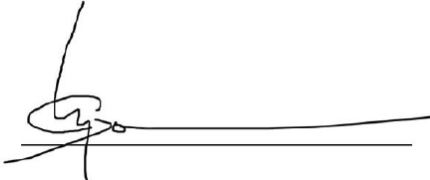
---

The logo for CoCo Yachts, featuring the text "CoCo Yachts" in a white, stylized, cursive font centered within a solid blue rectangular background.

The undersigned approves, in name of CoCo Yachts B.V., the publication of this report on <http://repository.tudelft.nl/> in July 2022.

Name: M. Francis

Date: 18-07-2022

Signature: A handwritten signature in black ink, consisting of a stylized 'G' followed by a horizontal line and a vertical stroke, positioned over a horizontal line.

# Preface

Before you lies the thesis "Design and Feasibility of a 30- To 40-Knot Emission-Free Ferry". This report has been written to fulfill the graduation requirements of MSc in Marine Technology at the Delft University of Technology. I was occupied with researching and writing this thesis from November 2021 till July 2022.

This project was performed in cooperation with CoCo Yachts, a naval architecture company based in Gorinchem specialised in designing high-speed vessels. Together with CoCo Yachts, the topic of this thesis was determined, aiming to research the technical and economic feasibility of a 200-passenger, 30- to 40-knot, emission-free ferry operating on the Zhuhai-Shenzhen route in the Chinese Pearl River Delta.

I would like to thank my supervisors for their excellent support and guidance during the duration of this project. Austin Kana, thank you for continuously guiding me in the right direction and giving prompt responses to my questions and meeting requests, despite your busy schedule. Moreno Francis, thank you for being my daily company supervisor, your sharp feedback, and helpful advice.

I would like to thank the management of CoCo Yachts, Henk van Herwijnen and Mirella Colon, for allowing me to research this interesting topic and being open to a technical or non-technical conversation at all times. I am also thankful for my other colleagues at CoCo Yachts, who were always friendly and helpful, which led to an enjoyable working atmosphere.

At last, my parents and friends deserve a particular note of thanks for their support, kind words, and laughs.

I hope you enjoy reading this thesis.

*Patryk Doornebos  
Delft, July 2022*

# Abstract

This thesis evaluates the technical and economic feasibility of a 200-passenger, 30- to 40-knot, emission-free ferry operating on the Zhuhai-Shenzhen route. This route has a length of 25 nautical miles and is located in the Chinese Pearl River Delta. The Pearl River Delta is one of the world's most densely urbanized regions and faces numerous social, health, and economic issues due to air pollution. Examples include global warming and harm to public health, including reduced lung function and even premature deaths. Part of this air pollution is caused by internal combustion engine (ICE) emissions. The reference vessel of this thesis, the Coastal Cruiser 200 (CC-200), also uses ICEs as part of its propulsion system. A next-generation CC-200 may implement zero-emission propulsion technologies to negate its contribution to the total ICE emissions.

During this thesis, a literature review was performed to find the most technologically advanced emission-free energy carriers and propulsion systems. Detailed data of the CC-200 was used to examine the impact on the ferry's weight when switching to a zero-emission power plant and identify various weight-saving measures. Besides weight reduction, the application of hydrofoils was identified as a method to improve the ferry's efficiency. A software tool used to calculate the hydrodynamics of high-speed craft called Autowing was applied to collect quantitative data on the hydrofoil system's performance. The performance of the ferry's propulsion system was analyzed based on available data of the CC-200 and propeller calculations using Wageningen B-series open water diagrams. The obtained qualitative and quantitative data from research and literature was integrated into a parametric model designed to assess the technical feasibility of the 200-passenger, 30- to 40-knot, emission-free ferry. Finally, an economic feasibility assessment was performed based on the results of the developed parametric model and collected quantitative data related to the purchase, operation, and maintenance costs of the CC-200 and the developed zero-emission ferries.

The technical analysis showed that it is technically feasible to operate a 200-passenger, 30-knot, emission-free ferry on the Zhuhai-Shenzhen route when implementing a battery-, compressed hydrogen-, or liquid hydrogen energy carrier system, hydrofoils, and all identified weight-saving measures. Meanwhile, the economic analysis showed that the operation of these three ferry configurations may or may not be economically feasible, with a yearly total cost of ownership (TCO) of 60 to 161 % of the CC-200's yearly TCO, depending on the ferry configuration.

At last, this thesis concludes that the operation of a 200-passenger, 30-knot, emission-free ferry on the Zhuhai-Shenzhen route has the highest likelihood of being both technically and economically feasible when implementing a thruster propulsion system, hydrofoils, and a Li-ion battery energy carrier system. This zero-emission ferry configuration complies with the set technical requirements and has an estimated yearly TCO of 60 to 107 % of the CC-200's yearly TCO.

# Contents

<b>Preface</b>	<b>ii</b>
<b>Abstract</b>	<b>iii</b>
<b>Nomenclature</b>	<b>vii</b>
<b>List of Figures</b>	<b>x</b>
<b>List of Tables</b>	<b>xii</b>
<b>1 Introduction</b>	<b>1</b>
1.1 Project background . . . . .	1
1.1.1 CoCo Yachts and fast ferries . . . . .	1
1.1.2 Social and environmental relevance of the research . . . . .	2
1.1.3 Health relevance of the research . . . . .	2
1.1.4 Economic relevance of the research . . . . .	3
1.1.5 Technological developments and ethical relevance of the research . . . . .	4
1.2 Research objective and sub-questions . . . . .	4
<b>2 Zero-emission ferry requirements and the state-of-the-art</b>	<b>6</b>
2.1 The Coastal Cruiser 200 and the Zhuhai-Shenzhen crossing . . . . .	6
2.2 Emission-free Coastal Cruiser 200 requirements . . . . .	8
2.3 State-of-the-art zero-emission ferries . . . . .	8
2.3.1 The latest developments in zero-emission ferries . . . . .	9
2.3.2 Most prominent challenges for zero-emission fast ferries . . . . .	11
2.3.3 Conclusion: state-of-the-art zero-emission ferries and remaining gaps . . . . .	13
<b>3 Optimizing the efficiency of fast ferries</b>	<b>14</b>
3.1 Lowering the mass of the Coastal Cruiser 200 . . . . .	14
3.1.1 Switching from a diesel-driven to a zero-emission ferry . . . . .	14
3.1.2 Weight-saving measures for the zero-emission CC-200 . . . . .	15
3.2 Hydrofoils . . . . .	17
3.2.1 The basics and working principles of hydrofoils . . . . .	18
3.2.2 Designing the hydrofoil system . . . . .	23
<b>4 Emission-free energy carriers</b>	<b>32</b>
4.1 Batteries . . . . .	32
4.1.1 Energy density of Li-ion batteries . . . . .	34
4.1.2 Costs and lifetime of Li-ion batteries . . . . .	34
4.1.3 Safety of Li-ion batteries . . . . .	35
4.1.4 Charging capabilities of Li-ion batteries . . . . .	36
4.1.5 Availability of Li-ion batteries . . . . .	37
4.1.6 The most suitable Li-ion battery type . . . . .	37
4.1.7 Commercially-available marine Li-ion batteries . . . . .	38
4.2 Hydrogen fuel cells . . . . .	38
4.2.1 Fuel cell types . . . . .	38
4.2.2 PEM fuel cell costs and lifetime . . . . .	41
4.2.3 Hydrogen production . . . . .	41
4.2.4 Hydrogen storage . . . . .	42
4.2.5 Safety of using hydrogen as an energy source . . . . .	44
4.3 Conclusion: the most suitable energy carriers . . . . .	45

<b>5</b>	<b>Propulsion systems</b>	<b>46</b>
5.1	Propellers, thrusters, and waterjets	46
5.1.1	Propellers	46
5.1.2	Thrusters	48
5.1.3	Waterjets	50
5.1.4	Conclusion: propellers, thrusters, and waterjets	52
5.2	The design of thrusters mounted to a hydrofoil system.	52
5.2.1	The thruster's propeller performance	52
5.2.2	Foil-thruster mounting and interaction.	55
5.2.3	Electric motors and gearboxes.	56
5.2.4	Conclusion: the design of a thruster mounted to a hydrofoil system.	57
<b>6</b>	<b>Modeling the technical feasibility of a zero-emission ferry</b>	<b>58</b>
6.1	Parametric model flowchart	58
6.2	Details of the parametric model	60
6.2.1	Inputs	60
6.2.2	Weight calculation	60
6.2.3	Hydrofoil and resistance model	60
6.2.4	Power demand and propulsion system selection	63
6.2.5	Energy demand and energy carrier selection	63
6.3	Results of the parametric model	64
6.3.1	Designing a zero-emission ferry with minimal speed and range requirements	64
6.3.2	The impact of altering the required speed and range.	66
6.3.3	Comparing a compressed hydrogen-, liquid hydrogen-, and battery-powered ferry.	68
6.3.4	The technical boundaries of a zero-emission ferry	71
6.3.5	Parametric model sensitivity analysis	75
6.4	Conclusion: the technical feasibility of a zero-emission ferry	77
<b>7</b>	<b>Economic feasibility of a zero-emission ferry</b>	<b>79</b>
7.1	Capital expenditures	79
7.1.1	CAPEX of the battery-powered ferry	80
7.1.2	CAPEX of the compressed hydrogen-powered ferry	80
7.1.3	CAPEX of the liquid hydrogen-powered ferry	81
7.2	Operational expenditures	81
7.2.1	OPEX of the Coastal Cruiser 200	81
7.2.2	OPEX of the battery-powered ferry	83
7.2.3	OPEX of the compressed hydrogen-powered ferry	84
7.2.4	OPEX of the liquid hydrogen-powered ferry.	85
7.3	Total cost of ownership.	85
7.4	Conclusion: the economic feasibility of a zero-emission ferry	86
<b>8</b>	<b>Conclusion and recommendations</b>	<b>87</b>
8.1	Conclusion	87
8.1.1	Contributions	89
8.2	Recommendations	89
8.2.1	Hydrofoil system	89
8.2.2	Low-emission, carbon-neutral, and future emission-free energy carriers	89
8.2.3	Validation	90
8.2.4	Economic feasibility	90
8.2.5	Larger ferries	90
8.2.6	System interfaces	91
8.3	Personal reflection	91

---

<b>References</b>	<b>101</b>
<b>A Hydrofoils: calculations and results</b>	<b>102</b>
A.1 The chord length of the hydrofoils . . . . .	102
A.2 Autowing: working principles and methods . . . . .	103
A.3 Autowing lift and drag data with corresponding curve-fitted mass-resistance equations . . . . .	104
A.4 Validating the hydrofoil system mass . . . . .	105
<b>B Propulsion system: calculations and results</b>	<b>107</b>
B.1 The efficiency of waterjets integrated with a hydrofoil system . . . . .	107
B.2 Results: propeller open water characteristics . . . . .	108
B.3 Overview: specifications of electric motors and gearboxes . . . . .	109
<b>C Parametric model</b>	<b>111</b>
C.1 Parametric model: inputs . . . . .	111
C.2 Parametric model: pseudocode . . . . .	112
<b>D Economic feasibility</b>	<b>118</b>
D.1 CAPEX calculations . . . . .	118
D.1.1 CAPEX of the battery-powered ferry . . . . .	118
D.1.2 CAPEX of the compressed hydrogen-powered ferry . . . . .	119
D.1.3 CAPEX liquid hydrogen-powered ferry . . . . .	119

# Nomenclature

## Abbreviations

Abbreviation	Definition
3D	Three-dimensional
'80s	1980s
'90s	1990s
AC	Alternating current
AFC	Alkaline fuel cell
AoA	Angle of attack
CAPEX	Capital expenditures
CC-200	Coastal Cruiser 200
CEO	Chief executive officer
CFRP	Carbon fiber-reinforced polymers
CH <sub>2</sub>	Compressed hydrogen
CO <sub>2</sub>	Carbon dioxide
CPP	Controllable pitch propellers
DC	Direct current
DNV	Det Norske Veritas
DSOC	Delta state of charge
ECA	Emission Control Area
EPA	Environmental Protection Agency
ETS	Emissions Trading System
FPP	Fixed pitch propellers
ft	Feet (1 ft = 0.3048 m)
GDP	Gross domestic product
GFRP	Glass fiber-reinforced polymers
GT	Gross tonnage
H <sub>2</sub>	Hydrogen
ICE	Internal combustion engines
ITTC	International Towing Tank Conference
IMO	International Maritime Organization
ISO	International Organization for Standardization
kN	Kilonewton
KOH	Potassium hydroxide
kW	Kilowatt
LCO	Lithium Cobalt Oxide
LFP	Lithium Iron Phosphate
LH <sub>2</sub>	Liquid hydrogen
LHV	Lower heating value
Li-Polymer	Lithium-Polymer
Li-ion	Lithium-ion
LMO	Lithium Manganese Oxide
LNG	Liquefied natural gas
LTO	Lithium Titanate Oxide
MARIN	Maritime Research Institute Netherlands
MCFC	Molten carbonate fuel cell
MGO	Marine gasoil
MJP	Marine Jet Power

Abbreviation	Definition
MW	Megawatt
N/A	Not available or not applicable
NACA	National Advisory Committee for Aeronautics
NAVAIS	New, Advanced and Value-added Innovative Ships
$NH_3$	Ammonia
Ni-Cd	Nickel-cadmium
Ni-MH	Nickel-metal hydride
NM	Nautical mile (1 NM = 1.852 m)
NMC	Nickel Manganese Cobalt
$NO_x$	Nitrogen oxides
NOAA	National Oceanic and Atmospheric Administration
$OH$	Hydroxide
OPEX	Operating expenditures
PAFC	Phosphoric Acid fuel cell
PEM	Proton Exchange Membrane
PhD	Doctor of Philosophy
PowerCell	PowerCellution Marine System 200
MS200	
RPM	Revolutions per minute
SAE	Society of Automotive Engineers
$SO_x$	Sulfur oxides
SOFC	Solid oxide fuel cell
TCO	Total cost of ownership
TrAM	Transport: Advanced and Modular
US	United States
USD	United States Dollar
VIP	Very important person
WHR	Waste heat recovery
WSM	Weight-saving measures

## Symbols

Symbol	Definition	Unit
\$	Dollar (USD)	[\$]
$A$	(Planform) area	[ $m^2$ ]
$AR$	Aspect ratio	[-]
$C_D$	Drag coefficient	[-]
$C_L$	Lift coefficient	[-]
$E_{tot}$	Total energy demand	[kWh]
$J$	Advance number	[-]
$K_T$	Thrust coefficient	[-]
$K_Q$	Torque coefficient	[-]
$M_{ec}$	Energy carrier mass	[kg]
$n_{motor}$	Rotational speed of the motor	[RPM]
$n_{prop}$	Rotational speed of the propeller	[RPM]
$P_B$	Brake power	[kW]
$P_D$	Delivered power	[kW]
$P_{D_{hump}}$	Delivered power at the resistance hump speed	[kW]
$P_{D_{op.}}$	Delivered power at the operational speed	[kW]
$pf_{min}$	Minimum power factor	[kW/RPM]
$t$	tonne	[ $10^3 \text{ kg}$ ]

Symbol	Definition	Unit
$T$	Thrust	[N]
$V$	(Ship) speed	[ $m\ s^{-1}$ ]
$V_{ec}$	Energy carrier volume	[ $m^3$ ]
$V_a$	Speed of advance	[ $m\ s^{-1}$ ]
$V_{design}$	Design (ship) speed	[ $m\ s^{-1}$ ]
$V_j$	Discharge velocity	[ $m\ s^{-1}$ ]
$w$	Wake coefficient	[-]
$Q$	Volume flow rate	[ $m^3\ s^{-1}$ ]
$R_{tot}$	Total resistance	[kN]
$R_{hump}$	Resistance at the resistance hump speed	[kN]
$R_{op.}$	Resistance at the operational speed	[kN]
$S$	Wetted surface area	[ $m^2$ ]
$\eta_O$	Propeller open water efficiency	[-]
$\eta_{O_{hump}}$	Propeller open water efficiency at the resistance hump speed	[-]
$\eta_{O_{op.}}$	Propeller open water efficiency at the operational speed	[-]
$\rho$	Density	[ $kg\ m^{-3}$ ]
$\rho_{sw}$	Seawater density	[ $kg\ m^{-3}$ ]

# List of Figures

1.1	Illustration of a Coastal Cruiser 200 vessel (Peng Xing 16) [25]	1
1.2	The rise of atmospheric carbon dioxide levels in the last 60 years [97]	2
1.3	A map of the Pearl River Delta region in China [131]	3
1.4	Benefit-cost ratio for an ECA for the Pearl River Delta region [107]	3
2.1	The Peng Xing 15 [25]	7
2.2	A map of the Zhuhai-Shenzhen crossing [168]	7
2.3	MF Ampere [44]	9
2.4	Rendering of Medstrom [171]	9
2.5	Sea Change [138]	10
2.6	Beluga24 [78]	11
3.1	The 150-passenger catamaran ferry used in Gurit's case study [38]	16
3.2	The Jetfoil, a high-speed hydrofoil ferry [165]	18
3.3	Typical relation between resistance/thrust and speed for a hydrofoil vessel [23]	18
3.4	Basic foil geometry in 2- and 3D [69]	19
3.5	Submerged and surface-piercing hydrofoils [118]	19
3.6	Restoring roll moments for (a) surface-piercing and (b) fully submerged foils [189]	20
3.7	The aircraft (a), tandem (b), and canard (c) hydrofoil configurations [189]	21
3.8	The PS-30 hydrofoil ferry in service [184]	22
3.9	The ELECTRA hydrofoil ferry concept [22]	22
3.10	Autowing and experimental total resistance data comparison for a Hysuwac configuration [115]	24
3.11	The NACA63-615 foil as modeled in Autowing	25
3.12	The NACA63-615 foil profile [122]	26
3.13	The geometry of the hydrofoil system modeled in Autowing	27
3.14	Initial pressure distribution (bar) of the pressure side of the forward foils at 30 knots and 3-degree angle of attack	27
3.15	Initial pressure distribution (bar) of the suction side of the forward foils at 30 knots and 3-degree angle of attack	27
3.16	The hydrofoil resistance at 30 knots as a function of the ferry's mass (equation 3.4)	29
4.1	Energy density comparison of main battery cell types [18]	33
4.2	Number of cycles to reach 80% capacity as a function of DSOC for two NMC and one LTO battery [70]	35
4.3	The BB Green, a fast electric commuter vessel using an LTO Li-ion battery pack [162]	36
4.4	Illustration of the PemGen 500kW fuel cell manufactured by Nedstack [133]	39
4.5	The 200 kW FCwave fuel cell module manufactured by Ballard Power [109]	40
4.6	An example of a Gardner Cryogenics liquid hydrogen tanker [27]	44
5.1	Electric motor part-load efficiency (as a function of % full-load efficiency) [46]	47
5.2	An example of a diesel-powered hydrofoil ship with an angled propeller shaft [114]	47
5.3	A rendering of Hydromaster's high-speed thruster [77]	48
5.4	The FHE-400 "Bras D'Or" [92]	49
5.5	The propulsion system arrangement of Argo, a zero-emission hydrofoiling container ship [96]	49
5.6	A general configuration of a waterjet [45]	50
5.7	The waterjet propulsion system of the Jetfoil 929 [189]	51
5.8	Example of a result from PropCalc [87]	53

---

5.9	An electric motor from The Switch [134] . . . . .	56
6.1	A flowchart of the developed parametric model . . . . .	59
6.2	Overview of a technically-feasible, 30-knot zero-emission ferry with a range of 30 NM [134] [150] [77] [80] [108] . . . . .	65
6.3	The zero-emission ferry's mass as a function of its required speed . . . . .	66
6.4	The zero-emission ferry's total used brake power as a function of its required speed . . . . .	66
6.5	The zero-emission ferry's total resistance as a function of its required operational speed . . . . .	67
6.6	The zero-emission ferry's energy consumption as a function of its required operational speed . . . . .	67
6.7	The mass of the energy carrier system as a function of the required range . . . . .	68
6.8	The volume of the energy carrier system as a function of the required range . . . . .	68
6.9	An engineering model of the SF-BREEZE, including the placement of its LH2 tank [147] . . . . .	70
6.10	The FerryCHARGER used to charge the electric, 400-passenger MF Suløy ferry [57] . . . . .	71
6.11	The technical boundaries of the battery-powered ferry . . . . .	72
6.12	The technical boundaries of the compressed hydrogen-powered ferry . . . . .	73
6.13	The technical boundaries of the liquid hydrogen-powered ferry . . . . .	74
7.1	Price of the European Union's carbon permits [51] . . . . .	82

# List of Tables

2.1	Main particulars of the Coastal Cruiser 200 [76] [74]	7
2.2	Details around the Zhuhai-Shenzhen route [55] [47] [58]	8
2.3	Weight comparison of a zero-emission ferry vs. two traditional diesel-driven ferries	12
2.4	Comparison of the Beluga24 and the zero-emission concepts of the Coastal Cruiser 200 and 300 [58] [174]	13
2.5	Overview of state-of-the-art zero-emission ferries [8] [17] [149] [147] [152] [182] [67] [29] [174] [58] [139]	13
3.1	Summary of five case studies researching the structural weight saving of using a CFRP hull [38] [127] [72] [95] [28]	16
3.2	Summary of (dis)advantages of fully submerged and surface-piercing foils	20
3.3	Overview of discussed hydrofoil ferries [189] [153] [117] [48]	23
3.4	Comparing the lift/drag ratio of four NACA profiles	25
3.5	Specifications of the defined hydrofoil system geometry	27
3.6	Lift and drag data results from experiments using Autowing	28
3.7	Autowing results of the hydrofoil lift and drag forces at the resistance hump (21 and 23 knots)	30
4.1	The selection of to be compared Lithium-ion battery types	33
4.2	Energy densities of LMO, NMC, LFP and LTO battery cells [190] [124]	34
4.3	Life-cycle cost comparison of LMO, NMC, LFP and LTO batteries [13]	35
4.4	Safety rating of LMO, NMC, LFP and LTO batteries for marine applications	36
4.5	Charging capability of LMO, NMC, LFP and LTO batteries for marine applications	37
4.6	Availability of LMO, NMC, LFP and LTO batteries for marine applications	37
4.7	Complete comparison of LMO, NMC, LFP and LTO batteries	37
4.8	Specifications of commercially available Li-ion battery modules [186] [50] [36]	38
4.9	Overview of PEM fuel cell specifications from four different manufacturers [133] [109] [146] [147]	40
4.10	Cost and lifetime estimate of PEM fuel cells [31] [64] [147] [180] [164]	41
4.11	Overview of different high-pressure hydrogen storage tanks [147] [81] [6]	42
5.1	Comparing the total resistance, open water efficiency, and delivered propeller power at hump and operational conditions	55
6.1	Comparison of a compressed hydrogen-, liquid hydrogen-, and battery-powered ferry	69
6.2	Overview of the reached technical limits of the battery-powered ferry	72
6.3	The impact of hydrofoils on a 30-knot, 30 NM, battery-powered ferry	73
6.4	Overview of the reached technical limits of the compressed hydrogen-powered ferry	73
6.5	Overview of the reached technical limits of the liquid hydrogen-powered ferry	74
6.6	The impact of the hydrofoil chord on the lift-drag ratio	75
6.7	The impact of the available energy carrier volume on the zero-emission ferry's maximum range	76
7.1	Estimated total CAPEX of the battery-powered ferry as a percentage of the CC-200's total CAPEX	80
7.2	Estimated total CAPEX of the compressed hydrogen-powered ferry as a percentage of the CC-200's total CAPEX	81
7.3	Estimated total CAPEX of the liquid hydrogen-powered ferry as a percentage of the CC-200's total CAPEX	81

---

7.4	Estimated yearly OPEX of the current CC-200 . . . . .	83
7.5	Estimated yearly OPEX of a battery-powered ferry . . . . .	84
7.6	Estimated yearly OPEX of a compressed hydrogen-powered ferry . . . . .	85
7.7	Estimated yearly OPEX of a liquid hydrogen-powered ferry . . . . .	85
7.8	A comparison of the yearly TCO of the zero-emission ferries as a percentage of the CC-200's TCO . . . . .	86
7.9	OPEX, CAPEX, and TCO of the CC-200 and the battery-, compressed hydrogen-, and liquid hydrogen-powered ferries . . . . .	86
A.1	Specifications of the defined hydrofoil system geometry . . . . .	104
A.2	Lift and drag data results from experiments using Autowing (appendix) . . . . .	105
A.3	Calculations of the hydrofoil system mass by volume (chapter 3.2) . . . . .	106
B.1	PropCalc results: propeller open water characteristics based on the defined inputs and tested range of velocities and thrusts (chapter 5.2.1) . . . . .	109
B.2	The technical specifications of a selection of electric motors from The Switch [140] [141] . . . . .	109
B.3	The dimensions of a selection of electric motors from The Switch [140] [141] . . . . .	110
B.4	The technical specifications of a selection of gearboxes from ZF [151] . . . . .	110
B.5	The dimensions of a selection of gearboxes from ZF [151] . . . . .	110

# Introduction

Over the years, the adverse effects of air pollution are becoming more and more visible. At the same time, interest in reducing or eliminating internal combustion engine emissions is increasing. This also applies to emissions released by fast ferries, whose relatively large engines can discharge significant amounts of greenhouse gases and substances like  $SO_x$ ,  $NO_x$ , and particulate matter. In this section, the relevance of research into zero-emission ferries will be described from various perspectives. Together with the project background, the research question and corresponding sub-questions are defined, giving a clear overview of the goal of this thesis.

## 1.1. Project background

### 1.1.1. CoCo Yachts and fast ferries

This project is done in cooperation with CoCo Yachts, a naval architecture company based in Gorinchem, the Netherlands. CoCo Yachts specializes in the development of high-speed vessels, including (fast) ferries, patrol boats and yachts. The company was founded in November 2011 and currently has 15 team members.

Fast ferries are part of CoCo Yachts' core business. This thesis' center of attention is the Coastal Cruiser ferry series, designed to transport people, cars, and cargo in coastal areas. Coastal Cruisers can have lengths ranging from 20 to 125 meters and achieve speeds of 10 to 60 knots [54].

More specifically, this project focuses on the Coastal Cruiser 200 (CC-200), shown in figure 1.1 and discussed in more detail in chapter 2.1. The CC-200 is used as a reference for defining the technical and economic requirements of the zero-emission ferry studied in this thesis.



Figure 1.1: Illustration of a Coastal Cruiser 200 vessel (Peng Xing 16) [25]

### 1.1.2. Social and environmental relevance of the research

The International Maritime Organization (IMO), an agency formed to promote maritime safety, is currently adopting measures to cut greenhouse gases and other emissions like  $SO_x$  and  $NO_x$  from shipping. The IMO greenhouse gas regulations have entered into force from January 1, 2013 and apply to all ships of 400 gross tonnage and above [83].

Although the CC-200 has a gross tonnage below 400 and the IMO regulations do not apply to it, they do show that there is an aim to reduce greenhouse gas emissions [73]. Greenhouse gases trap and hold heat in the earth's atmosphere, ultimately leading to global warming. Carbon dioxide ( $CO_2$ ) is one of the most problematic greenhouse gases according to the Environmental Protection Agency (EPA) and takes up around 6% of the exhaust gas composition of a typical marine diesel engine [129] [181]. According to NOAA's Climate.gov, the atmospheric  $CO_2$  levels have increased at an annual rate that is 100 times quicker compared to previous natural increases over the past 60 years, reaching a record of 412.5 parts per million [97], as seen in figure 1.2.

#### ATMOSPHERIC CARBON DIOXIDE (1960-2021)

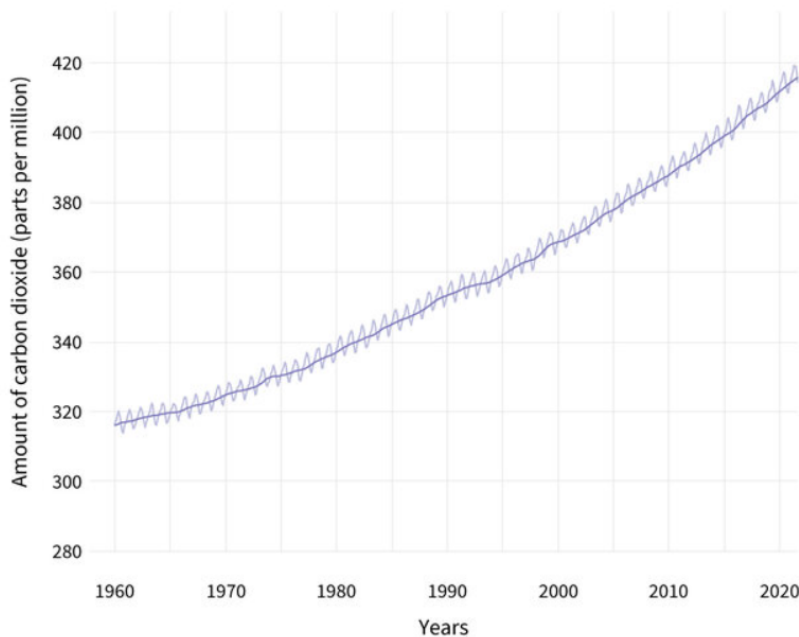


Figure 1.2: The rise of atmospheric carbon dioxide levels in the last 60 years [97]

If the current trend continues, scientists fear that the worst effects of global warming, like extreme weather, rising sea levels, and animal extinctions, are inevitable [111]. Meanwhile,  $CO_2$  emissions due to maritime transport currently reach around 940 million tonnes per year and are responsible for roughly 2.5% of global greenhouse gas emissions [154]. Therefore, research into zero-emission marine vehicles will play a vital role in reducing greenhouse gas emissions from shipping and complying with the IMO's initial strategy.

### 1.1.3. Health relevance of the research

The adverse social and environmental effects of greenhouse gas emissions only represent a part of the reason why internal combustion engine emissions should be reduced or eliminated. A marine internal combustion engine also emits substances like  $SO_x$  and  $NO_x$ , which cause air pollution and can lead to direct health risks for persons in the vessel's environment. Globally, around 66,000 people die prematurely due to ship-related air pollution each year, and one-third of these deaths happen in China [107].

Another problem is smog, partly caused by internal combustion engine emissions. Since 2000, the days on which widespread smog has been encountered have sharply increased in the Pearl River Delta, a region in China where the CC-200 frequently sails [187]. A map of the Pearl River Delta can

be seen in figure 1.3. Smog and air pollution from marine engine emissions can cause reduced lung function and difficulty in breathing [187]. A reduction in harmful emissions would therefore be beneficial to public health.



Figure 1.3: A map of the Pearl River Delta region in China [131]

#### 1.1.4. Economic relevance of the research

Due to health-related problems, ICE emissions are a source of indirect costs for the economy and society. A study conducted in 2016 concluded that  $SO_x$ ,  $NO_x$ , and other ICE emissions in the Pearl River Delta had the highest total economic loss in 2013, being 14,768 to 25,305 million USD [105]. This was the equivalent of 1.4% to 2.3% of the local gross domestic product (GDP). The results show that stricter control policies should be implemented to reduce air pollution and, therefore, lower economic loss.

This conclusion is in line with another study, which found that an Emission Control Area (ECA) in the Pearl River Delta region would result in economic benefits of around \$1.65 billion each year and avoid about 1,400 premature deaths in 2030, as illustrated in figure 1.4 [107].

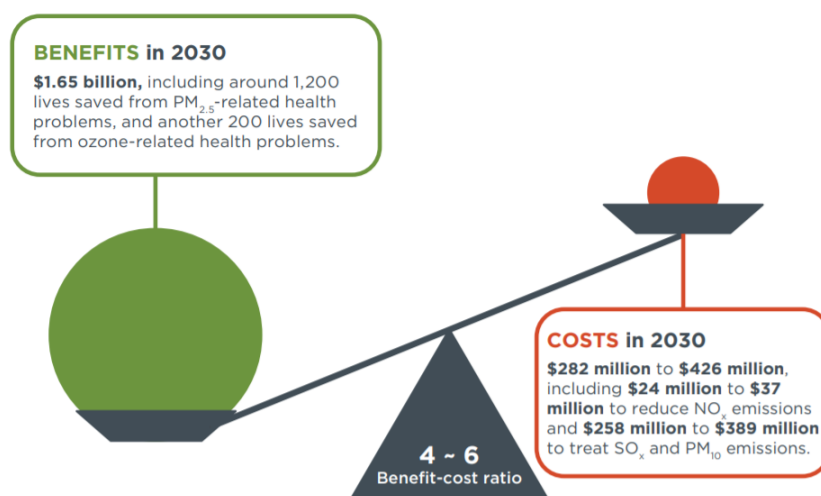


Figure 1.4: Benefit-cost ratio for an ECA for the Pearl River Delta region [107]

### 1.1.5. Technological developments and ethical relevance of the research

ICE emissions result in societal, environmental, and economic damages. However, a large part of the damages caused by ICE emissions and, in turn, air pollution is not paid for by the engine owner. As a result, an ethical dilemma arises. A ferry operator could choose an ICE-based propulsion system, traditionally the cheapest option in most situations. However, when factoring in the indirect costs due to ICE emissions, an emission-free propulsion system may be the better choice, even though it is more expensive for the operator. Society will have to pay for the indirect costs either way, so it may be better to invest now instead of suffering from the negative consequences later.

The good news is that in some applications, technological developments make it possible to eliminate internal combustion engine emissions. To illustrate this, examples of various state-of-the-art zero-emission ferries are given in chapter 2.3.

## 1.2. Research objective and sub-questions

To negate the aforementioned social, environmental, health, economic, and ethical issues related to ICE emissions, ships built in the future will have to implement emission-free propulsion technologies, which affects their design and operation. As highlighted in chapter 2.3, zero-emission ferries are already operational. However, as concluded in chapter 2.3.3, no state-of-the-art zero-emission ferries have been found that would match the technical specifications and operational requirements of the CC-200. For this reason, CoCo Yachts is interested in the design and feasibility of a fast emission-free ferry similar to the CC-200, which leads to the main research question of this thesis:

**How technically and economically feasible is a 200-passenger, 30- to 40-knot, emission-free ferry operating on the Zhuhai-Shenzhen route in the Pearl River Delta?**

---

To achieve this project's goal, the main research question has been divided into a number of sub-questions. First of all, the requirements of the zero-emission ferry must be carefully drawn up to correctly assess its technical and economic feasibility, leading to the following sub-question, answered in chapter 2.2:

*What are the requirements of an emission-free ferry operating on the Zhuhai-Shenzhen route in terms of transit speed, minimum range, operational profile, passenger capacity, safety and comfort, and costs?*

Next, research was done into state-of-the-art zero-emission ferries in chapter 2.3, which helped to identify the main gaps between the required zero-emission ferry and the state-of-the-art:

*What is state-of-the-art in zero-emission ferries, and what are the challenges and gaps when comparing the state-of-the-art to the zero-emission ferry's requirements?*

---

To help overcome the challenges associated with designing a zero-emission ferry that complies with the technical and economic requirements as set in chapter 2.2, a number of design choices could be made that would improve the ferry's efficiency at its operational speed. This proposition leads to the following sub-question, answered in chapter 3:

*Which design choices can be made for fast ferries that could result in an improved efficiency at operational speeds?*

---

The specifications of a zero-emission ferry's energy carrier significantly contribute to its technical and economic feasibility. Therefore, a detailed study into emission-free energy carriers is required, leading to the next sub-question, answered in chapter 4:

*What emission-free energy carriers are most suitable to be applied on a fast ferry and are available now or in the coming five years?*

---

The performance of the zero-emission ferry's propulsion system plays an important role in the ferry's technical feasibility. In this thesis, the propulsion system has been defined as the system that transforms the electrical energy of the ferry's energy carrier into a thrust used to propel the vessel. The components of the ferry's propulsion system are studied by the following sub-question, answered in chapter 5:

*What is expected to be the most technically feasible propulsion system for a fast, emission-free ferry?*

---

To assess the technical feasibility of a zero-emission ferry, the knowledge related to the previous sub-questions could be combined into a model. To achieve this, the following sub-question is investigated in chapter 6:

*How can the technical feasibility of a 200-passenger, 30- to 40-knot emission-free ferry be determined?*

Once the technical feasibility of a zero-emission ferry can be determined, the design choices and components required to achieve a technically-feasible zero-emission ferry design can be found. This leads to the following sub-question, answered in chapter 6.3:

*What combination of design choices in terms of the emission-free energy carrier, weight-saving measures, the hydrofoil system, or the propulsion system is expected to result in the most technically feasible zero-emission ferry configuration?*

---

At last, a complete feasibility assessment requires research into not only a ferry's technical specifications but also its economic characteristics. Therefore, chapter 7 aims to answer the sub-question:

*How economically feasible are the developed technically-feasible zero-emission ferry concepts?*

---

To summarize, the main goal of this thesis is to study the technical and economic feasibility of a zero-emission ferry with requirements based on the CC-200 operating on the Zhuhai-Shenzhen route. To achieve this goal, information related to reducing power demand, emission-free energy carriers, and propulsion systems is studied. Next, the obtained knowledge is combined into a model that assesses the technical feasibility of the zero-emission ferry. At last, the feasibility study is finalized with an economic assessment of the zero-emission ferry concept(s).

# 2

## Zero-emission ferry requirements and the state-of-the-art

Chapter 2 starts with an overview of the CC-200 and its main operating profile. Using this information, the requirements of the zero-emission ferry can be drawn up in chapter 2.2, which are required to make a conclusion on its technical and economic feasibility. Thus, the following sub-question is answered:

*What are the requirements of an emission-free ferry operating on the Zhuhai-Shenzhen route in terms of transit speed, minimum range, operational profile, passenger capacity, safety and comfort, and costs?*

Furthermore, a study into the state-of-the-art in zero-emission ferries will help identify the challenges to be solved. Therefore, chapter 2.3 will answer the sub-question:

*What is state-of-the-art in zero-emission ferries, and what are the challenges and gaps when comparing the state-of-the-art to the zero-emission ferry's requirements?*

### **2.1. The Coastal Cruiser 200 and the Zhuhai-Shenzhen crossing**

Maritime transport has traditionally been among the slowest forms of transportation. The average speed of conventional ferries ranges between 16 and 18 knots [85]. However, since some countries started to experience the "money-rich, time-poor" phenomenon, describing people with little leisure time despite having a high disposable income, the demand for fast ferry transport increased significantly. This mainly happened during the '80s and '90s, when fast ferry transport became one of the fastest-growing sectors within the maritime transport sector [102]. Currently, the fastest passenger ferry can reach speeds of up to 58.1 knots [125], significantly reducing passenger travel times.

The CC-200 is a fast ferry developed by CoCo Yachts. A CC-200 named the Peng Xing 15 is illustrated in figure 2.1. The vessel has an aluminum catamaran hull designed to have an excellent performance in rough sea conditions, maintain its service speed in waves, and provide a comfortable trip for the passengers and crew. The separation between the two demi-hulls of the catamaran provides an improved roll stability and therefore helps the safety and comfort on board of the vessel.

The CC-200 is powered by two MTU 12V2000M72 main diesel engines, each driving one MJP 650 waterjet through a ZF 3050 gearbox [76]. Each engine delivers a power output of 1,080 kW at 2,250 RPM. This results in a speed at a full load of 31.5 knots.

The ferry's catamaran hull allows for a large deck area, resulting in the capability to accommodate 199 passengers. This is divided into 163 economy seats, 28 business seats, two VIP rooms for four, and two crew cabins for four.



Figure 2.1: The Peng Xing 15 [25]

The main particulars of the CC-200 are summarized in table 2.1.

Table 2.1: Main particulars of the Coastal Cruiser 200 [76] [74]

Main particulars Coastal Cruiser 200	
Hull type	Aluminium catamaran
Length x beam x draft	40.0 x 9.3 x 1.2 m
Main engines	2x MTU 12V2000M72
Power	2x 1,080 kW @ 2,250 rpm
Speed @ full load	31.5 knots
Passenger capacity	199

The main operator of the CC-200, a Chinese company called Shenzhen Pengxing Shipping Co., Ltd, mainly uses the ferry to sail on the route in China from Zhuhai to Shenzhen, shown in figure 2.2:

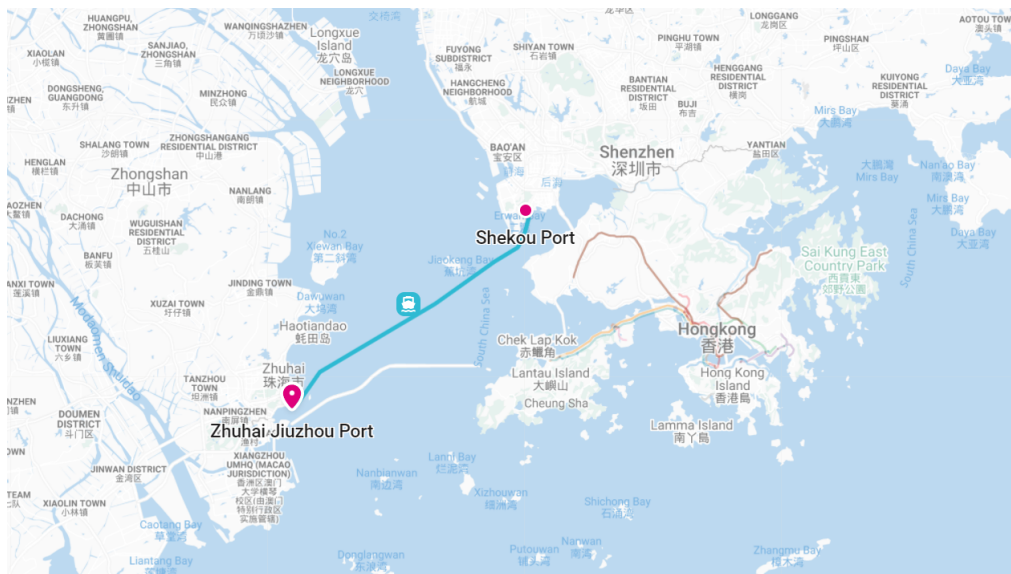


Figure 2.2: A map of the Zhuhai-Shenzhen crossing [168]

Commuters use the CC-200 to sail from Zhuhai to Shekou, which is an area in Shenzhen, or vice versa. From the perspective of Zhuhai, the Shekou ferry terminal is located on the other side of the Pearl River Delta, as can be seen in figure 2.2.

The main details of the Zhuhai-Shenzhen route and the CC-200's operating profile are summarized in table 2.2.

**Table 2.2:** Details around the Zhuhai-Shenzhen route [55] [47] [58]

<b>Zhuhai-Shenzhen route</b>	
Sailing distance	25 NM
Time in transit	50 minutes
Time maneuvering in port	10 minutes
Time in port between crossings	30 minutes
Number of crossings per day	9 (average)

## 2.2. Emission-free Coastal Cruiser 200 requirements

Based on the specifications of the CC-200, its operating profile, and the details of the Zhuhai-Shenzhen route, the following requirements were set for the zero-emission ferry studied in this thesis:

- **Transit speed.** The ferry must reach a transit speed of 30 to 40 knots. This is required so that the ferry is competitive with other modes of transport from Zhuhai to Shenzhen, such as the current CC-200, busses, and taxis. Taking a taxi from Zhuhai to Shenzhen takes around 90 minutes [168].
- **Minimum range.** The ferry must have a minimum range of 30 NM at service speed. This will allow the vessel to operate between the Zhuhai-Shenzhen route without refueling or recharging along the way. The minimum range includes a margin of safety in case of rough sea conditions or heavy loads.
- **Passenger capacity.** The ferry must have a passenger capacity of 200 passengers (including the crew), which is required to keep similarity to the CC-200.
- **Propulsion system.** The ferry must use a propulsion system and power plant that allow for zero-emission operation.
- **Operational profile.** The ferry must be able to operate on the same operating profile as the CC-200 sailing on the Zhuhai-Shenzhen crossing. Among others, this could mean that it must be able to recharge or refuel fast enough during the 30 minutes spent in port to make it to the other side again.
- **Safety and comfort.** The ferry must be at least as safe as the reference ferry, the CC-200. Also, the comfort levels of the zero-emission ferry must be similar to the CC-200, which means that the superstructure dimensions and interior arrangement will not be altered.
- **Economic feasibility.** To be feasible in all respects, the zero-emission ferry must be feasible from both a technical and financial perspective. In this thesis, it has been defined that economic feasibility is achieved when the zero-emission ferry's yearly total cost of ownership (TCO), which combines the capital and operational expenditures, is less or equal to the CC-200's yearly TCO. The CC-200's TCO will also account for the indirect costs caused by its ICE emissions. In this definition, a zero-emission ferry could therefore be economically feasible when it is more expensive to purchase but cheaper to run compared to the CC-200, or vice versa. The economic feasibility is further elaborated and studied in chapter 7.

## 2.3. State-of-the-art zero-emission ferries

This chapter will highlight a list of the latest zero-emission ferries. Together with the requirements set in chapter 2.2, a better understanding of the current gaps and challenges around zero-emission ferries is obtained.

### 2.3.1. The latest developments in zero-emission ferries

#### MF Ampere

One of the first real-world developments for zero-emission ferries started in 2012 when the Norwegian shipping company Norled won the contract to build and operate the world's first battery-powered ferry, MF Ampere. The 80-meter long catamaran ferry, illustrated in figure 2.3, began its operation in 2015 and operates in Norway on a route of roughly 3 NM [8]. During the 10 minutes of loading and unloading time, the ferry is recharged for the next trip. MF Ampere can accommodate up to 120 cars and 360 passengers and has two onboard 450 kW electric motors, allowing it to sail at a speed of 10 knots [8].



Figure 2.3: MF Ampere [44]

#### Medstraum

Although the MF Ampere was an excellent step towards a future with lower emissions, it is not suited as a replacement for a fast passenger ferry due to its relatively low maximum sailing speed.

A good progression towards fast zero-emission ferries was made with the start of the construction of Medstraum in June 2021 [149]. Medstraum (Norwegian for “with current”), illustrated in figure 2.4, is currently being built and will be operated in Norway. It will be equipped with two electric motors and a battery capacity of 1.5 MWh [149]. This allows Medstraum to sail with a service speed of 23 knots and complete its route in 36 minutes [149] [121]. Medstraum's hull and superstructure will be built using aluminum, lowering the vessel's weight and energy consumption compared to a steel superstructure. The zero-emission ferry is designed to carry around 150 passengers, made possible due to its length of 31 meters and a beam of nine meters [149]. Nevertheless, the desired service speed of 30+ knots is not reached.



Figure 2.4: Rendering of Medstraum [171]

### SF-BREEZE

The zero-emission ferries that were covered so far are all battery-powered. A straightforward alternative to batteries is hydrogen fuel cells. In 2016, a feasibility study of a hydrogen zero-emission ferry called SF-BREEZE changed the world's perspective on using hydrogen fuel cells as a power source for maritime use [147]. This study not only showed that it is feasible to operate a fast, hydrogen-powered, zero-emission ferry but showed how it should be done in great detail. The concept design of the aluminum catamaran ferry would be able to carry 150 passengers and hold 1,200 kilograms of liquid hydrogen [152]. Combined with a 4.92 MW installed fuel cell power, the ferry would operate at a speed of 35 knots [152]. The SF-BREEZE was designed to complete four 50-mile round trips per day and sail at a speed of 35 knots for about 60% of the transit time [175]. The ferry would refuel twice a day, being after the morning and afternoon peak commuter periods.

### Sea Change

Although the SF Breeze was never built, the same team that performed the study, Zero Emission Industries (formerly Golden Gate Zero Emission Marine), did eventually build and launch a zero-emission hydrogen-powered ferry named the Sea Change, illustrated in figure 2.5, in early 2021 [182]. This was the first hydrogen-powered vessel in the US and the first commercial hydrogen-powered ferry globally [67]. The Sea Change is designed to transport commuters around the bay of San Francisco, California. It is equipped with 360 kW of fuel cells and reaches speeds up to 22 knots [67]. With its length of around 21 meters, it can provide high-speed transport for up to 75 passengers [67].



Figure 2.5: Sea Change [138]

### Beluga24

A number of state-of-the-art zero-emission ferries with both battery- and hydrogen-driven propulsion systems have been highlighted now. However, these ferries do not show an element that may be interesting for the concept design of a zero-emission CC-200; hydrofoils.

Currently, a new 150-passenger zero-emission hydrofoil ferry called the Beluga24 is being developed and designed by a Swedish start-up company, Green City Ferries [29]. The Beluga24 is illustrated in figure 2.6. It will use proven hydrofoil technology, allowing the ship to lift itself halfway out of the water at high speed and reduce its water resistance significantly.



Figure 2.6: Beluga24 [78]

The CEO of Green City Ferries, Frederik Thornell, even made the following quote about the new ferry:

"We expect a consumption of 30 kWh per nautical mile at 30 knots, which is almost half of what a conventional catamaran consumes". [78]

#### **Zero-emission Coastal cruiser 300**

A study closely related to this research is the feasibility study of a fast electric passenger ferry performed by Moreno Francis in 2019, also in cooperation with CoCo Yachts [58]. This study investigated the feasibility of a zero-emission version of the Coastal Cruiser 300, a ferry with a passenger capacity of 300 and a maximum speed of 31 knots [58].

The study concluded that an electric version of this ferry was not technically feasible using the technologies that were available at the time. The batteries would increase the vessel's weight too much, resulting in too large of an increase in resistance and energy consumption. The study also concluded that a hydrogen-powered version of the Coastal Cruiser 300 would be technically feasible [58]. Still, it concluded that economic feasibility can not be achieved since the fuel costs would be significantly higher compared to the diesel-powered ferry [58].

#### **NAVAIS**

Lastly, NAVAIS is a promising project researching zero-emission ferries. The project aims to introduce a ferry product family that can be used in a platform-based modular product design method for double-ended ferries. In the next four years, the project's goal is to develop a "digital twin" of a double-ended battery-powered ferry for Europe with a capacity for up to 400 passengers and 120 cars, and a service speed of 8.5 to 23 knots [139].

### **2.3.2. Most prominent challenges for zero-emission fast ferries**

Although some concepts exist, fast zero-emission ferries have not become mainstream for several reasons, which are discussed in the next section.

#### **Technical challenges**

There are several technical challenges involved in building a fast zero-emission ferry that can compete in its technical specifications with its diesel-driven variant.

#### **Power**

One of the first technical challenges is the required power. Commonly, required ship power is roughly proportional to the cube of its speed [155]. Therefore, doubling the speed of a conventional

ferry from 15 knots to 30 knots will require roughly  $2^3 = 8$  times as much power.

### Weight

Due to the high power demand, larger power plants are required for fast ferries. Moreover, zero-emission power plants typically weigh more than diesel power plants. The combination of these effects cause weight to be one of the primary technical challenges when designing zero-emission ferries.

As an example, the parametric weight estimates of the SF-BREEZE concluded that the ferry would have a fully-loaded weight of 135.1 tonnes [147]. The study compared this weight to a similarly-sized diesel-driven ferry called Vallejo, which carries more passengers than the SF-BREEZE (300 vs. 150). The conclusion was that despite the lower passenger capacity, the estimated weight of the SF-BREEZE was 10% higher than the weight of the Vallejo [147]. Compared to the CC-200, which has a fully-loaded weight of around 120 tonnes, the SF-BREEZE is around 14% heavier, even though it carries fewer passengers and is significantly smaller in terms of its dimensions [74]. An overview of this comparison is given in table 2.3.

**Table 2.3:** Weight comparison of a zero-emission ferry vs. two traditional diesel-driven ferries

Ship	Passengers (-)	Dimensions (m)	Fully loaded weight (t)
SF-BREEZE	150	33.2 x 10.1 x 3.43	135.1
Vallejo	300	31.6 x 8.67 x 2.68	122.8
Coastal Cruiser 200	199	40.0 x 9.30 x 3.40	approx. 120

The relatively high weight of the SF-BREEZE is mainly caused by the weight and volume of the fuel cells and liquid hydrogen systems. A strengthening effect also plays a role. As the weight of the SF-BREEZE is higher compared to a similar diesel-powered ferry, it requires more power to sail at high speeds. Therefore, bigger and heavier hydrogen tanks and fuel cell systems are required, increasing weight, energy demand, and fuel consumption. Lastly, a 5% additional margin is also included in the SF-BREEZE weight estimate [147].

Another notable observation from the weight comparison is the small weight difference between the Vallejo and CC-200, even though the Vallejo can carry 50% more passengers. This can be explained by the Vallejo's significantly smaller dimensions compared to the CC-200. The smaller dimensions increase the passenger density on board the ship, enabling the Vallejo to carry 50% more passengers at a similar fully-loaded weight.

### Passenger capacity and operational profile

The development of the Beluga24 shows that despite the challenges, it may be possible to design a 30-knot zero-emission ferry that carries 150 passengers. However, this does not mean that a zero-emission version of the CC-200 is feasible. First, the zero-emission version of the CC-200 will have to carry 200 passengers instead of 150, an increase of 33.3 %. A feasibility study performed in 2018 and 2019 by Moreno Francis showed that an electric version of the Coastal Cruiser 300, with a passenger capacity of 300, was not technically feasible at the time [58]. Therefore, it could be said that somewhere in this range of passenger capacity lies a turning point where the zero-emission ferry becomes non-feasible. The question is whether the CC-200 is on the feasible or non-feasible side.

Besides, there is no known information about the operational profile of the Beluga24. It may have to sail shorter distances compared to the CC-200, increasing the chances of a technically feasible outcome. Also, it is still unknown whether batteries or hydrogen fuel cells will be used, which will likely impact the Beluga24's maximum sailing distance. Sailing a more considerable distance using hydrogen fuel cells is less of a challenge compared to batteries, as is discussed in chapter 4. Also, the engineering team could still alter the ferry's specifications to make it feasible. As an example, the promised speed of 30 knots may be lowered.

An overview of a selected set of specifications of the Beluga24 and the zero-emission concept designs of the Coastal Cruiser 200 and Coastal Cruiser 300 is presented in table 2.4.

**Table 2.4:** Comparison of the Beluga24 and the zero-emission concepts of the Coastal Cruiser 200 and 300 [58] [174]

Ship	Passengers (-)	Energy source (-)	Speed (knots)	Range (NM)
Beluga24	150	$H_2$ /batteries	30 (expected)	N/A
Coastal Cruiser 200 (zero-emission concept)	200	$H_2$ /batteries	30-40	30+
Coastal Cruiser 300 (zero-emission concept)	300	$H_2$	30	25 (depending on design)

### Safety challenges

At last, there is a challenge from the safety point of view. Zero-emission power plants can be seen as an increased risk due to their shorter proven track record compared to diesel power plants. Also, hydrogen, for example, is the lightest of all atoms, making it hard to contain. It is also highly explosive, ignites more quickly than natural gas, and has a wider flammability range [59]. Therefore, designers of zero-emission hydrogen ferries will need to account for detonation risks if there is a leak in the hydrogen tank(s).

Even energy carriers like batteries comes with safety risks. Lithium-ion batteries can experience thermal runaway. Once this happens, fires and explosions may occur on board the ship. Therefore, choosing a safe battery type and applying safety precautions when designing a battery-powered ship is crucial.

### Financial challenges

Apart from the technical challenges, a financial challenge is present. The feasibility study of the SF-BREEZE showed that at the economics of 2016, the cost of building the hydrogen zero-emission fast ferry would be 1.5 to 3.5 times more than a similar diesel ferry [147]. Meanwhile, the operating and maintenance costs would be two to eight times that of a comparable diesel ferry [147].

Battery-driven ferries struggle with a similar problem as most need organizational or governmental funding. In the case of the world's first electric zero-emission fast ferry, Medstram, the development was initiated by the TrAM project, which started in 2018 and secured €11.7 million in financing from the European Union's Horizon 2020 research and innovation program [149].

### 2.3.3. Conclusion: state-of-the-art zero-emission ferries and remaining gaps

An overview of the state-of-the-art in zero-emission ferries is given in table 2.5.

**Table 2.5:** Overview of state-of-the-art zero-emission ferries [8] [17] [149] [147] [152] [182] [67] [29] [174] [58] [139]

Zero-emission ferry	State of development	Energy source	Capacity (-)	Speed (knots)
MF Ampere	Operating since 2015	Batteries	360 pax, 120 cars	10
BB Green (chapter 4.1.4)	Built in 2016 (currently not used)	Batteries	80 pax	28
Medstram	In construction since June 2021	Batteries	150 pax	23
SF-BREEZE	Concept (2016)	$H_2$ fuel cells	150 pax	35 (60% of transit time)
Sea Change	Built in early 2021	$H_2$ fuel cells	75 pax	22
Beluga24	Expected initial operation in 2023	Batteries/ $H_2$ fuel cells	150 pax	30
Zero-emission CC-300	Feasibility study (2019)	$H_2$ fuel cells	300 pax	30
NAVAIS ferry family	Project ongoing	Batteries	≤ 450 pax, 120 cars	8.5-23

By comparing the state-of-the-art zero-emission ferries with the emission-free CC-200 requirements given in chapter 2.2, it can be concluded that no zero-emission ferry currently exists that meets the set requirements. The most prominent and identifiable gap is that no currently-operating, state-of-the-art, zero-emission ferry offers a passenger capacity of 200 in combination with a 30- to 40-knot service speed.

# 3

## Optimizing the efficiency of fast ferries

As discussed in the previous chapter, several technical challenges are involved with designing a technically feasible, high-speed, zero-emission ferry. To make a technically feasible outcome more likely, this chapter researches ways to optimize the efficiency of fast ferries. The following sub-question is answered:

*Which design choices can be made for fast ferries that could result in an improved efficiency at operational speeds?*

Identified measures that could improve a ferry's efficiency include implementing hydrofoils, weight-saving measures (e.g., using a fiber-reinforced composite hull), energy saving devices, wind-assisted propulsion, advanced control strategies (e.g., adaptive pitch control), and air lubrication.

However, not every identified measure is expected to be worthwhile. For instance, energy saving devices generally provide relatively small efficiency improvements and can only be used in combination with a propeller. The use of adaptive pitch control also poses a constraint on the ferry's propulsion system, as it requires using a controllable pitch propeller. Furthermore, wind-assisted propulsion is generally used on vessels with a lower sailing speed. Lastly, air lubrication may cause a significant improvement in the ferry's efficiency but generally requires a relatively large additional power for the air fans. Also, using air lubrication in combination with hydrofoils is not needed, as the hull will be lifted out of the water at service speed.

For these reasons, this chapter investigates how the mass of the CC-200 can be lowered and if hydrofoils can be used, as it is expected that these measures will have the most significant impact on the ferry's efficiency.

### 3.1. Lowering the mass of the Coastal Cruiser 200

A zero-emission ferry uses different power plant and auxiliary system components compared to a diesel-powered ferry. Chapter 3.1.1 studies how the ferry's mass changes due to the switch zero-emission. Moreover, one can also lower the mass of a zero-emission CC-200 by adopting various weight-saving measures, such as constructing the ferry's hull from carbon fiber instead of aluminum. These weight-saving measures are identified in chapter 3.1.2.

#### 3.1.1. Switching from a diesel-driven to a zero-emission ferry

When switching from a traditional, diesel-driven ferry to a zero-emission ferry, the mass may change due to the removal or addition of the following main components and systems:

- **The removal of the diesel engine(s) and propulsion-related system(s)**
- The added weight of the new energy carrier
- The added weight of the new electric motor(s) and gearbox(es)
- The added weight of the new propulsor(s)
- The added weight of a hydrofoil system

This subsection only covers the change of mass due to the removal of the diesel engine(s) and propulsion-related system(s) as it is fixed and known from the data of the CC-200. Meanwhile, the other items depend on the chosen requirements and components and will therefore be determined in subsequent chapters.

It is assumed that the following components are removed from the CC-200 when switching to an emission-free ferry:

- Diesel engine (2x)
- Generator set (2x)
- Gearbox (2x)
- Waterjet (2x)
- Fuel and lubrication oil tanks
- Fuel and lubrication oil systems
- Exhaust systems of the main and auxiliary engines
- Engine-related batteries, boxes, and chargers

The mass of these components is not disclosed in this thesis due to the confidential nature of the information. However, the resulting mass is used later in this thesis to determine the expected weight of the zero-emission ferry.

### 3.1.2. Weight-saving measures for the zero-emission CC-200

Together with the removed power plant components, the mass of the zero-emission CC-200 lowers due to a number of identified weight-saving measures that may be applied. This thesis identified the following measures, which are discussed next:

- Using fiber-reinforced composites
- Removing unnecessary items
- Reducing the mass of currently-equipped items

As a disclaimer, the exact weight saving resulting from these measures is not disclosed due to the confidential nature of the information, but is used in this thesis for estimating the mass of the zero-emission ferry.

#### Using fiber-reinforced composites

Fiber-reinforced composites were identified as a method to tackle one of the most significant challenges of zero-emission ferries, a high weight. As fiber-reinforced composites are lighter than most metals, the ferry's weight can be lowered by using fiber-reinforced composites to construct the ferry's hull and superstructure.

Standard classes of fiber-reinforced polymers are carbon fiber-reinforced polymers (CFRP) and glass fiber-reinforced polymers (GFRP). Studies have shown that carbon fiber-reinforced structures are approximately 20 to 30% lighter than glass fiber-reinforced structures [68]. Because of this, CFRP is one of the most suitable fiber-reinforced composites for marine applications and is the material this thesis will focus on [160]. Other reasons why CFRP may be preferred above aluminum are listed below:

- A higher strength-to-weight ratio, which improves efficiency and reduces operating costs.
- Excellent corrosion resistance, leading to fewer maintenance requirements.
- A higher stiffness, leading to improved stability and safety.

Unfortunately, the weight saving of using CFRP instead of metals is hard to calculate. CFRP is a nonhomogeneous material, which means that the material properties fluctuate depending on the direction of the force. In a CFRP ship hull, the fibers' orientation can be placed along the path of the load in a particular component, making a weight estimation based on material properties alone inaccurate.

For this reason, the weight saving of using a fiber-reinforced hull instead of a metal hull is estimated based on five case studies that researched this exact problem.

The five identified case studies concluded that a structural weight saving of 33 %, 45 %, 50 % (2x), or 52 % can be achieved when using a CFRP hull instead of an aluminum hull [38] [127] [72] [95] [28]. The results of the case studies are summarized in table 3.1. Figure 3.1 shows the Malolo Cat IV, a 150-passenger catamaran ferry that was used in Gerit's case study, which concluded that switching from aluminum to CFRP resulted in a structural weight saving of 50% [38].

**Table 3.1:** Summary of five case studies researching the structural weight saving of using a CFRP hull [38] [127] [72] [95] [28]

Ship	Structural weight saving	Researcher(s)
20-meter catamaran ferry	50%	Gurit Composite Engineering
40-meter catamaran ferry	33%	J. Kuzjatkin
13.7-meter electric yacht	45%	D. Oh, et al.
24-meter civil passenger ship	52%	T. Hertzberg
24-meter high-speed patrol craft	50%	M. Burman, et al.

For the zero-emission CC-200, CFRP could be applied as the material for the hull, superstructure, and U-shaped fender, which are currently constructed from aluminum. Considering that the hull of the CC-200 is already optimised for a low weight, a structural weight saving of 35% is assumed in this thesis.



**Figure 3.1:** The 150-passenger catamaran ferry used in Gurit's case study [38]

Besides saving weight, the use of CFRP can have other benefits too. Among them is the improved life span of the vessel. The design life span of the aluminum vessels designed by CoCo Yachts is 20 years, which includes a margin based on heavy operating conditions. The aluminum vessels could be operated for longer than 20 years, depending on their use and maintenance. However, using CFRP could increase the vessel's design life span, as CFRP hulls typically achieve a life span of 30 years or more [34].

This also helps to lower the environmental impact during the vessel's lifetime. A study on composite hulls for ferries found that a CFRP hull has a 33% higher environmental impact on ecosystems and human health and a 62% higher environmental impact on resources compared to an aluminum hull [34]. However, as a CFRP hull is lighter and reduces the ferry's fuel consumption, it was found that after three months of operation on the case study route in Norway, the damages of both hull types will reach a break-even point [34]. From that point, the study found that the ferry with an aluminum hull will cause higher environmental impacts compared to the CFRP ferry for the rest of its lifetime [34].

One concern of a composite hull might be its end of life. In contrast to an aluminum hull, a CFRP hull can not be melted, reshaped, and recycled at the end of its life cycle. Due to the bond and structure

of the fibers and resin, the material can take high temperatures and forces, making it hard to separate for recycling purposes. Recycling methods for fiber-reinforced composites do exist but require labor-intensive and complex processes. This is why in practice, many fiber-reinforced composites are dumped at the end of their lifetime [2]. However, if a vessel with a CFRP hull is built now, it is expected to have a lifespan of at least 30 years. During that time, new recycling options for fiber-reinforced composites could be introduced, allowing cheaper and easier material recycling with less environmental impact.

### **Removing unnecessary items**

The second identified weight-saving measure consists of the removal of unnecessary items onboard the ferry. Three item groups have been identified that are fitted to the CC-200 but are unnecessary when switching to zero-emission variant.

The first group of items is the four watertight doors that are placed between the engine room and auxiliary room in the bottom compartment of the CC-200. The main and auxiliary engines will be removed for the zero-emission ferry, and it will not be necessary anymore to keep these rooms separated watertight.

Next is the removal of the thermal insulation of the interior arrangement. The heat conductivity of composites can be around 40 times lower compared to aluminum [7]. Therefore, thermal insulation is unnecessary when a CFRP hull is used.

At last, the extra noise insulation of the auxiliary rooms will become unnecessary for a zero-emission ferry. The zero-emission ferry will most likely use electric motors instead of diesel engines. Since electric motors are much more silent compared to internal combustion engines, no additional noise insulation is required.

### **Reducing the mass of current items**

The third measure taken to lower the mass of the zero-emission ferry is replacing a number of items with lighter variants. For most items, this measure makes the ferry either more expensive or less comfortable, which is why the measure has not been taken for the original CC-200. However, since a low weight for the zero-emission ferry is such an important objective, it is expected that the advantages of the weight saved by this measure, such as a lower resistance, a higher range, and so forth, will outweigh the disadvantages it causes, such as higher costs or lower comfort levels.

A number of items onboard the CC-200 can be swapped out for lighter variants. First, the glass windows on the upper and main deck can be replaced by polycarbonate windows, saving around 50% in mass [143]. Next, the cooling water system can be replaced with an air cooling system, which is assumed to weigh 70% less as it eliminates the need for metal piping and carrying water in the system.

The mass of the electrical systems can also be reduced. The current lead-acid dead ship, emergency service, and radio batteries can be replaced with lighter Li-ion batteries, which are almost 60% lighter [101]. Also, the copper electric cables of the control, power, and communication systems can be replaced with aluminum cables, which will save around 40% in mass [40].

Lastly, the zero-emission ferry can be equipped with lighter seats. It was found that seats from the manufacturer YSmarines are between 22 and 39% lighter than the current seats, depending on whether they are standard or VIP seats [110].

## **3.2. Hydrofoils**

In 2019, Moreno Francis performed a feasibility study of a zero-emission version of the Coastal Cruiser 300 and studied the use of hydrofoils. The conclusion was that a battery- or hydrogen-powered ferry sailing at a speed of 30 knots would not benefit from implementing hydrofoils [58]. This was mainly the case due to the considerable weight of the vessel, which led to the need for an extensive hydrofoil system and, in turn, a lower effective lift coefficient.

Nevertheless, the use of hydrofoils is studied in this thesis too, as it is expected that hydrofoils may prove to be feasible for the zero-emission CC-200. The vessel's high weight was the main issue that led to an unfeasible solution in Moreno's feasibility study. It is expected that the latest battery technologies or hydrogen systems (chapter 4), the use of various weight-saving measures (chapter 3.1.2), and the ship's lower passenger capacity will result in a considerable reduction in mass. This increases the likelihood of a feasible hydrofoil system, as studies have shown that the effectiveness of hydrofoil systems is reduced as the ship size increases [116].



Figure 3.2: The Jetfoil, a high-speed hydrofoil ferry [165]

### 3.2.1. The basics and working principles of hydrofoils

Hydrofoils are submerged wings mounted on struts below the ship's hull. As the ship sails forward, the hydrofoils generate lift. At higher speeds, the hydrofoils can lift the ship out of the water, just like an airplane flies using its wings. As the density of water is about 800 times higher than the air density, hydrofoils can be made much smaller than aircraft wings and still provide enough force to fully lift a ship's hull out of the water. As a ship's hull is lifted out of the water, the hull resistance decreases. Due to hydrofoils, the conventional power-speed relationship is not applicable anymore.

The typical resistance curve for a hydrofoil ship is illustrated in figure 3.3. At low speeds, the resistance increases exponentially until it reaches the top of the resistance hump. At this point, the ship's hull is still in the water, and the total resistance is relatively high due to the hull's resistance and the hydrofoil's drag. As the speed increases, the hull lifts out of the water, and the resistance decreases. After the point of take-off speed, the ship's resistance rises again due to the increased drag of the hydrofoil system until the resistance matches the thrust, which is the ship's maximum speed.

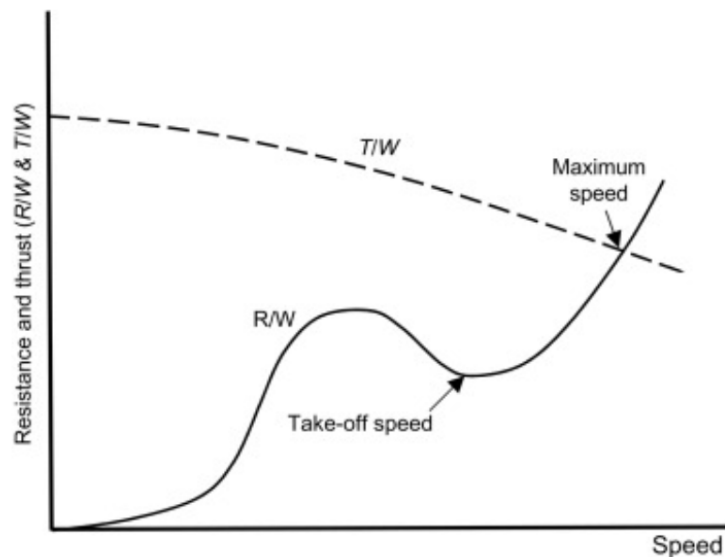


Figure 3.3: Typical relation between resistance/thrust and speed for a hydrofoil vessel [23]

The main particulars that define the geometry of a hydrofoil are the angle of attack, thickness, chord, camber line, and span, as illustrated in figure 3.4.

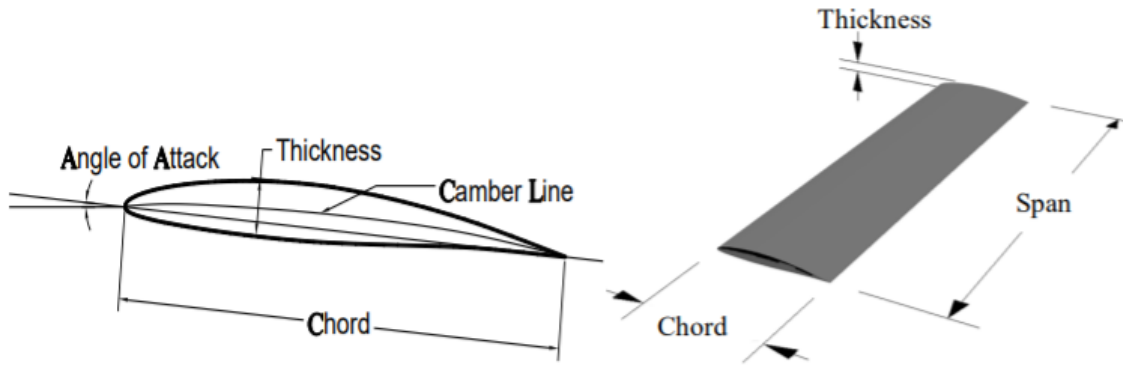


Figure 3.4: Basic foil geometry in 2- and 3D [69]

Using this geometry, the planform area can be defined as in equation 3.1:

$$A = \text{Span} \cdot \text{Mean Chord} \quad (3.1)$$

The lift is defined as the force component acting perpendicular to the direction of motion, while the drag is the force component acting parallel to the direction of motion. The lift and drag are usually nondimensionalized by the lift and drag coefficients:

$$\begin{aligned} C_L &= \frac{L}{\frac{1}{2}\rho V^2 A} \\ C_D &= \frac{D}{\frac{1}{2}\rho V^2 A} \end{aligned} \quad (3.2)$$

Designers of hydrofoils usually aim to maximize the ratio of these two coefficients (the lift/drag ratio) to maximize the efficiency of the hydrofoil.

### Categories of hydrofoils

Hydrofoils can be grouped into two main categories, fully-submerged hydrofoils and surface-piercing hydrofoils. These two categories of hydrofoils, illustrated in figure 3.5, will now be discussed.

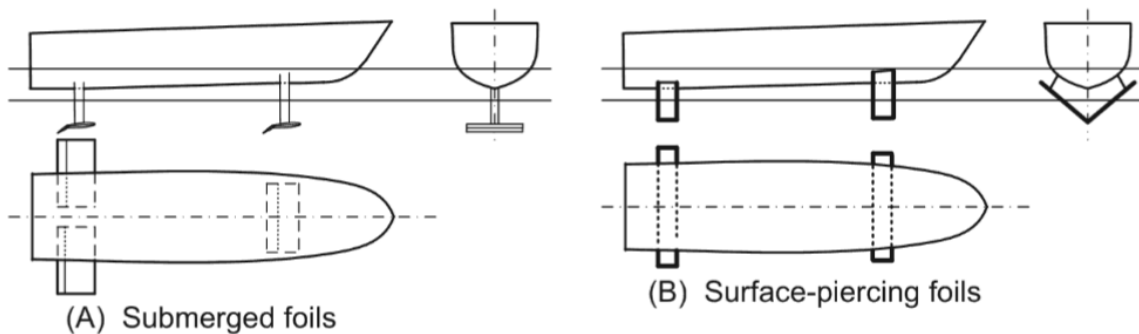
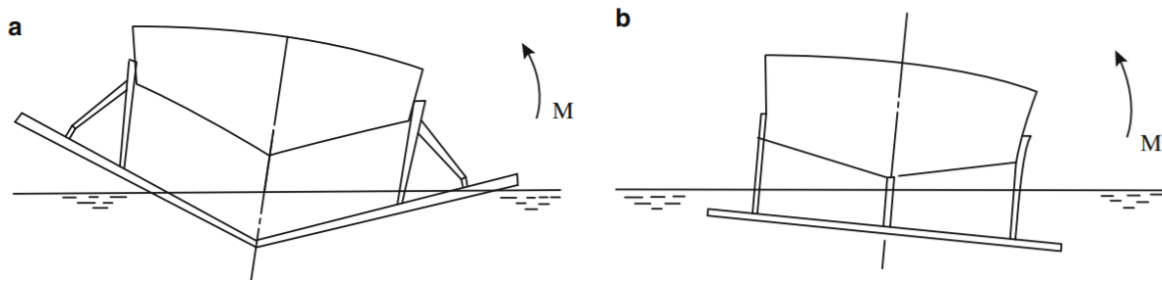


Figure 3.5: Submerged and surface-piercing hydrofoils [118]

### Fully-submerged foils

Fully-submerged foils are wholly immersed in the water, except for the non-lifting struts that provide the support. Typically, they are designed to operate at an immersion greater than the foil chord. This is because the lift of the foil reduces as it approaches the water surface, an effect called lift degradation. Although lift degradation decreases the foil's lift/drag ratio, it can be used to stabilize the vessel in heave, roll, and pitch direction. As the vessel rolls, one side of the foils comes closer to the water surface, which decreases its lift. This leads to a correcting roll moment, as shown in figure 3.6(b). Still, the roll moment is not as effective as the correcting roll moment for surface-piercing foils, which is

discussed in the next subsection. Therefore, a fully-submerged foil system needs active flaps to further increase this restoring roll moment and stabilize the vessel.



**Figure 3.6:** Restoring roll moments for (a) surface-piercing and (b) fully submerged foils [189]

The main advantages of submerged foils include seaworthiness and maneuverability. Due to the active control system applied on submerged foils and the fact that the foils are constantly immersed, the vessel experiences little motions and speed losses in rough waves. This is attractive for a ferry, as the passengers will feel more comfortable and are less likely to become seasick. Also, flaps that are part of the active control system allow the ferry's operator to achieve an inward heeling angle for the ship to minimize its turning circle, which improves high-speed maneuverability. Figure 3.2 shows an example of this inward heeling angle.

#### Surface-piercing foils

Surface-piercing foils are constructed to have a considerable angle between the two planes and often have a "V" shape. This results in stabilization forces that are more effective compared to fully submerged foils. Besides the advantage of passive stability, surface-piercing foils can achieve good maneuverability performance in restricted waterways due to their small overall size.

However, surface-piercing foils also have disadvantages. First, since a part of the surface-piercing foils penetrates the free water surface, their lift/drag ratio is inferior to fully-submerged foils [69]. Furthermore, the docking of a vessel with surface-piercing foils can be complicated because the foils are wider than the vessel's beam. Cavitation is another commonly identified disadvantage but usually only occurs at speeds above 45 knots, which is not the case for this thesis [189]. Lastly, surface-piercing foils can pose limitations for waterjet propulsion systems due to the lack of an advanced active control system, which increases the likelihood of the rear foil coming too close to the water surface, making it more challenging to design a reliable waterjet intake [189].

The advantages and disadvantages of fully-submerged and surface-piercing foils are summarized in table 3.2.

**Table 3.2:** Summary of (dis)advantages of fully submerged and surface-piercing foils

<b>Fully-submerged foils</b>	
<i>Advantages</i>	<i>Disadvantages</i>
High seaworthiness in rough waves	Requires an active control system
Good high-speed maneuverability	No inherent stability
<b>Surface-piercing foils</b>	
<i>Advantages</i>	<i>Disadvantages</i>
Passively controlled (less complexity)	Inferior lift/drag ratio
Good maneuverability in restricted waterways	Docking is more complicated
	More challenging in case of waterjet propulsion

After weighing the advantages and disadvantages, it was decided to continue researching fully-submerged foils. The zero-emission CC-200 will sail along the coast of the South China Sea. Thus, the advantage of high seaworthiness is attractive to enhance the passengers' comfort. Furthermore, the higher lift/drag ratio will help to increase the chances of a technically-feasible solution. At last, the improved high-speed maneuverability is a significant benefit as the ferry will be operating at a speed of 30 to 40 knots.

### Hydrofoil configurations

There are three hydrofoil configurations possible when it comes to maintaining stability in the pitch direction. First is an aircraft configuration where the main lifting foil is placed forward and a smaller stabilizing foil is placed aft. An alternative is the tandem configuration where both foils support an equal load. At last, there is the canard configuration where the main lifting foils is placed aft and a smaller stabilizing foil is placed forward of the ship. These three hydrofoil configurations are illustrated in figure 3.7. Chapter 3.2.2 will discuss which configuration was chosen for the zero-emission ferry.

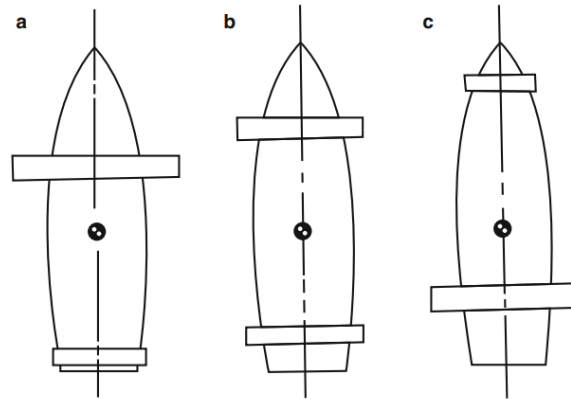


Figure 3.7: The aircraft (a), tandem (b), and canard (c) hydrofoil configurations [189]

### The challenges of implementing a hydrofoil system

When implementing a hydrofoil system on a vessel, the designers are bound to come across a specific set of challenges. This subsection gives an overview of all the identified challenges that should be considered when designing a hydrofoil vessel.

- **Weight.** It is important to keep the weight of a hydrofoil vessel as low as possible. According to the results of several studies, a heavier vessel requires a larger hydrofoil system, which decreases the foil's effective lift coefficient [58] [116].
- **Cooling system.** Cooling systems in ships typically use seawater as a medium to extract heat from the power plant. Traditional seawater intakes for cooling systems are located at the ship's hull, which will not function once the hull is above the water surface. Therefore, a hydrofoil ship's cooling system should be designed to extract seawater from the foils or use a different medium.
- **Propulsion system.** Traditional propulsion systems may have to be significantly altered to work in combination with a hydrofoil system. For example, how can a propeller be mounted to a hydrofoil, and how will the propeller be driven? If a waterjet is used, how can a reliable water intake be ensured? How is that water guided into the waterjet pump, which may be located inside the ship's hull?
- **Stability.** This challenge is particularly relevant for fully-submerged foils, which do not have inherent stability. This means the vessel will likely require an expensive and complex active control system.
- **Cavitation.** Cavitation could be a challenge when implementing a hydrofoil system. If cavitation occurs, it can damage the surface of the hydrofoils and lower their efficiency.
- **Docking.** A challenge for surface-piercing foil ships is the docking maneuver. As surface-piercing foils are often wider than the ship's beam, the docking procedure will likely be more complicated.

### The state-of-the-art in hydrofoils

This chapter will give a short overview of the state-of-the-art in hydrofoil ships. No currently-operating zero-emission hydrofoil ships have been identified, only concepts. Therefore, the overview will include the most relevant "traditional" hydrofoil vessels and three concepts of zero-emission hydrofoil ferries.

#### Traditional hydrofoil ferries

A hydrofoil ship similar to the CC-200 in terms of passenger capacity is the RHS 200. This 210-238 passenger monohull ferry delivered in 1981 has an installed power of 3,828 kW and uses surface-piercing foils to achieve an operating speed of 35 knots [189].

Another relevant ferry is the "PS-30", which was operated in the Pearl River Delta and is illustrated in figure 3.8. The 301-passenger ferry was built in 1995 and used fully-submerged foils and a gas turbine power plant of 6,368 kW to achieve a service speed of 43 knots [189].



Figure 3.8: The PS-30 hydrofoil ferry in service [184]

### Zero-emission hydrofoil ferry concepts

Now, a selection of zero-emission hydrofoil ferry concepts is highlighted, as no such vessels have been identified that are currently in operation.

A 100% electric hydrofoil ferry concept is the Candela P-30, expected to be realized and launched in 2022 [39]. Using fully-submerged, computer-controlled hydrofoils, the designers claim that the ferry will consume 80% less energy (3 kWh/NM) than conventional ships when cruising at 20+ knots [153]. The P-30 provides space for up to 30 passengers and can sail at a speed of 20 knots for up to 60 nautical miles, but can also reach speeds of 30+ knots if necessary [153].

Another concept is the 300-passenger MobyFly 30. According to MobyFly, this ferry will be able to travel at speeds over 37 knots, all while requiring up to 70% less energy than current diesel ferries [117]. No information has been found on the realization of the MobyFly 30, as the company is planning to launch their smaller-sized hydrofoil boats of 10- and 18-meter length first.

The last concept example is the 150-passenger ELECTRA, designed by Boundary Layer Technologies, a California-based startup. The ferry is illustrated in figure 3.9. The company claims that the ferry, using fully-submerged hydrofoils, will be able to cruise at 40 knots, have a range of 100 nautical miles, and be equipped with 9,000 kWh of batteries [48].



Figure 3.9: The ELECTRA hydrofoil ferry concept [22]

The main characteristics of the highlighted hydrofoil ferries are summarized in table 3.3:

**Table 3.3:** Overview of discussed hydrofoil ferries [189] [153] [117] [48]

Hydrofoil ferry	State of development	Energy source & propulsion	Capacity (-)	Service speed (knots)
RHS 200	Delivered in 1981	Diesel engines, FPPs	210-238 pax	35
PS-30	Delivered in 1995	Gas turbines, water jets	294 pax, 9 crew	43
Candela P-30	Concept, realization plans for 2022	Batteries, propellers	30	20
MobyFly 30	Concept	Batteries, thrusters (expected)	300	38 (top speed)
ELECTRA	Concept	Batteries, propellers	150	40

### 3.2.2. Designing the hydrofoil system

To determine whether hydrofoils improve the zero-emission ferry's efficiency, it must be determined if the total propulsive power of the ferry is lower when a hydrofoil system is applied. As such, this chapter covers the design of a hydrofoil system in three parts.

First, the geometry of the zero-emission ferry's hydrofoil system is set based on the CC-200, findings from literature, structural considerations, and Autowing. Autowing is a software tool used for calculating the hydrodynamics of various high-speed craft and is further detailed in the next subsection [11]. Furthermore, resistance data of the hydrofoil ferry operating in various conditions is obtained by modeling the foil geometry in Autowing. Lastly, a method is developed that gives a better understanding of the ferry's resistance hump (figure 3.3). The resistance at the hump must be known to ensure the ferry has a high enough installed power to overcome the hump and reach its desired operating speed.

#### Autowing: methods and algorithm

The lift and drag of a hydrofoil system can be determined using Autowing [11]. Autowing is a software tool developed by Nikolai Kornev from the University of Rostock in Germany. It can model the complex hydrodynamics of high-speed craft using the vortex lattice method. For hydrofoil calculations, Autowing models a wing configuration advancing at a constant speed in an incompressible, inviscid, and irrotational fluid domain [176]. Free surface effects are accounted for by a surface vorticity, represented as a number of closed discrete vortex frames (the vortex lattice method) [176]. Effects of viscosity are also considered by an iterative procedure following viscous-inviscid flow interaction theory and boundary layer theory [176]. Autowing accounts for the frictional resistance, resistance due to lift, and wave-making resistance. More details about the method and algorithm of Autowing can be found in [176], [115], [89], and [90].

After tests, researchers found that lift coefficients at different Froude numbers and depths of submergence given by Autowing were in good agreement with experimental data acquired by the Krylov Institute and the Central Hydro-Aerodynamic Institute [176]. Additionally, various other studies found Autowing to be a suitable theoretical design tool and validated that the results of the tool are in good agreement with available experimental results from model tests [115] [90] [104] [91] [120].

For example, the PhD study of G. Migeotte used Autowing to validate the resistance, trim, and sinkage results for a catamaran using a Hysuwac configuration, which is a hydrofoil-assisted, planing catamaran of 40 meters in length (equal to the CC-200) [115]. The comparison of the total resistance as a function of the displacement Froude number can be found in figure 3.10. It can be seen that the predicted values are in good agreement with the available experimental values for the Hysuwac configuration. The displacement Froude numbers of the measured and predicted data points are in good agreement with those at the operational speed of the zero-emission CC-200. At a zero-emission ferry mass of 115 tonnes (estimate, not precisely known yet), a  $Fn_{\nabla}$  of 2.5 corresponds to roughly 33.4 knots, while a  $Fn_{\nabla}$  of 3.0 corresponds to roughly 40.1 knots. Therefore, this validation experiment was performed at conditions similar to those of the CC-200.

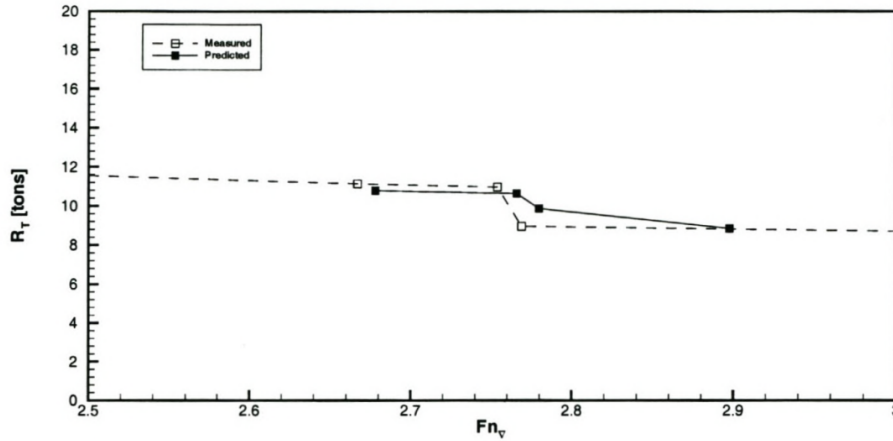


Figure 3.10: Autowing and experimental total resistance data comparison for a Hysuwac configuration [115]

Since Autowing's creators and several other studies have validated the design tool and no experimental data is available for the configuration in this thesis, it is assumed that the results obtained by Autowing are accurate enough for a preliminary assessment of the performance of a hydrofoil system. A more detailed explanation of the working principles and methods used by Autowing can be found in appendix A.2.

### The hydrofoil system's geometry

The geometry of the hydrofoil system is mainly determined by the following elements:

- The number of lifting foils.
- The span, chord, profile, and angle of attack of the lifting foils.
- The number of support struts.
- The span, chord, and profile of the support struts.

It is chosen to use two lifting foils, one placed aft of the ship and the other placed forward of the ship. Two lifting foils is the most common number on fully submerged-foils, both on already-built and concept ships, as was seen in chapter 3.2.1.

As seen in chapter 3.2.1, an aircraft, tandem, or canard configuration can be chosen for the hydrofoil system. From research done into state-of-the-art hydrofoil ferries, it seems that there is no consensus on which of the three configurations is best as all of them are applied on various vessels. For example, Electra and the Candela P-30 use an aircraft configuration, MobyFly and Argo (figure 5.5) use a tandem configuration, and the Jetfoil uses a canard configuration (figure 5.7) [48] [153] [117]. In this thesis, it has been chosen for a tandem configuration with equally-sized foils to minimize the geometry's complexity (fewer parameters) and keep an equal aspect ratio for both foils, as is discussed next.

Hydrofoils generally achieve higher lift/drag ratios by enlarging their aspect ratio (AR), meaning a longer span and a shorter chord. This is why gliders, which need a high lift/drag ratio, have long and narrow wings. From experiments with the Autowing software, it was also found that a longer span significantly improves the lift/drag ratio, while a longer chord can negatively impact the lift/drag ratio. Therefore, the decision was made to make the span of the foils as long as possible and equal to the ferry's beam, which is nine meters.

The chord of the lifting foils should be as short as possible, but structural considerations constrain it. In the Hydrofoil Handbook, written by Hoerner et al., an expression for the maximum allowable aspect ratio of the foil was derived based on the foil's strength [79]. Since the hydrofoil span is known, the equation can be rewritten (equation 3.3) to find the minimum chord length:

$$c_{\min} = \left( \frac{1.92}{b} \cdot \sqrt{\frac{\sigma}{f}} \cdot \frac{t/c}{\sqrt{F_L/s}} \right)^{-3/2} \quad (3.3)$$

With:

- $c_{min}$ , the minimum chord length of the foils [m]
- $b$ , the maximum length between the struts of the foils [m]
- $\sigma$ , the yield stress of the foil material [MPa] (276 MPa for Aluminum 6061 [10])
- $f$ , the safety factor [-] ( $f = 1.15$ ) [79]
- $t/c$ , thickness ratio of the used foil profile [-]
- $F_L$ , Lift force of the hydrofoil [N]
- $s$ , the span of the hydrofoil [m]

With the help of a developed MATLAB script listed in appendix A.1, the minimum chord length of the hydrofoils was determined to be 0.68 meters. However, the chord length of the foils was set to 0.80 meters for an additional margin of safety.

The profile of hydrofoils used in marine applications is often cambered because the foils have to provide lift in one direction [35]. To find a well-performing foil profile for the hydrofoils, four NACA profiles of similar thicknesses have been tested with Autowing in the same operating conditions and compared on their lift/drag ratios.

The geometry of the four selected foils was extracted from a foil database called Airfoil Tools [4]. The first tested foil is the NACA 4418, a widely tested foil in the NACA 4-digit database, which was also used in a recent study related to vortex-shedding of hydrofoils [170]. Next, two NACA 16- and 66-profiles were tested, as a study found them to be common hydrofoil shapes for sub-cavitation levels ( $\leq 40$  knots) [35]. Lastly, a NACA 63-615 foil was tested, which has a slightly higher camber and is listed on the Airfoil Tools database as having one of the highest lift/drag ratios out of the NACA 6-series database [4].

The inputs of the computational experiments were set to the following. The speed was set to 30 knots, equal to the operating speed of the current CC-200. The angle of attack was chosen equal to three degrees, which seems realistic at a design speed of 30 knots based on table A.2 and was also chosen as the test angle for the ferry's resistance hump in chapter 3.2.2. The profiles' span was set to nine meters, equal to the span of the hydrofoil geometry as previously determined. Likewise, the chord of the profiles was set to 0.80 meters, equal to the determined chord length for the hydrofoil system. The rest of the inputs for Autowing are equal to those used for the experiments of the entire hydrofoil configuration, as listed in appendix A.3. The configuration of the NACA 63-615 profile modeled in Autowing can be seen in figure 3.11.

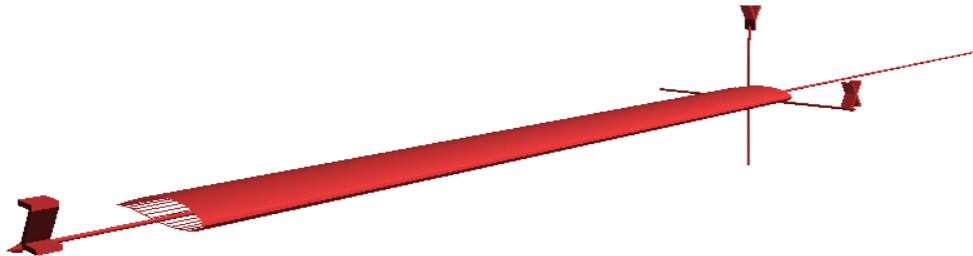


Figure 3.11: The NACA63-615 foil as modeled in Autowing

The results listed in table 3.4 show that the lift/drag ratios of the NACA profiles are in relatively close proximity to each other. Still, it can be seen that the NACA 63-615 foil profile (illustrated in figure 3.12) has the highest lift/drag ratio. As a result, it is selected as the foil profile for the hydrofoil system of this study's zero-emission ferry.

Foil profile	Angle of attack [deg]	Speed [knots]	Lift/drag ratio [-]
NACA 4418	3	30	20.62
NACA 16-015	3	30	20.83
NACA 66-215	3	30	20.50
NACA 63-615	3	30	21.18

Table 3.4: Comparing the lift/drag ratio of four NACA profiles

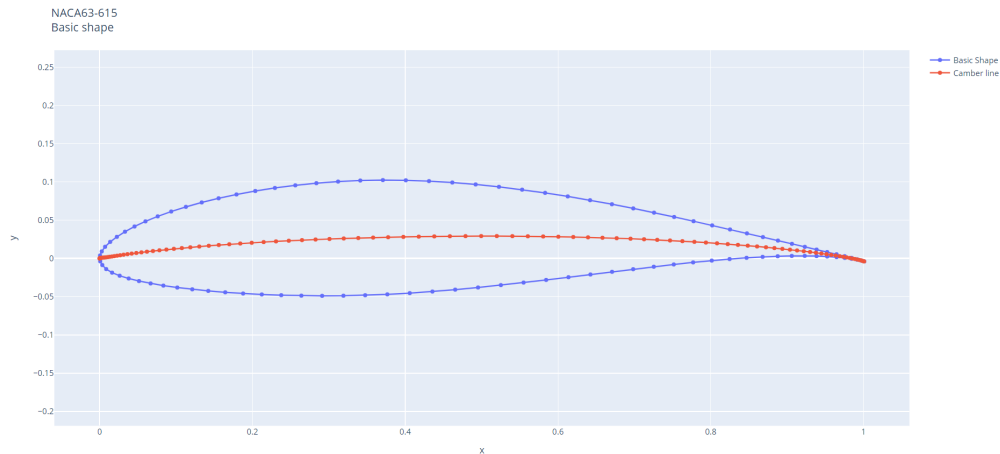


Figure 3.12: The NACA63-615 foil profile [122]

The effective angle of attack of the lifting foils is variable, both because the hydrofoil system will be equipped with an active control system and because the angle of attack will depend on the mass of the zero-emission ferry. A higher angle of attack increases the lift of the foils and vice-versa.

The hydrofoil system also consists of four support struts, connecting the lifting foils to the hull of the zero-emission ferry. According to Molland et al., the submergence of the hydrofoils should be at least 1.5 times the chord to avoid most free surface effects, which negatively affect the foil's lift/drag ratio [118]. For an additional margin of safety, the submergence of the foils was chosen to be two times the chord, or 1.6 meters. It was assumed that in foilborne condition, the zero-emission ferry's hull would be lifted 1 meter above the free water surface. Therefore, the span of the support struts is 2.6 meters. The support struts will have a symmetrical NACA profile because they should not generate any forces in a direction perpendicular to the water flow. The forward support struts are constructed from a NACA 0015 profile, while the aft struts will be constructed from a thicker NACA 0024 profile to accommodate a possible propeller shaft or a water intake.

As can be seen in chapter 2.3, the struts of most hydrofoil systems are placed to the outside of the ship. Therefore, the choice has been made to place the struts at three meters from the longitudinal axis. In other words, the span between the struts is six meters. In the modeled geometry, the distance between the lifting foils was chosen to be 16 meters, while the distance from the center of gravity and a lifting foil is eight meters (tandem configuration). However, this can be adapted without many consequences based on the center of gravity of the final ferry, its mass moment of inertia, and design preferences. For example, the ratio of the distance between the foils and the total ship length is slightly smaller compared to other state-of-the-art ferries (chapter 2.3), which adds a margin of safety. By making this distance larger, the aft lifting foil would experience a more uniform incoming flow, likely resulting in a better lift/drag ratio.

The main specifications of the hydrofoil system geometry are summarized in table 3.5. The geometry modeled in Autowing is illustrated in figure 3.13. This is half of the entire geometry, as it is mirrored around the x-axis. Also, the length of the support struts modeled in Autowing stops at the free water surface because the software did not support calculations in which the foils move through water and air simultaneously. Therefore, the resistance of the part of the struts above the water surface was not accounted for. However, it was assumed that this resistance is negligible compared to the resistance of the hydrofoil system below the free water surface and the air resistance of the ferry itself. Additionally, a number of safety margins were applied where possible to compensate for the resistance that is not accounted for by Autowing. These include a shorter distance between the lifting foils, a thicker chord, longer struts, and a relatively high frontal area and air resistance coefficient for the wind resistance calculation (chapter 6).

**Table 3.5:** Specifications of the defined hydrofoil system geometry

	Foils [-]	Span [m]	Chord [m]	Profile [-]	AoA [deg]
Lifting foils	2	9	0.8	NACA 63-615	Variable
Forward support struts	2	2.6	0.8	NACA 0015	0
Aft support struts	2	2.6	0.8	NACA 0024	0

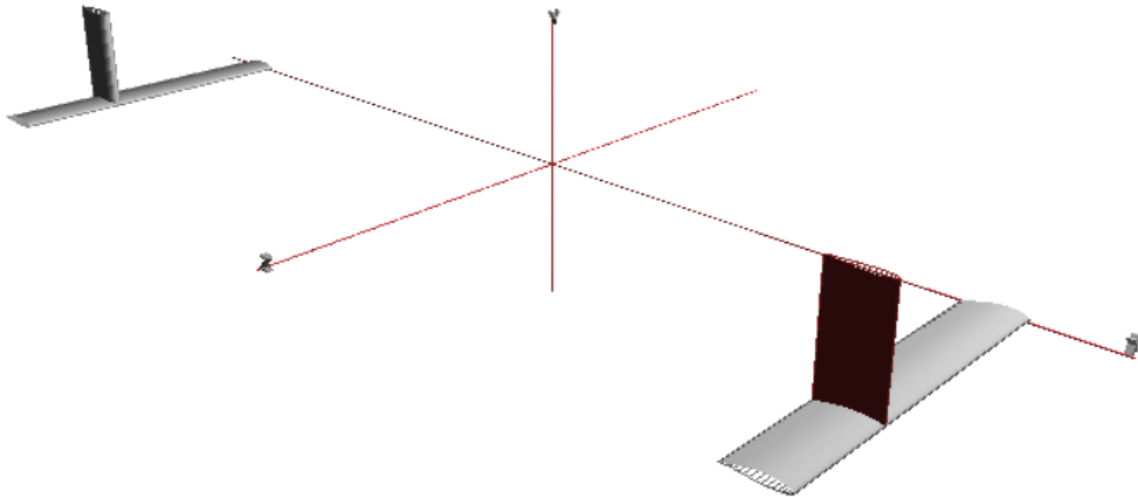


**Figure 3.13:** The geometry of the hydrofoil system modeled in Autowing

**Estimating the resistance of the hydrofoils**

One of the goals of studying a hydrofoil system is determining what resistance a hydrofoil ferry will encounter. This resistance can then be compared to the resistance of a ferry in the same conditions, but without hydrofoils, to make a conclusion on the effectiveness of a hydrofoil system.

**Autowing: Summary of the results**

The hydrofoil resistance was estimated using Autowing and the hydrofoil geometry modeled in figure 3.13. After running an iterative calculation, Autowing outputs a file containing pressure distributions, the wave surface after the hydrofoils, the vortex distribution, the vortex wake, and most importantly, the total forces acting on the hydrofoil geometry (lift and drag forces, as well as the lift/drag coefficient). As an illustration, the initial pressure distribution of the forward foils at a speed of 30 knots and angle of attack of three degrees is given in figures 3.14 and 3.15, where the pressure values are given in bars.

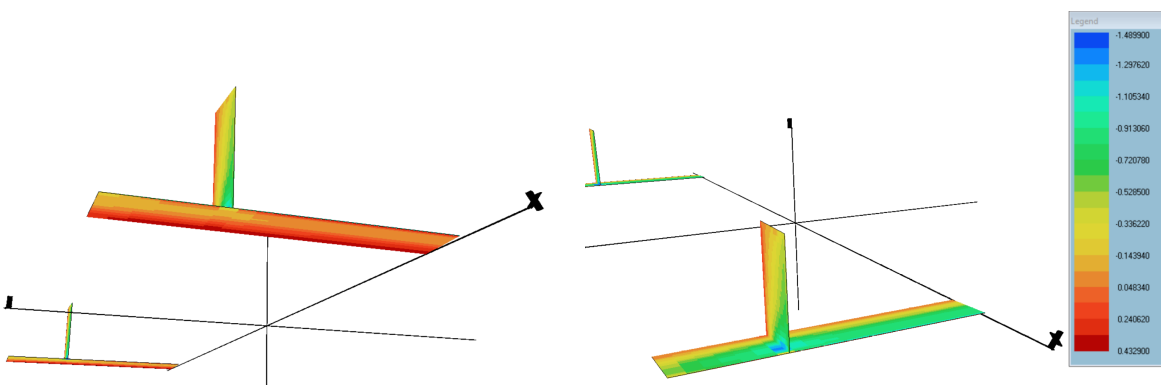


**Figure 3.14:** Initial pressure distribution (bar) of the pressure side of the forward foils at 30 knots and 3-degree angle of attack

**Figure 3.15:** Initial pressure distribution (bar) of the suction side of the forward foils at 30 knots and 3-degree angle of attack

Data of the hydrofoil system's lift and drag forces was collected for speeds of 30, 32, 34, 36, 38, and 40 knots, as well as varying angles of attack to account for a differing total mass of the zero-emission ferry, which is still unknown. The acquired data is listed in table 3.6.

**Table 3.6:** Lift and drag data results from experiments using Autowing

Speed [knots]	Angle of attack [deg]	Lift [t]	Drag [t]	Lift/drag [-]
30	4	132.6	-8.06	16.44
30	3.5	124.7	-7.38	16.89
30	3	116.6	-6.74	17.31
30	2.5	108.5	-6.14	17.67
30	2	100.3	-5.58	17.97
32	4	150.1	-9.28	16.17
32	3	131.9	-7.77	16.97
32	2.5	122.7	-7.08	17.32
32	2	113.4	-6.44	17.60
32	1.5	104.1	-5.85	17.80
34	2.5	137.8	-8.01	17.20
34	2	127.4	-7.28	17.49
34	1.5	116.9	-6.61	17.69
34	1	106.3	-5.98	17.76
36	2	142.1	-8.17	17.39
36	1.5	130.4	-7.41	17.59
36	1	118.6	-6.71	17.68
36	0.5	106.3	-6.04	17.59
38	1	131.6	-7.47	17.61
38	0.5	117.9	-6.72	17.52
38	0	104.9	-6.06	17.32
40	0.5	130.2	-7.45	17.48
40	0.25	122.7	-7.06	17.38
40	0	115.8	-6.70	17.28

The objective is to estimate the resistance of the hydrofoils based on the mass and speed of the zero-emission ferry. Therefore, the lift of the hydrofoils was assumed to equal the ship's mass. Drag is another word for the resistance of the hydrofoils. By curve fitting the lift and drag force data for each tested speed, equations (speed-specific) were obtained that estimate the resistance of the hydrofoils based on the mass of the ferry. These are listed in appendix A.3 and are used to estimate the ferry's hydrofoil resistance in a parametric, technical feasibility model covered in chapter 6.

For example, the mass-resistance equation for a sailing speed of 30 knots is given in equation 3.4. Its plot, together with the data points from Autowing, is illustrated in figure 3.16.

$$R_{foils} = 0.000369325 \cdot M_{ferry}^2 - 0.00923751 \cdot M_{ferry} + 2.79409 \quad (3.4)$$

With:

- $R_{foils}$ , the resistance of the hydrofoils in tonnes at 30 knots
- $M_{ferry}$ , the mass of the zero-emission ferry in tonnes

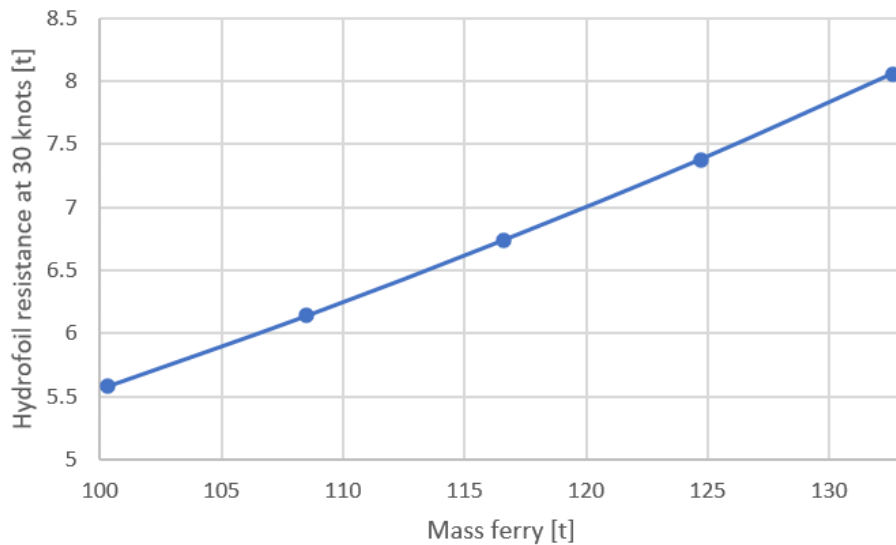


**Figure 3.16:** The hydrofoil resistance at 30 knots as a function of the ferry's mass (equation 3.4)

In table 3.6, it can be seen that the acquired lift/drag ratios range between 16.2 and 18.0. To validate these results, they were compared to lift/drag data from literature.

First of all, the acquired lift/drag ratios are somewhat higher but in reasonably good agreement with the lift/drag ratios of existing hydrofoil vessels built in the 20th century, which range between 8 and 12.5 [42]. A number of possible reasons would explain the lower lift/drag ratios of the existing vessels. First, the used configurations vary extensively, as the compared hydrofoil vessels use other foil profiles, arrangements, aspect ratios, and speeds that are often higher than 40 knots. Additionally, the lift/drag ratios could be based on the whole vessel (including air resistance), while the acquired lift/drag ratios are based on the hydrofoil resistance only. For the zero-emission CC-200, it should be noted that the effective lift/drag ratios will lower once the (air) resistance of the hull itself is added, which can be significant considering the relatively high operational speed of 30 to 40 knots.

A different study found that at 75 knots, a lift/drag ratio of 50 is achievable [19]. Moreover, researchers that performed experimental validation of lift and drag forces on an asymmetrical hydrofoil found that for an angle of attack between zero and three degrees, the lift/drag ratio can be between 92.6 and 18.5, respectively [30]. Although the results of these studies can not be compared directly to the results of Autowing because of the varying foil geometry and conditions, they prove that higher lift/drag ratios can be achieved. Therefore, it is assumed that the obtained lift/drag ratios are not unreasonably high and can be achieved in practice.

At last, something can be said about the interaction between the two foils from the acquired results of the computational experiments. Generally, it was seen that the aft foil provided slightly less lift and had a lower lift/drag ratio compared to the forward foil, presumably due to an interaction between the foils. In the experiment of figure 3.14 and figure 3.15, both foils provided 116.59 tonnes of lift in total. The forward foil was responsible for roughly 53% of the total lift, while the aft foil caused roughly 47% of the total lift. If the forward foil provides more lift compared to the aft foil, a disruption in the balance of the system may be created. However, it is assumed that this can be compensated by the hydrofoil's active control system, increasing the angle of attack of the aft foil, or by placing the aft foil a further distance from the ferry's center of gravity.

### The resistance hump

Hydrofoil ferries experience a resistance hump, as explained in chapter 3.2.1 and illustrated in figure 3.3. When designing a hydrofoil ferry, it is important to determine the speed at which the hump occurs and the magnitude of the resistance at the hump. If the resistance at the hump is significantly larger than the resistance at the ferry's operational speed, it has to be accounted for in the choice of the ferry's propulsion system and power plant to make sure that the hump can be overcome and the operational speed can be reached.

Determining the exact speed at which the resistance hump occurs is complex. At this speed, the hull of the ship is causing drag as it is still partially submerged and the ferry experiences lift and drag forces caused by the hydrofoil system. Moreover, various interactions occur between the foils and the hull. At speeds close to the resistance hump, the hydrofoil lift is in the same order of magnitude as the dynamic suction forces of the ship's hull, all while the two have a strong interaction with each other [115]. This interaction often results in sudden and significant resistance changes around the resistance hump.

A PhD thesis studying hydrofoil-assisted catamarans found that the resistance hump of a hydrofoil ship frequently occurs at a volumetric Froude number  $Fn_{\nabla}$  of 1.5 [115]. In this thesis, it has been assumed that the resistance hump will occur at a volumetric Froude number  $Fn_{\nabla}$  of 1.7. This decision was made to add a slight margin of safety to the hump resistance calculation and because the resulting resistance hump speed matched more closely with known resistance hump speeds of similar hydrofoil crafts, which lie between 20 and 22 knots [35]. The volumetric Froude number  $Fn_{\nabla}$  is given in equation 3.5:

$$Fn_{\nabla} = \frac{V}{\sqrt{g^3 \nabla}} \quad (3.5)$$

By rewriting the equation for the ship's speed, it was determined that depending on the inputs of the parametric model covered in chapter 6, the resistance hump of the zero-emission ferry would occur at a speed between 21 and 23 knots.

With the resistance hump speed determined, the total resistance can be calculated by adding all separate resistance components of the ferry at this speed. The resistance components consist of wind resistance, frictional and residual hull resistance, and hydrofoil resistance. The methods used for calculating the wind, frictional, and residual hull resistance are shown in chapter 6. The hydrofoil resistance and lift at the resistance hump speed were again determined with the help of Autowing. The modeled geometry shown in figure 3.13 was used. The angle of attack was assumed to be three degrees as it could be determined to be the optimum angle for operational speeds (table A.2), but could be altered in a more detailed design stage to expedite or delay the resistance hump. This is because a lower angle of attack generally lowers the lift and vice versa, affecting the magnitude of the total resistance as well. The results resistance hump speeds of 21 and 23 knots are given in table 3.7:

**Table 3.7:** Autowing results of the hydrofoil lift and drag forces at the resistance hump (21 and 23 knots)

Speed [knots]	Angle of attack [deg]	F_lift [kg]	F_drag [kg]	Lift/drag ratio [-]
21	3	59,160	3,161	18.72
23	3	70,059	3,816	18.36

### The mass of the hydrofoil system

When a hydrofoil system is added to a ferry, its mass should be accounted for. In this thesis, the mass of the hydrofoil system is estimated using equation 3.6. This equation is derived by A. Rofolo, who based it on estimations from various hydrofoil designers [161].

$$M_{foils} = (0.020 + 0.031 \sqrt{\frac{M_{tot}}{100}}) \cdot M_{tot} \quad (3.6)$$

With:

- $M_{foils}$ , the mass of the hydrofoil system [t]
- $M_{tot}$ , the total mass of the ferry, including the hydrofoils [t]

Depending on the ferry's speed and range requirement, the parametric model covered in chapter 6 used this equation to calculate an expected hydrofoil system weight of six to eight tonnes.

This outcome was validated in appendix A.4 by estimating the hydrofoil system weight based on the volume of the foils and the density of the material. This resulted in a mass of around 4.30 tonnes for aluminum, 2.80 tonnes for CFRP (both lower than the result of Rofolo's equation), and 12.5 tonnes for steel (higher than the result of Rofolo's equation), assuming the foils are not hollow (appendix A.4).

Therefore, it could be possible for the mass to become lower, as room inside of the foils is likely needed for a possible propeller shaft or flap system.

For these reasons, it could be said that the expected hydrofoil system weight of six to eight tonnes is overestimated when considering the hydrofoils are expected to be constructed from aluminum or CFRP. However, if a zero-emission hydrofoil CC-200 were to be built, it would need local structural reinforcements on the hull to cope with the forces from the struts, which can lift the entire ferry's weight. These structural reinforcements will add weight. Therefore, a high margin of safety is taken for the expected hydrofoil system weight, which is assumed to compensate for the (not accounted for) added weight of the structural reinforcements.

# 4

## Emission-free energy carriers

Chapter 4 studies several emission-free energy carriers that may be applied to fast ferries. From research into literature and data from manufacturers, properties like the energy density, safety, and availability are compared. This allows the most suitable emission-free energy carriers to be selected. Ultimately, the aim of chapter 4 is to answer the sub-question:

*What emission-free energy carriers are most suitable to be applied on a fast ferry and are available now or in the coming five years?*

The primary emission-free energy carriers that have been identified and will be researched in this chapter are batteries and fuel cells. More specifically, the following batteries and fuel cells will be discussed:

- Batteries
  - Lead Acid
  - Ni-Cd/Ni-MH
  - Li-Polymer
  - Li-ion
    - \* Lithium Cobalt Oxide (LCO)
    - \* Lithium Manganese Oxide (LMO)
    - \* Nickel Manganese Cobalt (NMC)
    - \* Lithium Iron Phosphate (LFP)
    - \* Lithium Titanate Oxide (LTO)
- Fuel cells
  - High-temperature fuel cells
  - Low-temperature fuel cells
    - \* Proton Exchange Membrane (PEM) fuel cells
    - \* Alkaline (AFC) fuel cells
    - \* Phosphoric Acid (PAFC) fuel cells

### 4.1. Batteries

Batteries are available in all kinds of shapes, sizes, and types. This chapter will select and compare the most relevant battery types for maritime applications.

As discussed in chapter 2.3.2, the weight of a zero-emission ferry is often relatively high due to its considerable energy requirement. Therefore, energy density is crucial when looking at a suitable battery type. The volumetric energy density (Wh/l) should be sufficient to fit in the vessel's battery compartment, and the gravimetric energy density (Wh/kg) is essential to minimize the added weight due to the battery pack.

By comparing the energy densities of the main battery cell types in figure 4.1, it can be concluded that Li-ion batteries have the highest gravimetric and volumetric energy densities. Therefore, the choice is made to restrict the battery study to Li-ion batteries.

Other battery technologies that were briefly examined but were not selected due to the five-year availability constraint include lithium-sulfur, solid-state, lithium-air, and graphene batteries.

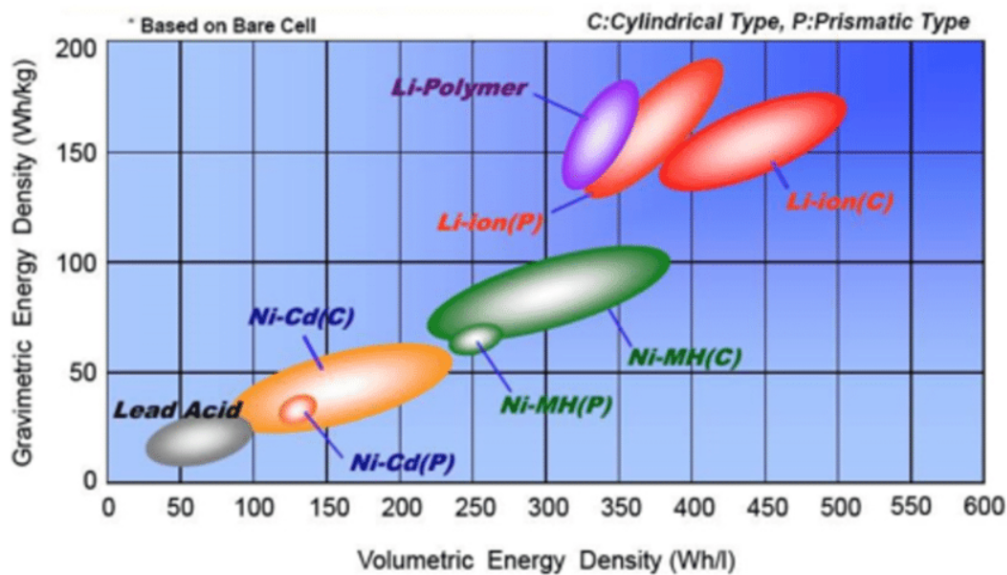


Figure 4.1: Energy density comparison of main battery cell types [18]

It must be noted that not all Li-ion batteries are equal. By changing the compounds used at the cathode and anode, Li-ion batteries show different properties in terms of energy density, charging capability, safety, expected lifetime, and more.

The Li-ion battery types shown in table 4.1 were identified and are researched next to find the most suitable one for a high-speed ferry.

Table 4.1: The selection of to be compared Lithium-ion battery types

Battery	Cathode	Anode
Lithium Cobalt Oxide (LCO)	$LiCoO_2$	Graphite
Lithium Manganese Oxide (LMO)	$LiMnO_2$	Graphite
Nickel Manganese Cobalt (NMC)	$LiNiMnCoO_2$	Graphite
Lithium Iron Phosphate (LFP)	$LiFePO_4$	Graphite
Lithium Titanate Oxide (LTO)	$LiFePO_4$	Lithium-titanate nanocrystals

For a clearer comparison, the LCO Li-ion battery was ruled out at the start of the study since it is not suitable to be applied in a marine transport environment.

LCO batteries are one of the most common Li-ion battery types but have three characteristics that make them unsuitable for fast ferries [159]. Firstly, LCO batteries are thermally unstable, especially when the cell size increases [32]. This is unattractive for marine applications, where large cell sizes are common. Secondly, the price of LCO batteries is rather high as they use a relatively large amount of cobalt. For this reason, the automotive industry is not using LCO batteries [178]. Lastly, LCO batteries have a limited life cycle of 500 to 1,000 cycles, depending on the depth of discharge and temperature [172]. This is unattractive for a high-speed ferry that is expected to have a long life span and may have to be charged frequently.

For the remaining four Li-ion batteries - LMO, NMC, LFP, and LTO - this thesis has identified the following criteria:

- **Energy density.** The battery's energy density should be as high as possible to maximize the energy storage for a certain mass or volume.

- **Costs and life span.** The battery's costs and life span are crucial for the ferry's economic feasibility. A cheap battery with a long lifetime will allow the ferry operator to minimize costs and increase profitability.
- **Safety.** Safety risks for passengers aboard a ferry should be minimized, making the battery's safety rating a crucial criterion.
- **Charging capabilities.** Ferries tend to have a demanding operational profile, which is why the chosen Li-ion battery should offer satisfactory charging capabilities to cope with the most intensive times of the day, such as rush hours.
- **Availability.** Ideally, manufacturers designing marine battery systems using the selected Li-ion battery are already operational.

#### 4.1.1. Energy density of Li-ion batteries

LMO batteries have an energy density of 100-140 Wh/kg [190]. NMC batteries have a significantly higher energy density of 140-200 Wh/kg, which is one of the reasons why they are often used in electric vehicle applications [190]. LFP batteries have an energy density of 90-140 Wh/kg [190]. Lastly, LTO batteries have a relatively low energy density of 45-100 Wh/kg [124]. The results are summarized in table 4.2.

**Table 4.2:** Energy densities of LMO, NMC, LFP and LTO battery cells [190] [124]

Battery	Energy density (Wh/kg)
LMO	100-140
NMC	140-200
LFP	90-140
LTO	45-100

It should be noted that this comparison is made on a battery cell level. For a functioning energy carrier, a battery system must be built around the battery cells, which adds weight. Therefore, the energy density on a system level may change.

As an example, the LTO battery's energy density is much lower compared to the NMC battery's on a cell level. However, the difference becomes smaller when comparing the battery types on a system level. Echandia, a manufacturer of LTO battery systems for marine applications, claims that the energy density of an NMC battery on a system level is between 10-12 kg/kWh (or 83.3-100 Wh/kg), while that of an LTO battery system varies between 13.5-14.5 kg/kWh (or 69-74 Wh/kg) [49].

#### 4.1.2. Costs and lifetime of Li-ion batteries

The cost of a Li-ion battery strongly depends on the materials used in its compound. A battery that uses cobalt, for example, is often relatively expensive, as cobalt is one of the most costly materials used in batteries [136]. However, the sole cost of a Li-ion battery is not interesting when no information is known about its lifetime. A battery that requires a higher initial investment but will operate without problems for years to come might be a better option than a cheap battery that will need to be replaced within a year. Therefore, the costs and lifetime will be looked at together. This way, the most cost-effective option is found using a life-cycle cost analysis method. In other words, the most cost-effective option will be found by looking at the battery's cost per kWh, per cycle, using formula 4.1:

$$Life-cycle\ cost = \frac{Battery\ cost\ per\ kWh\ of\ storage}{Cycle\ life} \quad (4.1)$$

A battery's cycle life depends on a few factors, such as its structure, usage, and the delta state of charge (DSOC). DSOC is a percentage that illustrates how much of the battery's total capacity is discharged per cycle. For instance, if a battery starts at 80% state of charge and ends at 20% state of charge before it is recharged again, the delta state of charge (DSOC) is 60%. The higher the DSOC, the shorter the battery's life cycle and vice versa. For this comparison, a DSOC of 100% is assumed.

The costs and life-cycle of NMC, LFP, and LTO batteries are retrieved from a comparative payback study of Li-ion batteries for Pacific NW ferries [13]. LMO batteries were not researched in this study. So, due to the sometimes varying results across different studies for the LMO battery's costs and life-cycle, LMO batteries were assumed to have a good cycle-life that is roughly equal to that of the NMC

battery and a relatively low cost that is roughly equal to the LTO battery [144] [190] [98]. The results are summarized in table 4.3.

**Table 4.3:** Life-cycle cost comparison of LMO, NMC, LFP and LTO batteries [13]

Battery	Cost (USD/kWh)	Cycle life at 100% DSOC (-)	Life-cycle cost (USD/(kWh*cycle))
LMO	700	8,000	0.0875
NMC	900	8,000	0.113
LFP	700	3,000	0.233
LTO	1,500	20,000	0.0750

The results show that the LTO battery is the most cost-effective option, mainly due to its much longer life cycle compared to the other batteries. It is then closely followed by LMO and NMC batteries, which are reasonably cost-effective options. The least cost-effective option is the LFP battery due to its relatively low life cycle.

Once again, it is important to note that results may vary depending on the DSOC. Furthermore, differences in cycle life, energy density, and costs may also be observed for batteries that use the same chemistry but are produced by different manufacturers. To illustrate this, figure 4.2 compares two NMC batteries from different manufacturers with an LTO battery in terms of DSOC and the number of cycles before the battery reaches 80% of its original capacity.

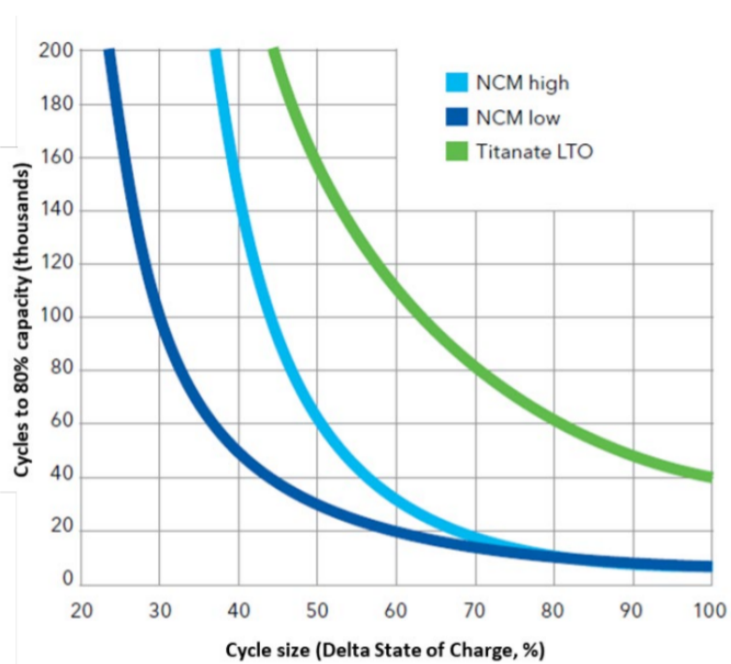


**Figure 4.2:** Number of cycles to reach 80% capacity as a function of DSOC for two NMC and one LTO battery [70]

### 4.1.3. Safety of Li-ion batteries

Safety is a crucial factor for batteries used in ferries. The most prominent safety risk of Li-ion batteries is thermal runaway, which happens when a battery cell is damaged or subjected to intense heat. The result is an exothermic reaction that propagates to other cells and is very difficult to stop. It can result in fires and explosions, which should be avoided at all costs on a passenger ferry.

First of all, the LMO battery is generally seen as a safe Li-ion battery type due to its high thermal stability [41] [123]. NMC batteries also provide reasonable safety and are the most popular Li-ion battery type in marine and automotive applications [41]. However, NMC batteries can have thermal stability risks, which may lead to thermal runaway [84].

LFP batteries are also considered as relatively safe, partly due to their lower energy density [190]. Batteries with lower energy densities are generally safer than batteries with higher energy densities

because they do not release as much heat in the event of a thermal runaway, which also decreases the likelihood of thermal runaway propagation.

At last, LTO batteries are the only battery types in this selection that use Lithium Titanium Oxide as their anode compound. As a result, the LTO battery is much more stable, robust, and resistant to mechanical abuse than any other Li-ion battery [49].

To conclude, the Li-ion batteries can be ranked from safest to least safe in the following order: LTO - LFP - LMO - NMC. In this ranking, LTO batteries are by far the safest choice. The results are summarized in table 4.4.

**Table 4.4:** Safety rating of LMO, NMC, LFP and LTO batteries for marine applications

Battery	Safety
LMO	Good
NMC	Average
LFP	Good
LTO	Very good

#### 4.1.4. Charging capabilities of Li-ion batteries

The charging capability of a battery is an important property needed to check whether it can cope with a ferry's operational profile. Charging capabilities are expressed in a C-rate, measured in  $h^{-1}$ . A battery charging at 1C will be fully charged in one hour, whereas 2C will fully charge the battery in half an hour.

A battery's maximum charge and discharge rates highly depend on the design of its cells. As such, typical charge and discharge rates for each of the Li-ion battery chemistries were not found in the literature. However, it is often seen that cells with a higher energy density can handle lower charging/discharging current and vice versa [70]. Therefore, an assumption could be made that NMC batteries have the least charging capabilities, followed by LMO and LFP batteries.

LTO batteries have the best charging capabilities, as they can double the charge rates of other battery chemistries while not affecting their life cycle in any significant way [13]. This is proved by the BB Green illustrated in figure 4.3, a 30-knot electric ferry that uses a 200 kWh LTO battery pack. Due to the relatively poor energy density of the LTO battery, the ferry has a range of 14 nautical miles [162]. However, the LTO battery pack can charge at a rate of up to 4C, which means the ferry can be fully recharged in 15 minutes [162].



**Figure 4.3:** The BB Green, a fast electric commuter vessel using an LTO Li-ion battery pack [162]

The results of the charging capability comparison are summarized in table 4.5.

**Table 4.5:** Charging capability of LMO, NMC, LFP and LTO batteries for marine applications

Battery	Charging capability
LMO	Good
NMC	Average
LFP	Good
LTO	Very good

#### 4.1.5. Availability of Li-ion batteries

The most significant factor influencing the availability of a select Li-ion battery is its chemistry. This is caused by a number of raw materials used in Li-ion batteries, which pose a high risk associated with their supply. These are included in the European Commission's list of critical raw materials [43].

A critical raw material that all Li-ion batteries have in common is lithium. In 2018, the total lithium production was 85,000 tons, of which 51,000 tons were supplied by Australia [100]. The total economically accessible global reserves are estimated to be 14 million tons, which equals 165 times the production volume in 2018 [100]. Besides that, lithium can be recycled from old batteries for at least 95% [94]. Therefore, lithium seems to be widely available in the long term unless its demand increases exponentially, which may be a risk due to the energy transition. This could be the motive behind adding lithium to the list of critical raw materials.

Another relevant critical raw material is cobalt, which is used in NMC batteries. Cobalt is extracted for 68% in the Democratic Republic of Congo, which has considerable political and ethical downsides [136] [43]. Therefore, the presence of cobalt negatively influences the availability of NMC batteries. However, unlike LCO batteries, which were ruled out at the start of the comparison, NMC batteries have nickel and manganese in their compound too, making the impact of using cobalt smaller. Furthermore, NMC batteries are currently the most popular Li-ion batteries in the marine industry, resulting in a very good availability [84].

LMO batteries are rarely used in marine applications as higher temperatures can significantly impact their life cycle [70]. Hence, it can be concluded that their availability is rather poor. LFP batteries, on the other hand, have a good availability since they do not contain any critical raw materials besides lithium and are already used in marine applications. For example, by the manufacturer Super B [99]. To end, the availability of LTO batteries is also considered satisfactory, considering Echandia is a manufacturer of LTO marine battery packs [49]. The availability of the Li-ion battery types is summarized in table 4.6.

**Table 4.6:** Availability of LMO, NMC, LFP and LTO batteries for marine applications

Battery	Availability
LMO	Average
NMC	Very good
LFP	Good
LTO	Good

#### 4.1.6. The most suitable Li-ion battery type

The previous subsections compared LMO, NMC, LFP, and LTO batteries based on energy density, life-cycle cost, safety, charging capability, and availability. The results from this analysis are summarized in table 4.7.

**Table 4.7:** Complete comparison of LMO, NMC, LFP and LTO batteries

Battery	Energy density (Wh/kg)	Life-cycle cost (USD/(kWh*cycle))	Safety	Charging capability	Availability
LMO	100-140	0.0875	Good	Good	Average
NMC	140-200	0.113	Average	Average	Very good
LFP	90-140	0.233	Good	Good	Good
LTO	45-100	0.0750	Very good	Very good	Good

It can be concluded that for the application of a fast electric ferry, either an LTO or NMC battery system will be the best option. LTO batteries perform the best in terms of life-cycle cost, safety, and charging capability while also having a good availability rating. On the other hand, NMC batteries have slightly higher life-cycle cost, deal with an increased risk of thermal runaway, and may have slightly

worse charging capabilities, but provide the highest energy density out of all options and are currently the most popular Li-ion battery option for the marine industry [84]. LMO and LFP batteries can be seen as satisfactory options at most, offering average or good scores across the board.

#### 4.1.7. Commercially-available marine Li-ion batteries

To truly test whether a certain Li-ion battery is technically feasible for use on a fast zero-emission ferry, more detailed and accurate specifications are needed. Therefore, specifications of several battery modules for marine applications have been collected and are shown in table 4.8. These specifications are compared in this subsection and are used in the parametric model of this thesis, which is discussed in chapter 6. In table 4.8, 'Grav. e. dens.' stands for gravimetric energy density, 'Vol. e. dens.' stands for volumetric energy density, 'C. charge' stands for continuous charge, and 'C. discharge' stands for continuous discharge.

**Table 4.8:** Specifications of commercially available Li-ion battery modules [186] [50] [36]

Battery module	Energy [kWh]	Grav. e. dens. [Wh/kg]	Vol. e. dens. [kWh/m <sup>3</sup> ]	C. charge [C]	C. discharge [C]
XMP 76P	7.636	100.5	118.7	3	5.5
XMP 98P	9.768	127.7	151.8	2.7	2.7
XMP 111E	11.10	146.1	172.5	1	2.3
XMP 125E	12.50	161.5	194.3	0.3	1
Dolphin Power	7.8	125.0	87.00	1.6	2.2
Dolphin Energy	10	166.7	116.0	0.4	0.5
Orca Energy	5.6	76.90	87.99	3	3
BM Cobra	11.7	130.0	131.3	N/A	N/A

In this table, the XMP modules are NMC Li-ion batteries manufactured by Xalt Energy [185]. The Dolphin and Orca modules are manufactured by Corvus Energy, but do not include specifications about the batteries' composition [50]. The BM Cobra is an LFP Li-ion battery module manufactured by Becker Marine [36].

By analyzing the table, it can be seen that the batteries with the highest energy densities have poorer continuous charging and discharging capabilities. As discussed previously, the energy density is critical, but the same can be said about the charging capability. It is found that the difference in energy density between fast-charging and slow-charging battery modules is not significant enough to easily be able to design a battery pack that stores enough energy for an entire day of operation (and can be charged at night). Therefore, a balance between the energy density and charging capability must be found.

Ultimately, it was concluded that the XMP 98P battery module provides the best balance between energy density and (dis)charging capability. It offers gravimetric and volumetric energy densities close to the energy-focused battery modules like the XMP 111E and XMP 125E. However, at the same time, it significantly improves the (dis)charging capability. Especially the continuous charging rate of 2.7C is seen as a substantial advantage, as the electric ferry could be fully recharged in just 18 minutes if enough power is available. This would fit perfectly in the 30 minutes spent in port by the CC-200 between trips. Therefore, the specifications of the XMP 98P were used to test the technical feasibility of the zero-emission ferry in chapter 6.

## 4.2. Hydrogen fuel cells

Instead of batteries, hydrogen fuel cells could power the zero-emission ferry. Hydrogen fuel cells rely on two electrochemical half-reactions (equation 4.2) to split hydrogen and generate electrical energy. As can be seen, a hydrogen fuel cell does not produce any harmful emissions, only pure  $H_2O$ .



### 4.2.1. Fuel cell types

Fuel cells can be divided into low-temperature fuel cells, which operate at 50°C to 220°C, and high-temperature fuel cells, which operate above 650°C. In this thesis, the following types of high- and low-temperature fuel cells were identified:

- High-temperature fuel cells
  - Molten Carbonate fuel cells (MCFC)
  - Solid Oxide fuel cells (SOFC)
- Low-temperature fuel cells
  - Proton Exchange Membrane fuel cells (PEMFC)
  - Alkaline fuel cells (AFC)
  - Phosphoric Acid fuel cells (PAFC)

It was decided to limit the scope of this thesis to low-temperature fuel cells due to the disadvantages associated with high-temperature fuel cells, which are discussed next.

First of all, high-temperature fuel cells need a start-up time of 30 minutes to multiple hours, depending on their size [135]. This is undesirable for a high-speed ferry as its operational profile requires power to be available immediately. The problem of prolonged start-up times could be solved by running the fuel cells continuously, but that would be inefficient. Secondly, load transients (0 to 100%) generally take much longer for high-temperature fuel cells. For instance, low-temperature PEM fuel cells have a load transient (0 to 100%) time of less than 10 seconds, while high-temperature SOFC can take up to 15 minutes, which is unattractive considering the ferry's dynamic operational profile [135]. Another reason not to use high-temperature fuel cells for a fast zero-emission ferry is their relatively low power density. For instance, SOFC fuel cells have a gravimetric power density of 20 to 230 (W/kg) and a volumetric power density of 8 to 60 (W/l) [135]. Meanwhile, as seen in table 4.9, PEM fuel cells achieve up to 229 W/kg and 138 W/l.

Due to the negative characteristics of high-temperature fuel cells, the following low-temperature fuel cell types will be studied; Proton Exchange Membrane (PEMFC), Alkaline (AFC), and Phosphoric Acid (PAFC).

#### Proton Exchange Membrane fuel cell

Of all commercially available fuel cell types, PEM fuel cells can achieve the highest power output per given weight or volume [132]. They also have a fast start-up time, even from subzero temperatures. Due to these properties, PEM fuel cells are considered one of the most versatile types of fuel cells and are being used in applications like transport and portable power with an excellent track record.

The most prominent manufacturers for large-scale PEM fuel cells are Nedstack, Ballard Power, PowerCellution, and Cummins. The fuel cells from these manufacturers will now be compared to find the module that offers the best overall properties.

Nedstack's most potent fuel cell module is the 'PemGen MT FCPI 500', illustrated in figure 4.4. It delivers a nominal electrical power of 500 kW, weighs 15,000 kilograms, and is built as a 20 ft ISO container (6.06 x 2.44 x 2.90 m) with a volume of 42.9  $m^3$  [133]. The fuel cell's nominal consumption is 59 kg/MWhe and it operates at 60°C, allowing a start-up time of about two minutes [180].



**Figure 4.4:** Illustration of the PemGen 500kW fuel cell manufactured by Nedstack [133]

The next manufacturer, Ballard Power, designed a specific module for marine vessels called 'FCwave.' It delivers a nominal power of 200 kW, and up to 6 modules can be installed with less than 5.5  $m^2$  of

floor space due to its compact footprint [109]. The FCwave offers a fuel efficiency of 56%, occupies a volume of  $1.98 \text{ m}^3$  ( $1.22 \times 0.738 \times 2.20 \text{ m}$ ), and weighs 875 kg [109].

The following PEM fuel cell, the Marine System 200, is manufactured by PowerCellution. Like the FCwave, the Marine System 200 is developed for marine applications and has a maximum output of 200 kW. It has a fuel efficiency of 54%, occupies a volume of  $1.45 \text{ m}^3$  ( $0.730 \times 0.900 \times 2.20 \text{ m}$ ), and weighs 1,070 kg [146].

Lastly, a number of PEM fuel cells are manufactured by Cummins [60]. The SF-BREEZE feasibility study performed in 2016 chose the Cummins fuel cells (previously manufactured under the company name 'Hydrogenics') for its concept design [147]. The authors of the SF-BREEZE feasibility study contacted Cummins and obtained the specifications for a 120 kW fuel cell module. This resulted in an efficiency of 59%, a volume of  $1.623 \text{ m}^3$  ( $1.99 \times 1.07 \times 0.762 \text{ m}$ ), and a weight of 800 kg [147].

An overview of the obtained specifications is given in table 4.9. As can be seen, the maximum output power is not equal for all fuel cells, but this is not a problem since multiple fuel cell systems can be connected in parallel to comply with higher power demands. However, for this reason, the fuel cells are compared on specific power ( $\text{kW}/\text{kg}$ ) and power density ( $\text{kW}/\text{m}^3$ ).

**Table 4.9:** Overview of PEM fuel cell specifications from four different manufacturers [133] [109] [146] [147]

	<b>Nedstack FCPI 500</b>	<b>Ballard FCwave</b>	<b>PowerCellution MS 200</b>	<b>Cummins 120 kW module</b>
Nominal power (kW)	500	200	200	120
Specific power (kW/kg)	0.0333	0.229	0.187	0.150
Power density (kW/m <sup>3</sup> )	11.66	101.0	137.9	73.94
Efficiency (%)	N/A	56	54	59

When comparing all fuel cell modules, it can be concluded that either the Ballard FCwave or PowerCellution Marine System 200 will be the best choice for the zero-emission ferry. The Ballard FCwave, illustrated in figure 4.5, has the highest specific power and should be used in an application where weight is a critical factor. Meanwhile, the PowerCellution Marine System 200 has the highest power density and should be used in an application where volume is critical.



**Figure 4.5:** The 200 kW FCwave fuel cell module manufactured by Ballard Power [109]

On a side note, it may be interesting to see that the Nedstack fuel cell module significantly underperforms on specific power and power density compared to modules of other manufacturers. A possible explanation for this rather big difference is that the Nedstack module looks bulkier compared to the other modules. Therefore, it could be that the Nedstack module, built as a 20 ft ISO container, is made to be very robust and used on the open deck, whereas the other modules focus on below-deck use.

At last, it is encouraging to see the advancements in fuel cell technology. In 2016, when the feasibility study of the SF-BREEZE was performed, the Cummins 120 kW module was selected as the best fuel cell option. Likely, the Ballard FCwave and PowerCellution MS 200 were not yet developed.

When comparing the Ballard FCwave with the Cummins 120 kW module, we see that the specific power increased by 53% and the power density increased by 37%, which is a considerable improvement.

### Alkaline fuel cell

The alkaline fuel cell is a low-temperature fuel cell that identifies itself by having an alkaline solution electrolyte. Although alkaline fuel cells have a reasonable efficiency of around 50 to 60% and are generally seen as low-cost systems, they have some notable disadvantages [20].

First of all, a separate KOH solution must be supplied to the fuel cell module [147]. In addition, alkaline fuel cells have a high intolerance to  $CO_2$ . Carbon dioxide can react with the fuel cell's alkaline electrolyte, leading to a loss in power. For these reasons, alkaline fuel cells are more complicated and heavier than PEM fuel cells [147]. On top of that, no heavy-duty alkaline fuel cell manufacturers specialized in marine applications have been found. As a result, alkaline fuel cells will not be studied any further as it can be concluded that PEM fuel cells are a better option for a fast zero-emission ferry.

### Phosphoric acid fuel cell

Phosphoric acid fuel cells (PAFC) use liquid phosphoric acid and carbon electrodes that support a platinum catalyst. Their operating temperature is generally on the higher side, being 150 to 200°C [61]. Combined with the sluggish kinetics of the PAFC reaction, phosphoric acid fuel cells have a warm-up time of 4 to 6 hours, which is very unattractive for a fast zero-emission ferry [147]. PAFC fuel cells also commonly run on natural gas, causing them to release  $CO_2$ . The manufacturers Fuji Electric and Doosan Fuel Cell do build PAFC modules that run on pure hydrogen, but they are designed to function as a stationary power plant [62] [173]. For these reasons, it is chosen not to further investigate phosphoric acid fuel cells.

## 4.2.2. PEM fuel cell costs and lifetime

The exact costs of PEM fuel cell modules are hard to determine as they largely depend on the production volume. Studies have shown that for the automotive industry, fuel cell prices could be higher than 1,000 \$/kW for a production volume of 500 to 1,000 mid-sized fuel cell vehicles per year, while the prices would drop to 50 \$/kW for 500,000 units due to economies of scale [31] [64]. Ballard, the manufacturer of the FCwave, also expects fuel cell costs to drop by as much as 70 to 80% once the annual production volume reaches 150,000 vehicles [142]. Researchers from the SF-BREEZE feasibility study found that for a one-time order of 5 MW, the estimated cost for a PEM fuel cell would be \$2,500/kW, which was given by the fuel cell manufacturer Cummins [147]. As such, it can be concluded that the costs quickly rise for low production volumes.

Additional costs that should be considered when designing a PEMFC power plant include the auxiliary systems and components like waste heat recovery (WHR) units, hydrogen and air delivery units or monitoring systems. Also, an investment in the onshore infrastructure may be needed, especially if compressed hydrogen storage is used. Nevertheless, this could also be true for a battery-powered vessel, which may require a power bank installed onshore to provide fast charging.

Like the cost, the lifetime of a PEM fuel cell is difficult to estimate. Nedstack claims its fuel cell has an operational lifetime of 24,000 hours, which is much more than the typical PEM fuel cell lifetime of 10,000 hours [180]. The fuel cell manufacturer Cummins estimated their fuel cells to last for 10,000 to 15,000 hours [147]. However, other studies expect a PEM fuel cell system to last for around 40,000 hours [164]. Like for batteries, the exact lifetime of a fuel cell depends on factors like its operating conditions and design.

The cost and lifetime estimations of PEM fuel cells are summarized in table 4.10.

**Table 4.10:** Cost and lifetime estimate of PEM fuel cells [31] [64] [147] [180] [164]

Fuel cell costs (\$/kW)	Lifetime (hours)
50 - 2,500 (depending on the production volume)	10,000-40,000 (depending on the fuel cell)

## 4.2.3. Hydrogen production

Unlike electricity, hydrogen is not currently produced on a massive scale, which may make the production, transport, and storage relatively costly.

Hydrogen is typically produced from the electrolysis of water. Therefore, electricity is required to produce hydrogen, which may come from non-renewable sources (e.g., fossil fuels) or renewable sources

(e.g., solar or wind). Therefore, a division is often made between grey hydrogen (produced from non-renewable sources) and green hydrogen (produced from renewable sources).

The hydrogen currently produced in China is mainly grey hydrogen and costs around \$6 to \$11 per kg [188]. However, the price of hydrogen can fluctuate quite significantly. For instance, gas prices have recently risen considerably in Europe for various reasons, causing the cost of grey hydrogen production to triple [75]. Luckily, China has set goals to decrease the cost of green hydrogen. China's goal is to produce green hydrogen for a cost lower than \$4.69 per kilogram by 2025 [188]. If it were economically feasible to use green hydrogen, the 'well-to-wake' emissions would be significantly decreased. To achieve this goal, multiple renewable energy production projects are in the pipeline, and hydrogen fuel production is being increased each year to achieve more significant economies of scale [188].

#### 4.2.4. Hydrogen storage

Hydrogen ( $H_2$ ) is the smallest and lightest gas molecule, causing it to have the highest gravimetric energy density of all known substances. Hydrogen has a lower heating value (LHV) of around 120 kJ/g, almost three times as much as diesel [119]. Unfortunately, the volumetric energy density of hydrogen is less attractive and depends on how it is stored.

Considering a fuel cell needs a continuous hydrogen supply to produce power, a hydrogen storage tank is required on board the vessel. Hydrogen can be stored in two main ways: as a compressed gas or as a liquid. These two are discussed in the following subsections.

##### Compressed hydrogen storage

The main advantage of compressed hydrogen storage is its lack of need for a complex thermal management system as the tanks operate at ambient temperature. Because of this, there is no loss of energy when hydrogen is not consumed.

Compressed hydrogen tanks are typically divided into four categories, type I to type IV. Type I tanks are the most basic tanks, usually constructed from carbon steel or aluminum, and can achieve pressure levels of around 200 to 300 bar [15]. Meanwhile, type IV tanks are the most advanced tanks. They are made of CFRP and use a polymer liner inside the tank. Type IV hydrogen tanks are the lightest of all and can withstand pressures of up to 700 bar [15].

A couple of years ago, few type IV tanks were commercially available as the technology was not fully developed [15]. However, due to recent developments, increasingly more companies are offering type IV hydrogen tanks. To illustrate the developments in the field of compressed hydrogen tanks, two Lincoln hydrogen tanks from the 2016 SF-BREEZE feasibility study will be compared to a number of state-of-the-art options [147]. The tanks are compared on the gravimetric and volumetric specifications (specs), which are defined as follows:

$$\begin{aligned} \text{Gravimetric spec} &= [\text{Empty tank mass (kg)}] / [\text{Mass of stored hydrogen (kg)}] \\ \text{Volumetric spec} &= [\text{Outer tank volume (L)}] / [\text{Mass of stored hydrogen (kg)}] \end{aligned} \quad (4.3)$$

The ideal high-pressure storage tank would have a gravimetric and volumetric spec close to zero. Or, in other words, be able to store a high mass of hydrogen relative to the weight and volume of the tank. The compressed hydrogen storage tanks are compared in table 4.11.

**Table 4.11:** Overview of different high-pressure hydrogen storage tanks [147] [81] [6]

Tank	Gravimetric spec (kg/kg)	Volumetric spec (L/kg)	Service pressure (MPa)	Type (-)
Lincoln 7,000 psi	16.21	49.69	48.26	N/A (composite)
Lincoln 10,000 psi	23.50	42.12	68.95	N/A (composite)
Quantum 332L	17.96	24.78	70	IV
Quantum 936L	10.62	41.6	35	IV
Luxfer M053H70	28.37	24.65	70	III

The Lincoln tanks displayed in table 4.11 were selected in the SF-BREEZE feasibility study, while the Quantum and Luxfer tanks are state-of-the-art. When comparing the 'old' Lincoln 10,000 psi to the 'new' Quantum 332L, which have similar service pressures, it can be seen that the gravimetric spec dropped by almost 24%, while the volumetric spec dropped by around 41% [81].

From the table, a balancing act between higher or lower service pressure can be clearly seen too, especially when comparing the Quantum 332L to the Quantum 936L. A high service pressure

compresses the hydrogen more and leads to a relatively low volumetric spec. However, more tank material is needed due to higher forces, which increases the gravimetric spec.

Out of the listed tanks, the best option would be the Quantum 332L or the Quantum 936L. The Quantum 332L is chosen above the Luxfer M053H70 because it offers a better gravimetric spec for a similar volumetric spec. The choice between the Quantum 332L and the Quantum 936L should be made based on their application. If weight is critical, Quantum 936L will be the best due to its lower gravimetric spec. If volume is critical, Quantum 332L will be the better choice due to its lower volumetric spec.

Lastly, it should be noted that the listed specifications are based on a single tank. For a marine application, multiple tanks are likely needed, which will be assembled together in pods. This increases the gravimetric and volumetric specifications. The feasibility study for the SF-BREEZE found that the pods have a minor penalty for the gravimetric spec, but the volumetric spec became 2.28 times larger [147].

### Liquefied hydrogen storage

The alternative to compressed hydrogen storage is liquefied hydrogen storage. Due to the characteristics of hydrogen, liquefied storage is done at a temperature below 20 to 30 Kelvin [15]. As the temperature difference between liquid hydrogen and ambient air could become as high as 290 Kelvin in summer, it is crucial to minimize heat transfer. Therefore, most liquid hydrogen tanks have a spherical or cylindrical shape to minimize the surface-to-volume ratio. It is estimated that around one-third of the stored hydrogen energy is needed to operate the cooling system that keeps the hydrogen in a liquid state [15].

In a liquid hydrogen tank, some hydrogen evaporates due to the heat exchange, causing an increase in pressure. If the hydrogen gas is not used by the fuel cells, it is usually released into the atmosphere using a blow-off valve. However, a zero-emission ferry has a predictable hydrogen demand, which means the bunkering of hydrogen can be planned, and this situation can be avoided. Besides, the evaporation problem is less severe for larger tanks, as the amount of hydrogen stored scales with tank volume (i.e., cube of the tank radius for a spherical tank), while the heat exchange scales with the tank surface (i.e., square of the tank radius for a spherical tank).

One of the most significant benefits of storing hydrogen in liquid form is the increase in volumetric energy density. When cooled to  $-253\text{ }^{\circ}\text{C}$ , hydrogen has a density of  $70.8\text{ kg/m}^3$  (14.12 L/kg) [177]. To get a better understanding of the gravimetric and volumetric specifications of a liquid hydrogen tank, a DOT-approved tank of 1,200 kg capacity designed by Gardner Cryogenics will be used as a reference, as no other detailed specifications for mobile liquid hydrogen tanks have been found. The authors of the SF-BREEZE feasibility study obtained the LH2 tank's specifications during a discussion with Gardner Cryogenics [147]. The Gardner Cryogenics liquid hydrogen tank, which weighs 10,440 kg when empty and has an outer volume of 29,760 L, holds 1,200 kg of liquid hydrogen, of which 1,000 kg can be delivered to the fuel cells [147]. The tank has an empty mass of 10,440 kg, a gravimetric spec of 9.4 kg/kg (including the mass of the evaporator), and a volumetric spec of 24.8 L/kg [147]. A ferry using a liquid hydrogen tank could be refueled directly from a liquid hydrogen tanker similar to the one illustrated in figure 4.6, provided by a gas supplier in the area.



**Figure 4.6:** An example of a Gardner Cryogenics liquid hydrogen tanker [27]

From this, it can be concluded that a liquid hydrogen tank is likely to be the better choice than a compressed hydrogen tank for large hydrogen storage demands, at least from a technical perspective. The volumetric spec is roughly equal to that of the compressed hydrogen tank with the best volumetric spec, the Quantum 332L. However, when multiple Quantum 332L tanks are grouped into a complete system, the volumetric spec is expected to worsen. When comparing the gravimetric spec, we see that the 9.4 kg/kg of the liquid hydrogen tank is much more preferable than the 17.96 kg/kg of the Quantum 332L. The Quantum 936L comes close to this gravimetric spec, with 10.62 kg/kg. However, its volumetric spec is much higher, being 41.6 L/kg.

#### **4.2.5. Safety of using hydrogen as an energy source**

As mentioned earlier, hydrogen is the lightest of all atoms. While this is an advantage for the gravimetric energy density, it does make it hard to contain. Hydrogen ignites more quickly than natural gas and has a wider flammability range [59]. Therefore, the safety aspect is important to consider.

Designers of zero-emission hydrogen ferries will need to account for detonation risks in case of a leak in the hydrogen tank. Hydrogen tends to release into a room in a high-speed, jet-like way, resulting in a concentrated pocket of gas with a high risk of detonation. Luckily, the safety risk can be minimized by correctly placing fans, ventilation shafts, and detectors.

Real-world use cases prove that hydrogen-powered vehicles can live up to a high degree of safety. For instance, the same technology that powers the Ballard FCwave fuel cell is used in more than 3,000 fuel cell electric trucks and buses running in China, Europe, and North America [109].

Furthermore, a concept risk assessment study of a hydrogen-driven, high-speed passenger ferry estimated that the risk related to hydrogen systems is relatively low, both in operation and during mooring in the harbor overnight [3]. The study estimated the risk pertaining to hydrogen systems to be less than 0.01 fatalities per  $10^9$  passenger-km, which is much lower than the beforehand anticipated risk tolerance level of 0.5 to 1.0 fatalities per  $10^9$  passenger-km [3]. As a reference, the Institute of Transport Economics estimated an average of 0.6 fatalities per  $10^9$  passenger-km for ferries and fast passenger boats in 1970-1994 [3]. This would mean that a modern-day hydrogen ferry would be significantly safer than an older diesel-driven ferry.

Safety concerns may also appear due to the significant pressures typically associated with hydrogen storage on a vessel, especially when hydrogen is stored in a compressed state. These concerns are often unnecessary, as experiences have shown that the high pressures are typically manageable from a technical perspective [15]. Still, design precautions are necessary to protect the pressure tank in an accident. These design precautions can lead to hydrogen tanks with minimal risk of explosion, even under extreme conditions. For instance, the hydrogen tank manufacturer Doosan performs drop tests from 150m, penetration tests, fire tests, and internal pressure tests to ensure their tanks are safe for mobile applications [82].

### **4.3. Conclusion: the most suitable energy carriers**

The goal of this chapter was to find the most suitable emission-free energy carriers for the zero-emission CC-200 that are available now or in the coming five years.

Chapter 4.1 investigated multiple types of Li-ion batteries and compared them based on properties like energy density, costs and lifetime, safety, charging capabilities, and availability. It was concluded that Nickel Manganese Cobalt (NMC) or Lithium Titanate Oxide (LTO) batteries are likely to be the most suitable battery option for the zero-emission ferry. More specifically, the NMC-type XMP 98P module produced by Xalt Energy was selected as the most suitable commercially-available battery type. Its specifications will be used to test the technical feasibility of the zero-emission ferry in chapter 6.

Chapter 4.2 studied hydrogen fuel cells. It was concluded that a Proton Exchange Membrane (PEM) fuel cell would be the most suitable energy carrier due to its highest power output per given weight or volume, short start-up time, commercial availability, and possibility to operate on pure hydrogen. In terms of hydrogen storage, both compressed and liquid hydrogen tanks could be the feasible. However, it is expected that due to the large temperature difference between liquid hydrogen and ambient air, liquid hydrogen storage will be better for higher energy demands (i.e., larger tanks) as the stored hydrogen scales with tank volume, while the heat exchange scales with tank surface. Meanwhile, compressed hydrogen storage is expected to be the better option for lower energy demands, as smaller hydrogen tanks can be used effectively.

# 5

## Propulsion systems

This chapter covers the propulsion system of the zero-emission ferry. First, three identified propulsion systems - propellers, thrusters, and waterjets - will be compared, after which the most feasible propulsion system for the zero-emission hydrofoil ferry is chosen. The next subsection discusses the performance of the propulsion system and its implementation into the ferry and hydrofoil system. All in all, the goal is to answer the following sub-question:

*What is expected to be the most technically feasible propulsion system for a fast, emission-free ferry?*

### 5.1. Propellers, thrusters, and waterjets

A propulsion system transforms the electrical energy of the ferry's energy carrier into a thrust used to propel the vessel. This thesis has identified three possible parts of the propulsion system that could be feasible on a zero-emission hydrofoil ferry; propellers, thrusters, and waterjets. This subsection considers the advantages and disadvantages of these propulsion systems, after which a propulsion system for the ferry's concept design is selected.

#### 5.1.1. Propellers

Propellers are usually divided into two main groups, fixed pitch propellers (FPPs) and controllable pitch propellers (CPPs).

Fixed pitch propellers are manufactured in a single block. As the name implies, the propeller's pitch can not be altered. Ships that do not require good maneuverability are generally equipped with a FPP. The advantages of FPPs include low purchase and maintenance costs and high efficiencies compared to CPPs [65]. On the other hand, FPPs have the drawback that the engine must be stopped and reversed if the vessel has to decelerate or sail backward. If the vessel is powered by 4-stroke engines, which are not reversible, a gearbox is needed to reverse the direction of the propeller.

Controllable pitch propellers have a hydraulic mechanism in their hub that enables control of the propeller blades' pitch. This requires a larger and more complex hub, making CPPs three to four times more expensive compared to FPPs and lowering their efficiency by 1-2% compared to FPPs [16]. The main advantage of a CPP is that the engine can continuously operate at its optimum load or revolution speed, even at lower speeds.

For a fast, zero-emission ferry, it is expected that FPPs are the better choice for a number of reasons. First, FPPs achieve slightly higher efficiencies and, therefore, increase the likelihood of a technically feasible zero-emission ferry. On top of that, electric motors can run efficiently at a much broader load range compared to diesel engines. Electric motors are usually designed to run at 50% to 100% of the rated load, as their efficiency remains near the peak value for these loads [46]. This is shown in figure 5.1. Besides, electric motors can generally provide their maximum torque from a standstill. At last, FPPs are cheaper to buy and maintain, making the economics of the ferry more attractive.

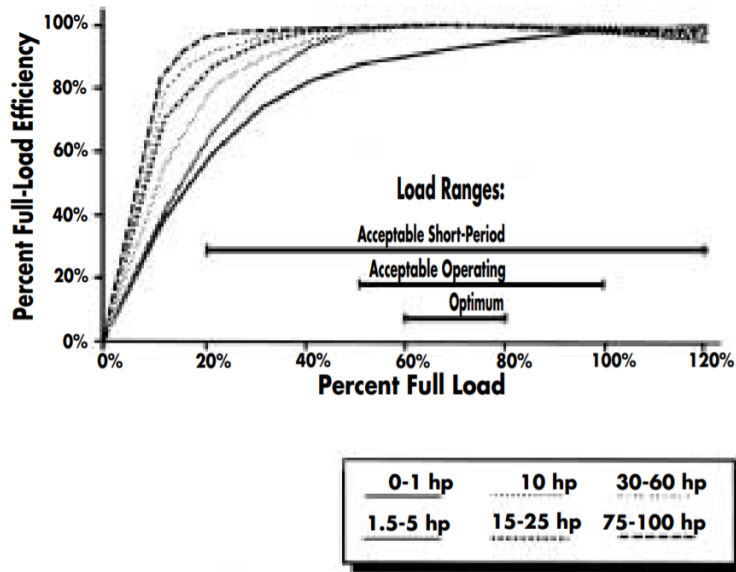


Figure 5.1: Electric motor part-load efficiency (as a function of % full-load efficiency) [46]

**Using propellers in combination with hydrofoils**

When a conventional ship is sailing, a boundary layer is created around its hull. Due to the boundary layer, the propeller water inflow, also known as the speed of advance ( $V_a$ ), is often lower than the ship speed ( $V$ ). This effect is accounted for with the wake coefficient ( $w$ ), which is the dimensionless expression of the difference between  $V_a$  and  $V$ :

$$w = \frac{V - V_A}{V} = 1 - \frac{V_A}{V} \tag{5.1}$$

When propellers are used in combination with a hydrofoil system, the wake coefficient of the propeller lowers as the distance between the hull and the propeller is increased. In fact, once the hull rises above the free water surface, it will not affect the propeller inflow. For the Foilcat hydrofoil ferry, which used propellers for its propulsion system, the wake coefficient was therefore deemed negligible [69]. This effect on the wake coefficient should be accounted for when modeling the propeller’s performance, as it can increase or decrease its efficiency, depending on the open water diagram. However, a study found that, in general, hydrofoil crafts have good flow conditions for propellers, making relatively high propulsive coefficients possible [24].

In terms of the design, an angled shaft can connect the propeller to an electric motor or engine on a hydrofoil ship. An illustration of this is given in figure 5.2.

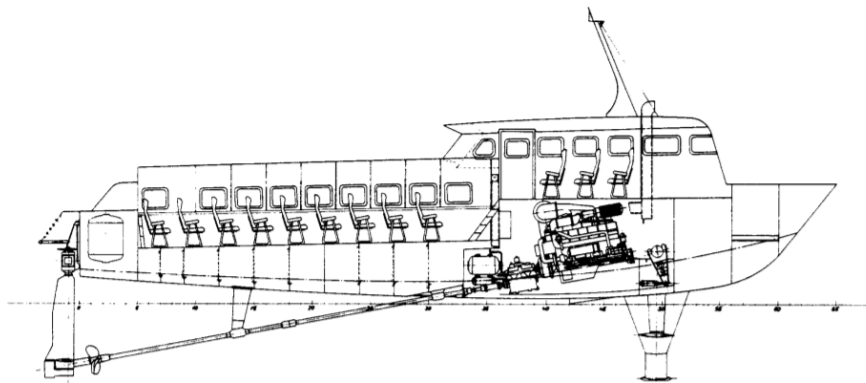


Figure 5.2: An example of a diesel-powered hydrofoil ship with an angled propeller shaft [114]

Unfortunately, several disadvantages are identified for this configuration. First of all, the propulsion system's efficiency is expected to decrease as the force delivered by the propeller is not directed straight aft, especially for larger angles. To keep the shaft angle as low as possible, the prime mover has to be placed far forward in the vessel, limiting the flexibility of its placement. Moreover, the relatively long propeller shaft and shaft bracket cause added weight and drag, which is not favorable for a zero-emission hydrofoil ship.

An alternative is to connect the prime mover to the propeller using a Z-drive or L-drive arrangement or by using "podded propulsors." However, in this thesis, it was chosen to define these propulsion systems as "thrusters," which are covered in the following subsection.

### 5.1.2. Thrusters

Thrusters are defined as propellers mounted to the prime mover using a Z-drive or L-drive arrangement or a prime mover located in a pod (so-called "podded propulsors"). Hydromaster is a Dutch manufacturer of various types of thrusters, such as the high-speed thruster illustrated in figure 5.3. The Hydromaster high-speed thruster is constructed from NACA profiles that achieve minimum drag for speeds between 28 and 30 knots. It is available in an L-drive or Z-drive configuration and features 360-degree steerability for increased maneuverability [77]. The thruster's stem section can be integrated into a carbon fiber hull, which is an advantage for the zero-emission CC-200 as it may use CFRP for its hull and superstructure.



Figure 5.3: A rendering of Hydromaster's high-speed thruster [77]

When deciding between a Z-drive or L-drive arrangement, the L-drive arrangement should be chosen if there is enough room in the vessel to mount the electric motor vertically. Else, a Z-drive can be chosen to allow the electric motor to be mounted horizontally, but this will introduce additional gear losses.

The main advantages of thrusters include that they are designed with electric motors in mind, have a compact design, generate low vibration and noise levels, and are highly adjustable to suit their application.

An alternative type of thruster is one where the electric motor is housed in a pod connected to the propeller. Such an arrangement is commonly referred to as a podded propulsor. However, it was found that podded propulsors are not suitable for a fast zero-emission ferry as they are usually designed to create high torques and propel larger vessels at relatively low speeds. As an example, the Azipod DZ980A (the smallest podded propulsor manufactured by ABB) has a power of 2.1 MW (roughly the same as the total propulsion power on the CC-200). However, it is designed for a service speed of 15 knots, which is significantly lower than the desired speed of 30 to 40 knots [14].

#### Using thrusters in combination with hydrofoils

Thrusters can be used in combination with a hydrofoil system, as proved by a number of real-life and concept designs. A real-life example of a thruster used with hydrofoils can be seen on the FHE-400

”Bras D’Or,” illustrated in figure 5.4. It features fully-submerged hydrofoils attached to vertical struts, which carry the Z-drive from the gas turbine to the supercavitating propellers aft of the hydrofoils [189]. Powered by a 16,549 kW gas turbine, the vessel could reach speeds of close to 60 knots in calm water [189].



**Figure 5.4:** The FHE-400 “Bras D’Or” [92]

A concept design example of thrusters used in combination with hydrofoils on a zero-emission hydrofoil ship can be found by looking at ARGO, a container ship designed by Boundary Layer Technologies [96]. When examining its propulsion system, it can be seen that the propellers are mounted at the level of the foils. They are connected to a Z-drive, leading to the electric motors placed inside the hull. The arrangement is illustrated in figure 5.5.

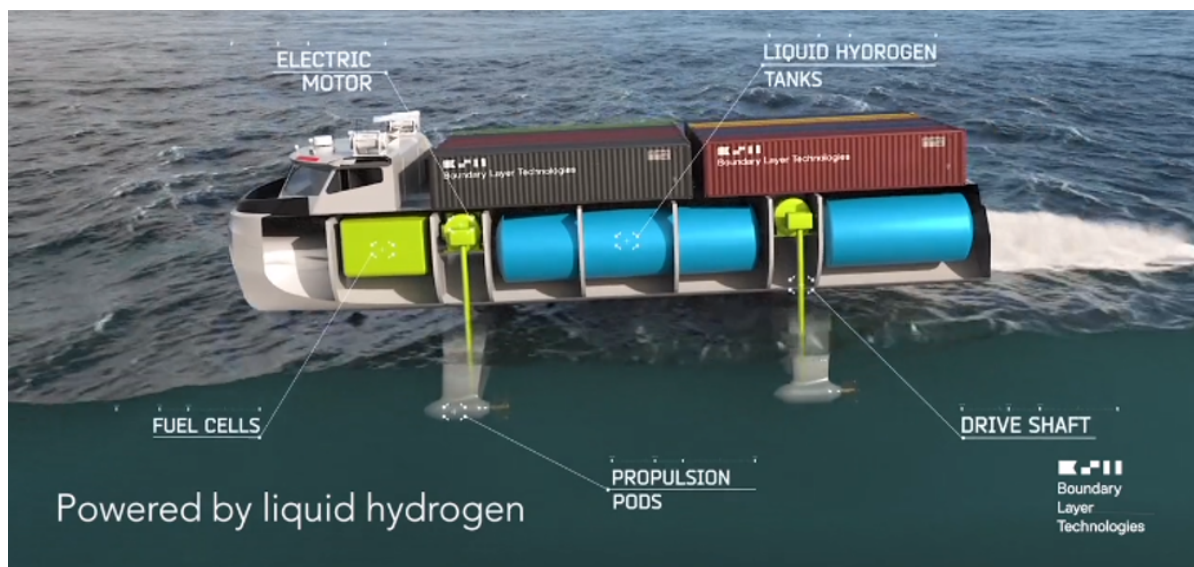


**Figure 5.5:** The propulsion system arrangement of Argo, a zero-emission hydrofoiling container ship [96]

As a last note, it was identified that most commercially-available thrusters would have to be adapted to achieve compatibility with a hydrofoil system. For one, the vertical shaft inside the thruster would have to be elongated due to the length of the hydrofoil struts. The components of the thruster and hydrofoils would also have to be designed so that the propeller shaft and other components would fit inside the hydrofoil strut profile. Moreover, it should be investigated how the bottom part of the thruster can be mounted to the bottom foils and if the thruster’s 360-degree steerability can be retained. Nevertheless, if the thruster lost its 360-degree steerability, the flaps on the hydrofoil system controlled

by the active control system could function as a rudder. In this thesis, it is assumed that this would provide sufficient maneuverability and all required modifications are technically feasible.

### 5.1.3. Waterjets

Traditionally, waterjets have been the propulsion system of choice for high-speed vessels. Generally, waterjets have superior propulsion efficiency at ship speeds above 25 to 30 knots [66].

The preference for using waterjets for high-speed applications can be seen when looking at various real-world fast catamaran ferries. For example, the 40-knot aluminum catamaran "Fast Ferry 4212" designed by Damen Shipyards uses four Kamewa waterjets for its propulsion system [53]. The "Blue Sea Jet," a 38-knot aluminum catamaran ferry operating in the Zhuhai region, also uses two Kamewa waterjets [158]. Even the case study ferry of this thesis, the CC-200, uses two MJP 650 CSU waterjets for its propulsion system [179].

A general configuration of a waterjet can be seen in figure 5.6. Waterjets generate thrust from the reaction force created by discharging a jet of water. The water flow is accelerated by the pump, which the primary mover drives through a shaft. Besides powering the pump, the primary mover must overcome hydraulic losses in the waterjet, inlet duct, and for the height difference and bends between the inlet and the pump.

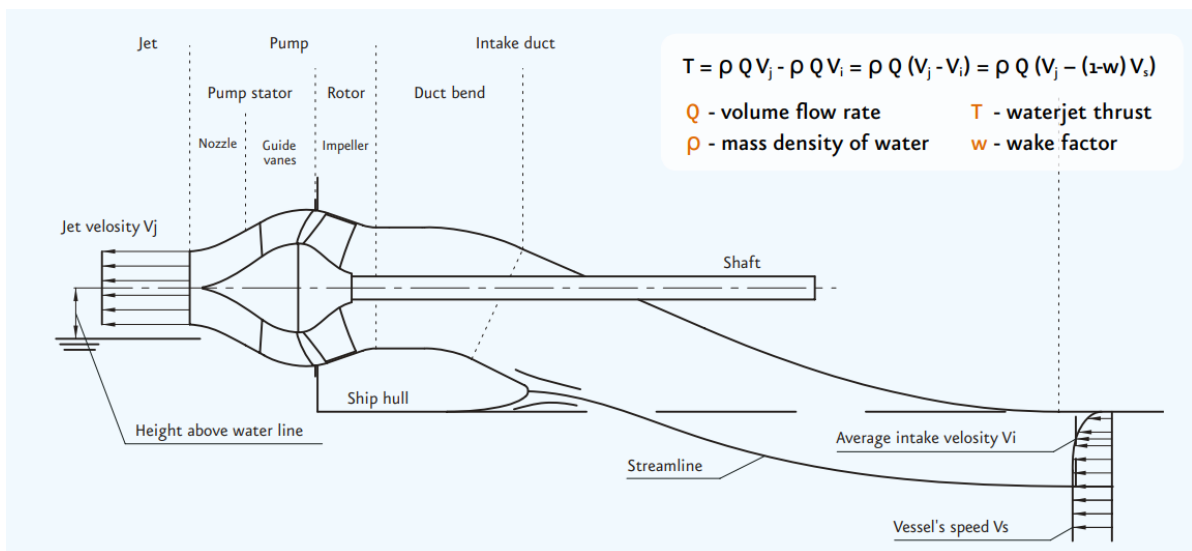


Figure 5.6: A general configuration of a waterjet [45]

An important advantage of waterjets is that cavitation is much easier to avoid for higher vessel speeds, avoiding damages, and increasing comfort [189]. Waterjets also have a relatively high power density, which allows for increased power outputs and small dimensions [66]. This is beneficial for a fast zero-emission ferry, as it allows more hydrogen or batteries to be stored on board the vessel, which increases the likelihood of a technically-feasible design. Lastly, waterjets emit little waterborne noise, which is advantageous for the marine environment near the vessel. Besides their lower efficiency at speeds below 30 knots, the main disadvantage of waterjets for non-hydrofoil, high-speed vessels is their high initial cost [113].

#### Using waterjets in combination with hydrofoils

Waterjets have been used in combination with hydrofoils in the past, as can be seen by looking at the configuration of the Jetfoil 929 (illustrated in figure 3.2). This 42-knot, 250-passenger ferry powered by gas turbines was operated near Hong Kong and was first launched in 1975 [189]. The configuration of the Jetfoil's waterjet propulsion system is illustrated in figure 5.7.

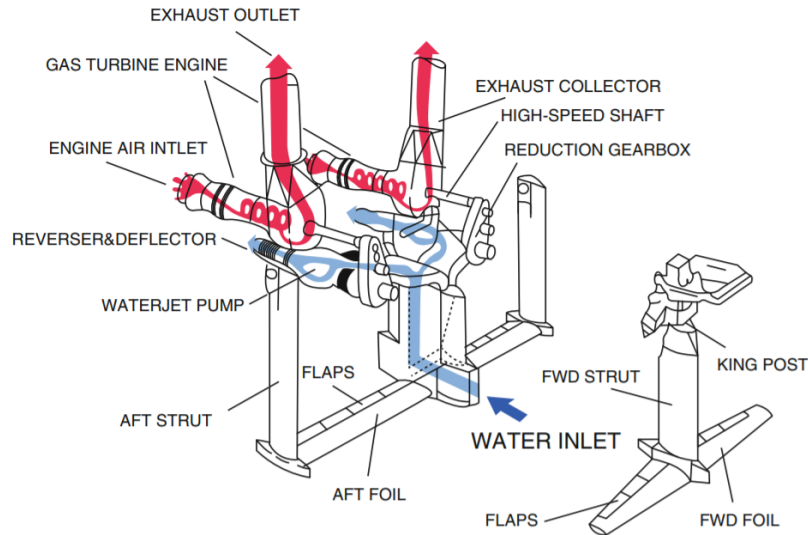


Figure 5.7: The waterjet propulsion system of the Jetfoil 929 [189]

For the zero-emission CC-200, a similar waterjet propulsion system could be designed. In comparison to the configuration of the Jetfoil 929, components related to the gas turbine engine (e.g., engine air inlet, exhaust outlet, exhaust collector) would be removed and components related to the electric motor would be added instead. Depending on the design choice, the electric motor could be placed and connected with a shaft in line with the waterjet pump for minimal mechanical losses, similar to figure 5.6.

While it is feasible to implement waterjets in combination with hydrofoils from a design perspective, it does introduce a set of technical challenges. As partly discussed in chapter 3.2, one of the challenges is the waterjet intake placement, usually located near the bottom of the hull. This configuration will not work for a hydrofoil ship as the hull rises out of the water at higher speeds. To fix this problem, the waterjet intake can be placed at the bottom of the aft struts, similar to the configuration of figure 5.7. Then, the water can be carried up through the struts into the hull and the waterjet pump, after which it is discharged from the aft of the vessel.

Unfortunately, additional challenges arise from this configuration. First of all, additional or thicker struts must be placed to allow for a high water flow. This increases the hydrofoil system's resistance and weight. Moreover, additional power is required to pump the seawater up through the struts due to the height difference and bends.

In appendix B.1, calculations have been made to estimate the additional power that would be needed to pump the seawater through the struts for the zero-emission CC-200. Due to the pressure loss caused by the strut height of 2.6 meters and two 90-degree bends, it was estimated that at 30 knots, the waterjets would require an additional power of around 536 kW (appendix B.1). For the CC-200, this equals to a power increase of 26.1% (appendix B.1).

The waterjet efficiency on the CC-200 is around 68% [179]. However, due to an increase in required power, the efficiency of a hydrofoil ferry will drop to around 53.9%, as shown by equation 5.2:

$$\eta_{waterjet,hydrofoils} = \frac{\eta_{waterjet,nominal}}{P_{additional}} = \frac{68\%}{1.261} = 53.9\% \quad (5.2)$$

While the waterjet efficiency has already dropped significantly, it is expected that this is still an optimistic estimate. The estimated total resistance of 80 kN used in the calculation is based on the hydrofoil geometry discussed in chapter 3.2.2. However, the aft struts have a thickness lower than the required inlet diameter of 0.65 m. In other words, they would have to be thicker, increasing the hydrofoil system's resistance. Additionally, the weight of the seawater in the struts should be considered in the design. Using the inlet diameter, strut height, and the density of seawater, it was determined that the weight of the water in one strut would be around 884 kg, which also increases the ferry's resistance (appendix B.1).

Because of these results and the significantly higher efficiency of a propeller operating in the conditions experienced by the hydrofoil CC-200 (discussed in chapter 5.2.1), it is concluded that waterjets are not the most efficient option for a 30- to 40-knot, zero-emission, hydrofoil ferry. Therefore, they are eliminated as a possibility for the propulsion system.

It is expected that waterjets may have been feasible for the Jetfoil because of its higher sailing speed and installed power. At speeds above 40 knots, propellers can become significantly less efficient, and cavitation can become a problem. Meanwhile, waterjets remain efficient at these higher speeds and have fewer issues with cavitation. Moreover, the additional required power needed to pump water up through the struts as a fraction of the total installed power may be smaller on the Jetfoil due to its significantly higher total installed power of 4,900 kW [189]. In that case, the reduction of the waterjet's efficiency would be less severe.

#### **5.1.4. Conclusion: propellers, thrusters, and waterjets**

This thesis has identified three main categories of propulsion systems that could be used for a fast, emission-free ferry. These include propellers, thrusters, and waterjets.

Waterjets are traditionally the propulsion system of choice for high-speed vessels. They provide a low risk of cavitation, have a relatively high power density, and emit little waterborne noise. However, using waterjets with a hydrofoil system would significantly lower their efficiency due to the pressure loss caused by the seawater that would have to be pumped through two 90-degree bends and a strut of 2.6 meters in height. Moreover, waterjets come with high initial costs. Therefore, it has been chosen to eliminate waterjets as a possible propulsion system for the zero-emission CC-200.

Thus, propellers and thrusters are left. When comparing these, the advantage of a propeller may be that it is cheaper. However, it comes with a significant set of disadvantages when combined with a hydrofoil system. First, additional support struts are required for the propeller shaft, which increases resistance and weight. Secondly, the propeller shaft should be designed to be as parallel as possible to the water surface. Therefore, it would be a long shaft, increasing resistance, weight, vibrations, and limiting the flexibility in the placement of the prime mover. Lastly, the propeller shaft is not likely to be perfectly parallel with the water surface, which means its generated force is not directed straight aft, decreasing its efficiency.

On the other hand, propellers mounted to L-drive or Z-drive thrusters provide a solution to some of these disadvantages. The thruster's propulsion shaft can be designed to be inside the struts, which does not cause a significant resistance, vibration, or weight increase. Besides, many thrusters have also been designed with electric motors in mind, which is an advantage for the zero-emission CC-200. Although most commercially available thrusters are designed for lower service speeds and are not plug-and-play compatible with hydrofoil ships, it is expected that modifications can be made to overcome these challenges, like mounting a custom propeller or electric motor, elongating the propulsion shaft, or eliminating the 360-degree steerability feature by fixing the bottom part of the thruster to the foils. For these reasons, thrusters are chosen as the propulsion system for the zero-emission CC-200 and are studied in more detail in the following chapter.

## **5.2. The design of thrusters mounted to a hydrofoil system**

This chapter investigates the design and performance of thrusters mounted to a hydrofoil system on the zero-emission CC-200. First, chapter 5.2.1 evaluates the propeller performance for various operating conditions relevant to the zero-emission ferry. Next, the interaction between the foils and the thruster is discussed in chapter 5.2.2. At last, a selection of electric motors and gearboxes for the zero-emission ferry is chosen in chapter 5.2.3.

### **5.2.1. The thruster's propeller performance**

Like a traditional propeller arrangement, a thruster also uses a propeller to transform the torque of the prime mover into a thrust. As discussed in chapter 5.1.1, it is expected that fixed pitch propellers are a better choice for a zero-emission hydrofoil ferry compared to controllable pitch propellers. Therefore, this section investigates the performance of a fixed pitch propeller mounted to a thruster on a hydrofoil ferry.

In this thesis, it was chosen to use a propeller from the Wageningen B-series propeller database, as their open water characteristics are known and validated. From the results of this chapter, it was found

that for the speed range of 30 to 40 knots, a Wageningen B-series propeller with the right diameter, pitch-diameter ratio, and blade area ratio can avoid cavitation and reach relatively high efficiencies. With the help of open water diagrams, thrust coefficients ( $K_T$ ), torque coefficients ( $K_Q$ ), and open water efficiencies are obtained based on the propeller's number of blades, the blade area ratio, the pitch-diameter ratio, and the advance coefficient ( $J$ ), where

$$K_T = \frac{T}{\rho \cdot n^2 \cdot D^4} \quad K_Q = \frac{Q}{\rho \cdot n^2 \cdot D^5} \quad J = \frac{V_A}{n \cdot D} \quad (5.3)$$

The computer program PropCalc, short for "Propeller Calculation," was used in this thesis to evaluate the open water characteristics of the used propeller [87]. PropCalc is a program created by Harm v. Keimpema and maintained by Erik Ulijn, who works as a teacher of the Ship Design, Production & Operations department at the Delft University of Technology [87]. The tool is based on publications of MARIN and reports of A.P. de Zwaan [87]. Using an optimization method based on a known velocity, thrust, and propeller diameter, PropCalc searches for the optimal open water efficiency configuration and displays the estimated or required thrust coefficient, torque coefficient, pitch-diameter ratio, and more. An example of a result is illustrated in figure 5.8:

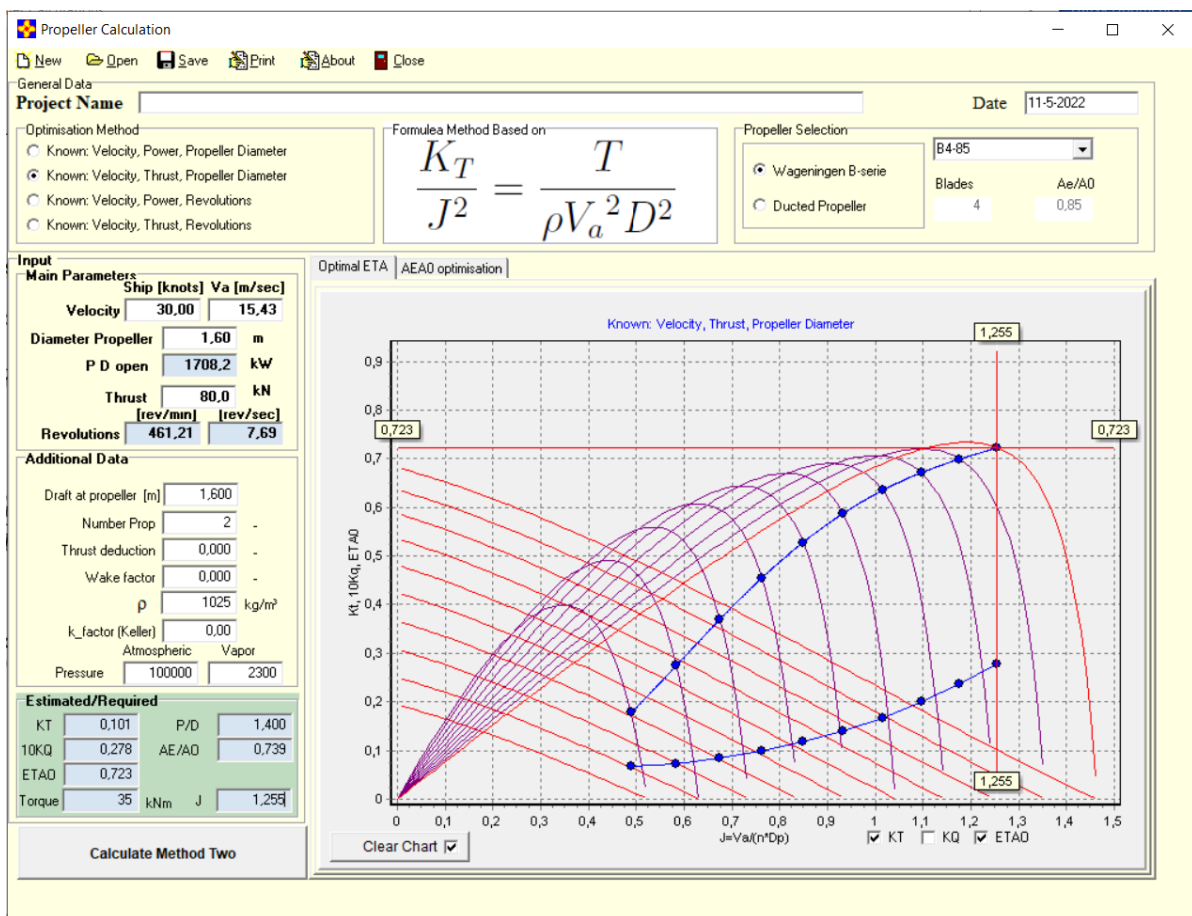


Figure 5.8: Example of a result from PropCalc [87]

The following list of inputs for PropCalc was used based on the operating conditions for the zero-emission CC-200:

- **Number of blades = 4.** It was assumed the propeller would have four blades, as it is one of the most common configurations. On top of that, the Candela-P30 hydrofoil ferry also uses a four-bladed propeller [153].
- **Blade area ratio (Ae/Ao) = 0.85.** Based on PropCalc experiments, the blade area ratio was chosen to be 0.85 to avoid cavitation based on Keller's constraint [137]. It was observed that the

propeller could be more efficient at operational speed with a lower blade area ratio. However, a blade area ratio of at least 0.85 was required to avoid cavitation at the ferry's resistance hump.

- **Velocity = [30 - 40] knots.** For the operating speed condition, the velocity was varied between 30 and 40 knots with a step size of 2 knots. Meanwhile, it was set to 22 knots for the resistance hump condition, based on the results of chapter 3.2.
- **Diameter propeller = 1.6 m.** In general, the propeller diameter should be as large as possible to achieve the highest efficiency [16]. For the zero-emission ferry, the maximum propeller diameter was assumed to be 1.6 meters, considering the nominal strut length below the water surface of 1.6 meters and clearances.
- **Thrust = [65 - 100] kN.** The total thrust of the ferry was assumed to equal the total resistance of the ferry, which could be estimated using the parametric model discussed in chapter 6 and the hydrofoil drag results from chapter 3.2. Depending on the velocity, values of the tested resistances lie between 65 and 100 kN.
- **Draft at propeller = 1.6 m.** The draft at the propeller was set to 1.6 meters, equal to the hydrofoil strut length below the free water surface (chapter 3.2.2).
- **Number of propellers = 2.** It was decided to use two propellers for increased redundancy and maneuverability, since the CC-200 also uses two waterjets.
- **Thrust deduction = 0.** In foilborne mode, the ferry's hull will not experience any additional resistance due to the propeller as it will be sailing above the water surface. Therefore, the thrust deduction coefficient was assumed to be 0.
- **Wake factor = 0.** In foilborne mode, the propellers operate in close to open water conditions as they do not experience any alterations in incoming flow due to the ship's hull. Therefore the wake factor is assumed to be negligible, just like on the Foilcat hydrofoil ferry [69].
- **rho.** The density of seawater, assumed to be  $1,025 \text{ kg/m}^3$ .
- **k\_factor (Keller) = 0.** The Keller correction factor, used for estimating the required blade area ratio, was assumed to be zero (normally for fast naval vessels) due to the relatively high sailing speed of the ferry [87].

Using the given inputs in the PropCalc tool, the propeller revolutions ( $n_{prop}$ ), thrust coefficients ( $K_T$ ), and torque coefficients ( $K_Q$ ) for various speeds and thrusts (based on the resistances) were acquired. The obtained data is listed in appendix B.2. As can be seen, the propeller revolutions range between 450.5 and 592.0 RPM, the thrust coefficients range between 0.064 and 0.11, and the torque coefficients range between 0.0202 and 0.0297. For a particular operating condition, these three values lead to the propeller torque using equation 5.4 and the delivered propeller power using equation 5.5. These equations are used in chapter 6 to select the appropriate electric motor and gearbox.

$$Q = K_Q \cdot \rho_{sw} \cdot D_{prop}^5 \cdot \left(\frac{n_{prop}}{60}\right)^2 \quad (5.4)$$

$$P_D = Q \cdot \pi \cdot \left(\frac{n_{prop}}{60}\right) \quad (5.5)$$

Additionally, the propeller revolutions, thrust coefficient, and torque coefficient data is used in the parametric model discussed in chapter 6 to assess the technical feasibility of the zero-emission ferry. From the results, it can be confirmed that the propeller's efficiency, which was found to be roughly 70% depending on the conditions, is significantly higher than the calculated waterjet efficiency of around 53.9% (chapter 5.1.3).

Besides the operational condition, propeller performance data at the resistance hump was also collected to find at which point the delivered power is highest. This is critical to know as the selected energy carrier and electric motors should be able to deliver this maximum power. Otherwise, the ferry might not be able to overcome the resistance hump or reach its desired operational speed.

For speeds of 30 to 40 knots and resistances at the resistance hump and foilborne conditions, estimated using the developed parametric model discussed in chapter 6, data of the propeller open water efficiency ( $\eta_O$ ) and delivered power ( $P_D$ ) is obtained from PropCalc and listed in table 5.1:

**Table 5.1:** Comparing the total resistance, open water efficiency, and delivered propeller power at hump and operational conditions

$V_{design}$ [knots]	$R_{hump}$ [kN]	$R_{op.}$ [kN]	$\eta_{O_{hump}}$ [-]	$\eta_{O_{op.}}$ [-]	$P_{D_{hump}}$ [kW]	$P_{D_{op.}}$ [kW]
30	90.3	78.9	0.728	0.722	1,448	1,687
32	92.1	81.3	0.728	0.716	1,485	1,871
34	92.4	82.0	0.728	0.706	1,490	2,031
36	94.6	85.3	0.727	0.699	1,534	2,260
38	97.9	90.0	0.726	0.693	1,602	2,539
40	100.1	94.1	0.726	0.687	1,647	2,821

From table 5.1, it can be observed that the resistance at the hump is expected to be higher than the resistance at operational speed for all design speeds. However, the delivered propeller power at operational speed is higher than the delivered propeller power at the hump speed for all design speeds. This is mainly caused by the significantly higher propeller revolutions needed at the operational speed. If the speed of the ferry increases, the propeller has to spin faster to generate the same amount of thrust. Another reason contributing to the increased delivered power at the operational speed is the propeller's lower open water efficiency, as seen in table 5.1.

Because of these results, it is assumed in the rest of the thesis that the delivered power in the operational condition is larger than the delivered power at the resistance hump. The most significant impact of this assumption is that the electric motors and gearboxes discussed in chapter 5.2.3 are selected based on the delivered propeller power in the operational (foilborne) condition.

### 5.2.2. Foil-thruster mounting and interaction

As discussed in chapter 5.1.2, a modified Hydromaster high-speed thruster was selected for the zero-emission ferry. A rendering of a standard Hydromaster high-speed thruster is given in figure 5.3. The upper section of the thruster, starting from the white part, could be placed inside the ferry's hull and connected to a gearbox and electric motor. The propeller shaft could be elongated and fitted through the support struts of the hydrofoil system. The black section of the thruster could be integrated with the hydrofoil system. Due to the modifications and lack of room available in the struts and foils, it is expected that retaining the 360-degree steerability feature of the thruster would be a considerable challenge. Therefore, it is assumed that the black part of the thruster will be fixed to the hydrofoils, and the vessel would maneuver using its two independent propellers and flaps on the hydrofoil struts, which would also be used for the active control system needed for fully-submerged foils. This design choice is expected to be the most feasible, as moving masses are minimized, and the thruster could be mounted with fewer modifications.

Considering the selected Hydromaster thruster is designed with a pulling propeller in mind, the propellers of the zero-emission ferry will be placed upstream of the hydrofoils. In other words, the propellers will be mounted on the opposite side of the hydrofoils compared to the propulsion system of Argo, illustrated in figure 5.5.

The propellers of the thrusters will be operating in close proximity to the hydrofoils, so it is expected that the two will experience an interaction that was not accounted for in the propeller's open water characteristics discussed in chapter 5.2.1.

Research studying the effect of the wake structure of a propeller operating upstream of a hydrofoil found that due to the presence of a hydrofoil, the pressure field on the pressure side of the propeller blades is altered, resulting in a higher  $K_T$  and  $K_Q$  [145]. However, because  $K_T$  increases relatively more than  $K_Q$ , the efficiency of the propeller increases by 2.33 to 2.92% for the conditions tested by the researchers (based on varying propeller loads) [145]. The paper also found that the drag coefficient of a NACA hydrofoil rudder became lower as the suction generated by the propeller decreased the pressure component of the hydrofoil's drag [145].

To conclude, when a propeller operates upstream of a hydrofoil, the propeller efficiency may increase by up to 2.92%, and the hydrofoil drag may become lower. However, as no study has been found that researched the effect on the lift coefficient of a lifting hydrofoil when a propeller is operating upstream, an assumption was made that any potentially negative effects on the hydrofoil's lift coefficient are balanced by the increased propeller efficiency and reduced hydrofoil drag, resulting in no lift, drag, or efficiency changes for the propeller or hydrofoil compared to operating in open water conditions.

### 5.2.3. Electric motors and gearboxes

The zero-emission ferry's electric motors will provide power to the thrusters. To match the optimal revolutions of the electric motors to the revolutions of the propeller, gearboxes are needed. The zero-emission ferry's electric motors and gearboxes are selected based on the required brake power ( $P_B$ ). The required brake power is determined by dividing the delivered power ( $P_D$ ) by the efficiencies of the propeller shaft, DC-DC converter, DC-AC converter, gearbox, and electric motor, as seen in equation 6.9.

Once the required brake power is known, an electric motor and gearbox of the appropriate size can be chosen. It has been decided to use electric motors from a manufacturer called "The Switch," as they are built for marine applications and can be delivered with various certifications, including DNV [140] [141]. Additionally, the manufacturer offers electric motors for a wide range of power requirements and openly lists their specifications. An electric motor from The Switch is illustrated in figure 5.9:



Figure 5.9: An electric motor from The Switch [134]

The technical specifications of a selection of electric motors from The Switch are listed in appendix B.3. The electric motors have been selected based on their output power at 1,500 RPM, which ranges from 810 to 2,200 kW. The most suitable electric motor for the zero-emission ferry depends on its requirements (e.g., operational speed and range) and is chosen by the parametric model covered in chapter 6.

During this research, it was also investigated whether it is better to use a bigger, higher-torque electric motor without a gearbox or a smaller, lower-torque electric motor with a gearbox. As shown in table B.1, a rough number for the expected propeller revolutions is 500 RPM. The largest electric motor from The Switch's 500-series (Frame 500-18) can output 1,000 kW at 500 RPM and has a total weight of 8,230 kg [141]. Meanwhile, the smaller Frame 450-8 has an output power of 1,070 kW at 1,500 RPM and has a total weight of 3,880 kg [140]. As seen later in this subsection, the weight of an appropriate gearbox for the drivetrain is around 750 kg. Together with the (smaller) Frame 450-8 electric motor, the total weight would be around 4,630 kg, against 8,230 kg for the larger electric motor, which would not need a gearbox. Because of the lighter weight and the fact that the efficiency of the smaller and larger electric motor is almost identical, it was decided to design the propulsion system using a smaller electric motor in combination with a gearbox [140] [141].

The gearbox used in the zero-emission ferry will be chosen out of the gearbox catalog of ZF, which designs gearboxes for marine propulsion systems [151]. ZF uses four duty classifications for their gearboxes; pleasure, light, medium, or continuous duty. As covered in chapter 2.1, the zero-emission ferry sails for roughly one hour for each one-way trip and does this nine times per day. Moreover, the ferry is operational 350 days per year [58]. Therefore, the ferry is in operation for  $1 \cdot 9 \cdot 350 = 3,150$  hours per year. To conclude, the selected gearbox should have a medium duty classification, with an engine operating hours limit of 4,000 hours per year [151].

The specific gearbox should be chosen based on its range of possible gear ratios and power factor.

The power factor is a metric used to assess the maximum torque the gearbox can withstand and is measured in  $kW/RPM$ . Therefore, the minimum power factor for a particular maximum brake power at a corresponding rotational speed can be found using equation 5.6:

$$pf_{min} = \frac{P_{B_{max}}}{n_{motor}} \quad (5.6)$$

With:

- $pf_{min}$ , the minimum power factor of the selected gearbox [kW/RPM]
- $P_{B_{max}}$ , the maximum expected brake power of the ferry [kW]
- $n_{motor}$ , the rotational speed at which the electric motor achieves the expected maximum brake power [RPM]

A list of the selected gearboxes that may be used for the zero-emission ferry and their technical specifications is listed in appendix B.3. The final selection will take place using the parametric model developed in this thesis, discussed in chapter 6.

#### 5.2.4. Conclusion: the design of a thruster mounted to a hydrofoil system

Chapter 5.2 researched the design and performance of a thruster propulsion system mounted to a hydrofoil ferry. By analyzing the performance of the thruster's propeller for various operating conditions using the PropCalc Tool, it was found that the propeller's efficiency at the operating speed would be roughly 70%. This confirms the hypothesis that the calculated waterjet efficiency of around 53.9% (chapter 5.1.3) would be lower than the efficiency of a propeller for a hydrofoil ferry. The required delivered power at the resistance hump and at the operational speed was also evaluated and compared. Even though the total resistance at the hump is larger than at the operational speed, the delivered power at the hump is smaller than at the operational speed. This is mainly caused by higher propeller revolutions needed to reach faster speeds, which increases the delivered power.

The interaction and mounting between the thruster and the hydrofoil were studied in chapter 5.2.2. It was assumed that the modifications required to make a thruster and hydrofoil system compatible are technically feasible. Furthermore, it was found that when a propeller operates upstream of a hydrofoil, its efficiency may increase, and the hydrofoil drag may become lower. However, as no research has been found studying the effects on the hydrofoil lift in this situation, it was assumed that any potential adverse effects on the hydrofoil lift are compensated by the increased propeller efficiency and decreased hydrofoil drag.

At last, chapter 5.2.3 identified a selection of electric motors and gearboxes that could be used by the zero-emission ferry. A number of electric motors from a manufacturer called "The Switch" were selected. It was also found that a smaller, lower-torque electric motor paired with a gearbox is significantly lighter than a bigger, higher-torque electric motor operating without a gearbox. Therefore, several gearboxes from the manufacturer ZF that could be used for the zero-emission ferry have been identified based on the gearboxes' classification, gear ratio, and power factor.

# 6

## Modeling the technical feasibility of a zero-emission ferry

This chapter focuses on modeling the technical feasibility of a zero-emission ferry and answering the following sub-question:

*How can the technical feasibility of a 200-passenger, 30- to 40-knot, emission-free ferry be determined?*

To determine the technical feasibility of a 200-passenger, 30- to 40-knot, emission-free ferry, a parametric model is developed. The model takes a set of inputs, including the required operating speed and range, and gives a conclusion on the technical feasibility of the ferry as an output, along with details like the best energy carrier to use and the ferry's energy consumption. Chapters 6.1 and 6.2 give an overview of all elements of the parametric model, while chapter 6.3 discusses the results of the parametric model.

### 6.1. Parametric model flowchart

The flowchart illustrated in figure 6.1 represents a simplified overview of the main parts of the developed parametric model and their interactions with each other. In the parametric model, a loop structure is applied as it starts with the "Weight calculation" block, which uses outcomes (e.g., mass of the energy carrier, hydrofoil system, and propulsion system) that are determined in a later stage of the model.

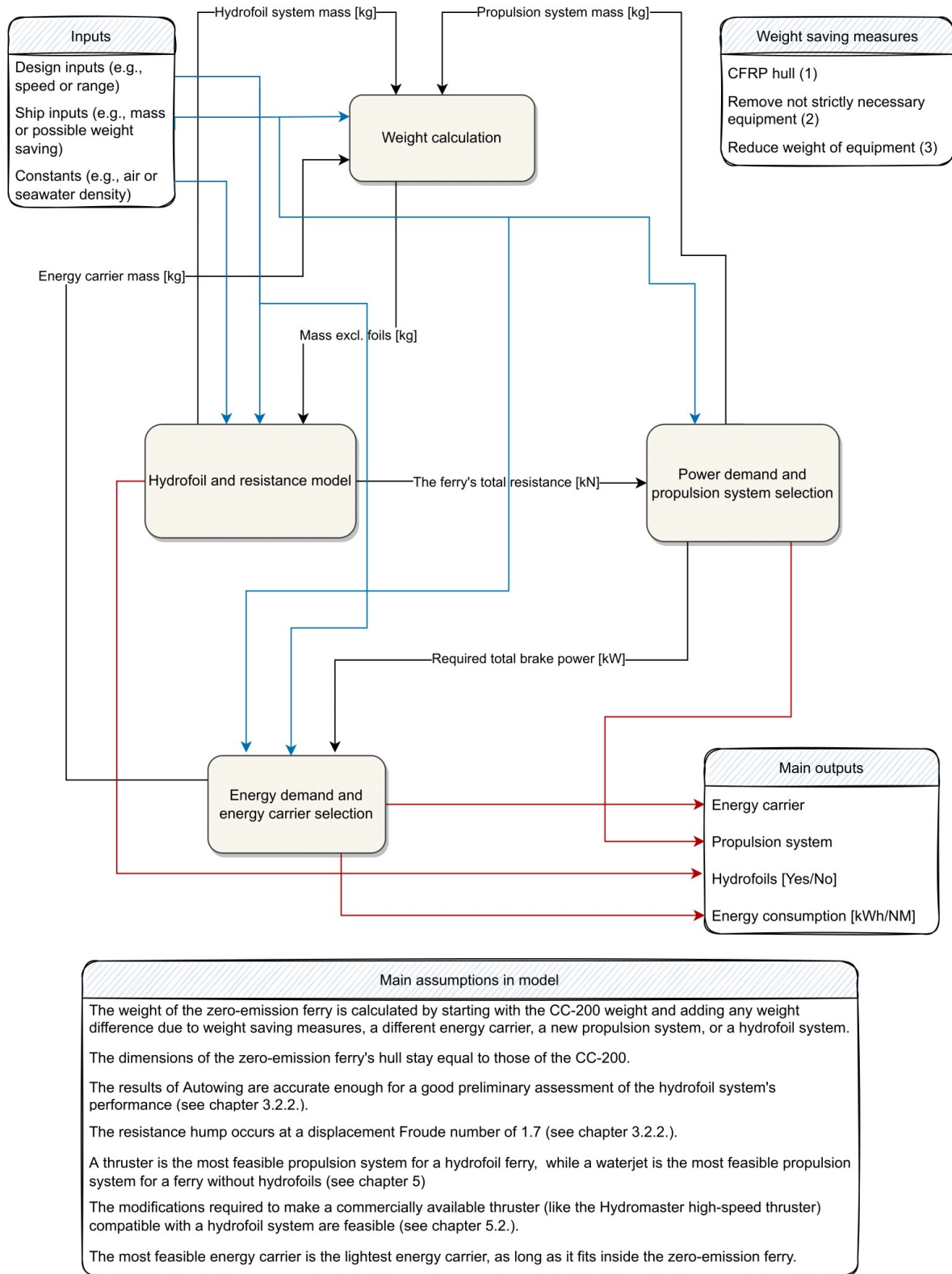


Figure 6.1: A flowchart of the developed parametric model

For a more thorough understanding of the methods, working principles, and loop structures of the parametric model, it is recommended to look at the model's pseudocode (appendix C.2) or the details of the parametric model discussed in chapter 6.2.

## 6.2. Details of the parametric model

This section discusses the main parts of the developed parametric model, being the:

- Inputs
- Weight calculation
- Hydrofoil and resistance model
- Power demand and propulsion system selection
- Energy demand and energy carrier selection

### 6.2.1. Inputs

The parametric model requires a number of inputs to run. The most important inputs are the design inputs, listed below. These consist of the design choices for the zero-emission ferry. The complete list of inputs (including ship inputs and constants) is listed in appendix C.1.

- **Design velocity [knots]**. The ferry's design velocity in knots. Valid values are 30, 32, 34, 36, 38, and 40, as per the available hydrofoil resistance data and the research question of this thesis.
- **Required range [NM]**. The ferry's required range in nautical miles.
- **Use of composites [-]**. Choice to enable a weight saving by the use of composites for the hull and superstructure.
- **Remove unnecessary items [-]**. Choice to enable a weight saving by removing unnecessary items.
- **Reduce weight of items [-]**. Choice to enable a weight saving by reducing the weight of currently-equipped items.

### 6.2.2. Weight calculation

The parametric model calculates the weight of the zero-emission ferry (excluding hydrofoils) by taking the weight of the CC-200 as a reference, subtracting any saved weight from the removal of propulsion-related systems and weight-saving measures, and adding the weight of the new energy carrier and propulsion system. This is illustrated by equation 6.1:

$$M_{excl.foils} = M_{CC200} - M_{CC200,pp} - M_{ws} + M_{ec} + M_{ps} \quad (6.1)$$

Where:

- $M_{excl.foils}$ , the mass of the CC-200 excluding the hydrofoil system [kg].
- $M_{CC200}$ , the maximum mass of the CC-200 [kg].
- $M_{CC200,pp}$ , the mass of the CC-200's propulsion-related systems [kg].
- $M_{ws}$ , the weight saving due to the selected measures [kg].
- $M_{ec}$ , the mass of the new energy carrier [kg], see chapter 4.
- $M_{ps}$ , the mass of the new propulsion system [kg], see chapter 6.2.4

Once the ferry's mass, excluding the hydrofoil system, is known, the hydrofoil system's mass can be estimated using the method described in chapter 3.2.2.

### 6.2.3. Hydrofoil and resistance model

In the model's part related to hydrofoils, the goal is to determine the difference in the ferry's resistance when hydrofoils are applied. The resistance of the hydrofoil ferry is found for both the operational speed and the resistance hump speed.

#### Hydrofoil and resistance model: operational speed

The total resistance of the hydrofoil ferry at operational speed consists of the resistance due to the hydrofoil system and the air resistance of the hull. Resistance data of the hydrofoil system has been collected using Autowing, as discussed in chapter 3.2.2. Using this data, a number of empirical relationships (equations A.4 till A.9) between the resistance of the hydrofoils and the mass of the ferry for

various speeds were created. These are used in the parametric model to determine the part of the total resistance caused by the foils.

The air resistance of the zero-emission ferry in foilborne mode is calculated using equation 6.2:

$$R_{air} = 0.5 \cdot \rho_{air} \cdot V_{air}^2 \cdot A_{frontal} \cdot C_{AA} \quad (6.2)$$

With:

- $R_{air}$ , air resistance [N].
- $\rho_{air}$ , air density [ $kg/m^3$ ].
- $V_{air}$ , air velocity [m/s], assumed equal to the ferry's speed.
- $A_{frontal}$ , frontal area of the ferry [ $m^2$ ].
- $C_{AA}$ , the ferry's air resistance coefficient [-].

The total resistance of the zero-emission hydrofoil ferry at operational speed is assumed to be the sum of the hydrofoil resistance and the air resistance.

### Hydrofoil and resistance model: resistance hump

The total resistance of the ferry at the resistance hump consists of the resistance due to the hydrofoil system and the residual, frictional, and air resistance of the hull. The methods and results of determining the hydrofoil resistance at the hump are described in chapter 3.2.2.

Additionally, the frictional and residual resistance coefficients must be found to determine the frictional and residual resistance of the ferry. The frictional resistance coefficient can be found using the ITTC-1957 formula, displayed in equation 6.3:

$$C_F = \frac{0.075}{(\log_{10} Rn - 2)^2} \quad (6.3)$$

With:

- $C_F$ , the frictional resistance coefficient [-]
- $Rn$ , the Reynolds number [-]

For the residual resistance coefficient, a method specific to the Coastal Cruiser series developed by Moreno Francis was used [58]. From his analysis, Moreno Francis concluded that:

- For the same family of catamarans, the residual resistance coefficient can be estimated with high enough accuracy based on one demi-hull parameter, the slenderness.
- A reasonable estimation of the residual resistance coefficient can be obtained using an exponential equation.
- An optimized hull form (e.g., the CC-200 hull) has a lower residual resistance coefficient compared to the results of the two studied systematic demi-hull series in Francis' research.

Using a number of chosen data points, two exponential functions for the residual resistance coefficient at a Froude number of 0.7 and 0.8 were formed by Moreno Francis [58]:

$$\begin{aligned} C_{R.7} \cdot 1,000 &= 0.43 + 115 \cdot \exp\left(-0.48 \cdot L/\nabla^{1/3}\right) \\ C_{R.8} \cdot 1,000 &= 0.26 + 90 \cdot \exp\left(-0.47 \cdot L/\nabla^{1/3}\right) \end{aligned} \quad (6.4)$$

With:

- $C_{R.7}$ , the residual resistance coefficient at a Froude number of 0.7 [-].
- $C_{R.8}$ , the residual resistance coefficient at a Froude number of 0.8 [-].
- $L$ , Length of the ship [m].
- $\nabla$ , the displacement volume of one demi-hull of the catamaran [ $m^3$ ].

These equations can then be interpolated or extrapolated over the ship's velocity to obtain the residual resistance coefficient at a specific speed [58]:

$$C_R = \frac{(V_{0.8}^{-2.8} - V^{-2.8}) \cdot C_{R,7} + (V^{-2.8} - V_{0.7}^{-2.8}) \cdot C_{R,8}}{V_{0.8}^{-2.8} - V_{0.7}^{-2.8}} \quad (6.5)$$

With:

- $C_R$ , the residual resistance coefficient [-].
- $V$ , the studied velocity of the ship [m/s].
- $V_{0.7}$ , the ship velocity at a Froude number of 0.7 [m/s].
- $V_{0.8}$ , the ship velocity at a Froude number of 0.8 [m/s].

Next, the wetted surface area of the vessel ( $S$ ) must be estimated, which can be done by equation 6.6, also found by Moreno Francis for the Coastal Cruiser series [58]:

$$S = 0.78 \cdot L \cdot \nabla^{1/3} + 8.2 \cdot \nabla^{2/3} \quad (6.6)$$

Note that for the resistance hump calculation, the demi-hull displacement volume is lower compared to a ferry without foils due to the lift of the hydrofoil system. As such, the wetted surface area becomes lower. This is accounted for in the parametric model.

Once the frictional coefficient, residual coefficient, and wetted surface area are known, the resistance caused by the interaction of the hull with the seawater can be calculated using equation 6.7:

$$R_{hull} = (C_F + C_R) \cdot 0.5 \cdot \rho_{sw} \cdot V^2 \cdot S \quad (6.7)$$

Now, the air resistance must be added using equation 6.2. For the resistance hump calculation, a 25% margin is also added due to a possible increased resistance in operational sea states, as recommended by Odd. M. Faltinsen [52]. In the end, the total resistance of the hydrofoil ferry at the resistance hump is found using equation 6.8:

$$R_{tot,hump} = (R_{air,hump} + R_{foils,hump} + R_{hull,hump}) \cdot 1.25 \quad (6.8)$$

The method concerning the ferry's residual, frictional, and air resistance described above is also used in the parametric model to calculate the resistance of a zero-emission ferry sailing without hydrofoils at a speed of 30 to 40 knots. For this calculation, the differences with the resistance hump calculation include:

- A higher speed (30 to 40 knots).
- A demi-hull displacement volume based on the mass excluding foils and not corrected for the hydrofoil lift.
- At the operational speed, a smaller frontal area for the air resistance calculation, as part of the ferry's hull remains below the free water surface.

### Hydrofoil and resistance model: conclusion

Using the methods described above, the following resistances can now be found:

- The resistance of the zero-emission hydrofoil ferry at the operational speed.
- The resistance of the zero-emission hydrofoil ferry at the resistance hump.
- The resistance of the zero-emission ferry without hydrofoils at the operational speed.

By comparing these resistances, the parametric model can find if and by how much the hydrofoil system lowers the total resistance of the ferry. Additionally, the resistance at the hump of the hydrofoil ferry can be compared with the resistance at the operational speed. That way, it can be found whether or not the resistance at the hump is greater than the resistance at the operational speed, and if so, by how much. If the total resistance at the operational speed lowers in the case of a hydrofoil ferry, a hydrofoil system is applied by the parametric model, which means all further calculations are based on the hydrofoil ferry's resistance.

### 6.2.4. Power demand and propulsion system selection

The power demand and propulsion system selection part of the parametric model is used to determine the required brake power for the zero-emission ferry and select a feasible electric motor and gearbox. In chapter 5, it was found that it is more efficient to use thrusters instead of waterjets on a hydrofoil ferry. Therefore, if a hydrofoil system is applied, the parametric model uses the propeller open water characteristics for further calculations. If a hydrofoil system is not applied, it was assumed that a waterjet would be used as it is also applied on the CC-200. However, as it was found that the hydrofoil system lowers the resistance between 30 and 40 knots (chapter 6.3), the waterjet calculations in the parametric model were simplified assuming a propulsion efficiency of 68% and a system mass of 20 tonnes.

For the propeller calculations, the open water characteristics found using PropCalc for a range of velocities and resistances are used (table B.1). In the parametric model, a linear curve fit was applied to the data points, allowing it to find the propeller's open water characteristics at a particular speed and resistance.

Once the propeller open water characteristics are known, the propeller torque and delivered power are found using equations 5.4 and 5.5. The required brake power is then determined using equation 6.9:

$$P_B = \frac{P_D}{\eta_{shaft} \cdot \eta_{dcdc_{converter}} \cdot \eta_{dcac_{converter}} \cdot \eta_{gearbox} \cdot \eta_{emotor}} \quad (6.9)$$

With:

- $P_B$ , the total required brake power per electric motor [kW]
- $P_D$ , the delivered power per propeller [kW]
- $\eta_{shaft}$ , the shaft efficiency, assumed to be 95% (typical shaft efficiency of 97% and additional transmission gear losses of the Z-drive of two percentage points [147]).
- $\eta_{dcdc_{converter}}$ , the efficiency of the DC-DC converter, assumed to be 98% [58].
- $\eta_{dcac_{converter}}$ , the efficiency of the DC-AC converter, assumed to be 98% [58].
- $\eta_{gearbox}$ , the gearbox efficiency, assumed to be 98% [151].
- $\eta_{emotor}$ , the efficiency of the electric motor, assumed to be 97.2% [140] [141].

Once the required brake power is determined, an appropriate electric motor and gearbox can be selected from table B.2 and B.4. Using the specifications of the selected electric motors and gearboxes, the parametric model also checks if the electric motor can produce the required torque and if the gearbox can handle the torque (based on its power factor).

At last, the added masses of the propulsion system components should be accounted for. The weight of the Z-drive thruster was determined to be around 4,500 kg including the propeller after contact with Jan Terlouw, who works at Hydromaster Propulsion Systems. Lastly, the weights of the electric motors and gearboxes are listed in table B.2 and B.4.

### 6.2.5. Energy demand and energy carrier selection

The next part of the parametric model calculates the energy demand of the zero-emission ferry and selects an energy carrier based on the outcome. Based on the input of the required range, the operational time of the ferry is calculated. By multiplying the operational time with the total brake power, the energy demand in kWh is obtained. The total brake power also includes the hotel load, which was assumed to be 50 kW for the CC-200.

Next, the model compares the three possible choices for the energy carrier determined in chapter 4; batteries or fuel cells combined with a liquid or compressed hydrogen storage.

For the batteries, chapter 4.1 has selected the XMP 98P module as the most feasible option. As such, the specifications of the battery module are programmed in the model, allowing it to calculate the total mass and volume of the battery system, the maximum power output, and the minimum charge time.

Chapter 4.2 found either the Ballard FCwave or the PowerCell MS200 to be the most feasible option for a fuel cell-powered ferry. In the parametric model, it has been assumed that the Ballard FCwave would be the better option in combination with liquid hydrogen storage. The liquid hydrogen tank would likely be placed on the ferry's top deck for venting purposes, just like on the SF-BREEZE

[147]. Therefore, the volume inside the ferry is not critical, which directs to the Ballard FCwave being the better choice, as it is more optimized for its specific power [ $kW/kg$ ] than its power density [ $kW/m^3$ ]. Using the specifications of the fuel cell and liquid hydrogen tank, the parametric model calculates the total mass and volume of the energy carrier system as well as the total range of the ferry.

For the compressed hydrogen-powered ferry, the PowerCell MS200 was chosen to be the most feasible option. As was seen in chapter 4.2, the volume of the compressed hydrogen tanks quickly scales, especially considering they will be placed in a pod arrangement. Therefore, a fuel cell with a high power density [ $kW/m^3$ ] like the PowerCell MS200 is more favorable. Again, the parametric model calculates this energy carrier system's total mass, volume, and range.

To conclude, for a fuel cell-powered ferry, the parametric model studies both a compressed hydrogen-powered ferry using PowerCell MS200 fuel cells and a liquid hydrogen-powered ferry using Ballard FCwave fuel cells.

Now that the total mass and volume of the three energy carriers are determined, the parametric model can make a conclusion on the best energy carrier to use. The parametric model has been programmed to select the energy carrier that is both the lightest and most compact. In the situation that none of the three options are both the lightest and most compact, it was assumed that there is a preference for the lightest energy carrier, as long as it fits a certain volume constraint based on the available room inside the ferry.

### 6.3. Results of the parametric model

This chapter discusses the results of the developed parametric model studying the technical feasibility of a zero-emission ferry with the requirements set in chapter 2.2. Consequently, the following sub-question is answered:

*What combination of design choices in terms of the emission-free energy carrier, weight-saving measures, the hydrofoil system, or the propulsion system is expected to result in the most technically feasible zero-emission ferry configuration?*

#### 6.3.1. Designing a zero-emission ferry with minimal speed and range requirements

The results of the parametric model depend on its inputs. In this section, the inputs of the parametric model are based on the minimum speed and range requirements for the emission-free CC-200 as listed in chapter 2.2. The zero-emission ferry must reach a transit speed of 30 knots and have a range of 30 NM. In this experiment, the following inputs are used:

- Transit speed = 30 knots.
- Range = 30 NM.
- The weight saving resulting from the use of composites for the hull and superstructure of the CC-200 is enabled.
- The weight saving resulting from the removal of unnecessary items on the CC-200 is enabled.
- The weight saving resulting from the reduction in weight of currently-equipped items on the CC-200 is enabled.
- All ship inputs specific to the CC-200 as listed in appendix C.1.
- Constants, air, and seawater properties as listed in appendix C.1.

The main results of the parametric model are summarized in figure 6.2. Note that the images of the propulsion and energy carrier system components are for illustration purposes only and are not always an accurate representation of the actually required components.

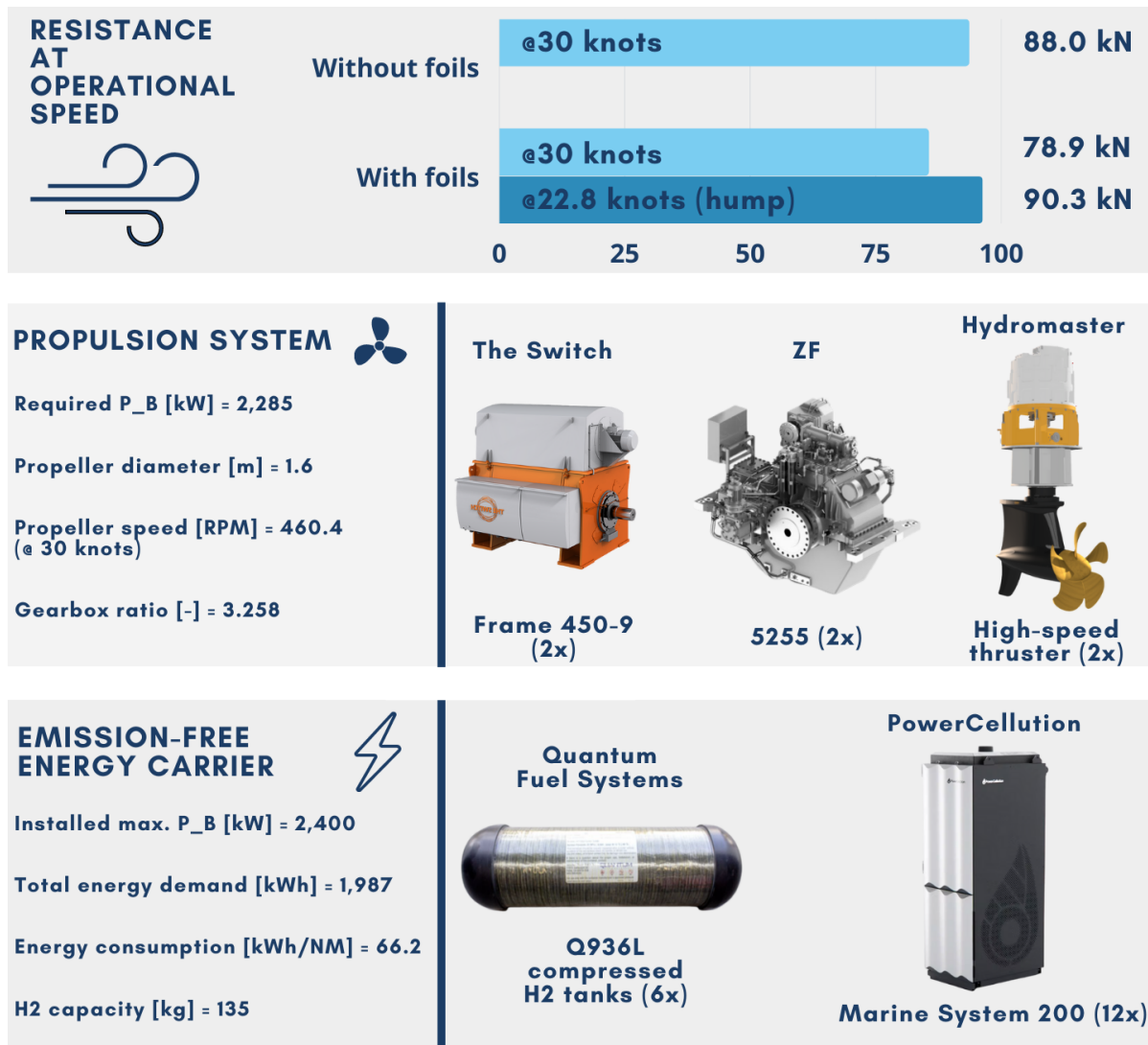


**Figure 6.2:** Overview of a technically-feasible, 30-knot zero-emission ferry with a range of 30 NM [134] [150] [77] [80] [108]

As can be seen, a hydrofoil system lowers the resistance of the zero-emission ferry by around 10 % at operational speed. The total mass of the zero-emission ferry would be around 120 tonnes, similar to the mass of the current CC-200. This shows that for the applied requirements, the zero-emission ferry would be heavier than the CC-200 if the lightest emission-free energy carrier would not have been chosen and the identified weight-saving measures would not have been applied. The required installed propulsion power for the ferry would be 2,285 kW, which is higher than the installed 2,160 kW on the CC-200, mainly due to a 15 % margin that is applied in the parametric model between the used brake power and required brake power [73].

It can be concluded that a zero-emission ferry with the aforementioned requirements is technically feasible. The zero-emission ferry would apply weight-saving measures, hydrofoils, a thruster propulsion system, and a compressed hydrogen energy carrier system to transport its passengers at a speed of 30 knots for a distance of 30 NM. In this configuration, the zero-emission ferry would have to be refueled with compressed hydrogen after every one-way trip, likely requiring a hydrogen refueling station to be built at the ports. Chapter 6.3.3 studies the limits of the compressed hydrogen-powered ferry to find if its range can be increased and the number of required refueling procedures can be lowered.

### 6.3.2. The impact of altering the required speed and range

The most important design inputs of the parametric model are the required speed and range. In the previous subsection, the model's results for a sailing speed of 30 knots and a range of 30 NM were discussed. However, the defined requirements of the zero-emission ferry state that it can have a sailing speed of up to 40 knots and a range of at least 30 NM. Therefore, the MATLAB code of the original parametric model was modified so that results could be plotted for an array of required input speeds and ranges. In this modified code, it has been assumed that a hydrofoil system will always lower the required power at operational speed, as the original parametric model found.

It is important to note that the plotted results illustrated in figures 6.3 till 6.6 are based on a ferry using a compressed hydrogen energy carrier. Using the parametric model, it was found that for an operational speed of 30 to 40 knots and a required range of 30 to 90 NM, the compressed hydrogen energy carrier is the lightest option and fits in the ferry at all times.

The results in this subsection have been obtained using the following design inputs:

- Transit speed = 30 to 40 knots, with a step size of 2 knots.
- Range = 30 to 90 NM, with a step size of 1 NM.
- The weight saving resulting from the use of composites for the hull and superstructure of the CC-200 is enabled.
- The weight saving resulting from the removal of unnecessary items on the CC-200 is enabled.
- The weight saving resulting from the reduction in weight of currently-equipped items on the CC-200 is enabled.
- All ship inputs specific to the CC-200 as listed in appendix C.1.
- Constants, air, and seawater properties as listed in appendix C.1.

First of all, figures 6.3 and 6.4 show how the zero-emission ferry's total mass and total used brake power depend on its required operational speed for three different range requirements.

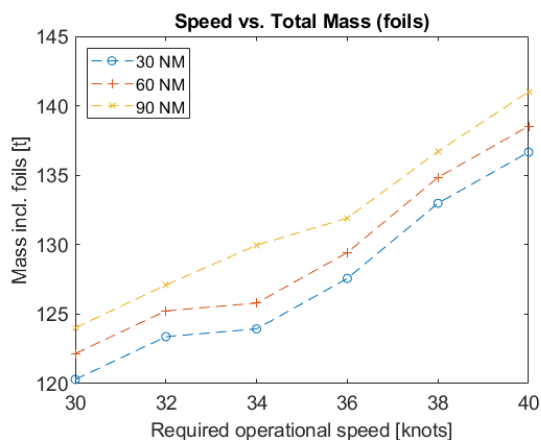


**Figure 6.3:** The zero-emission ferry's mass as a function of its required speed

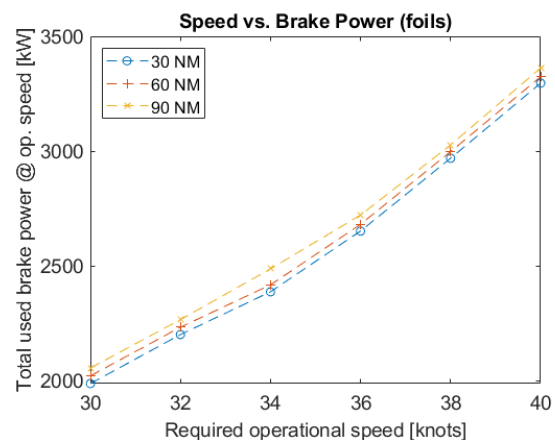


**Figure 6.4:** The zero-emission ferry's total used brake power as a function of its required speed

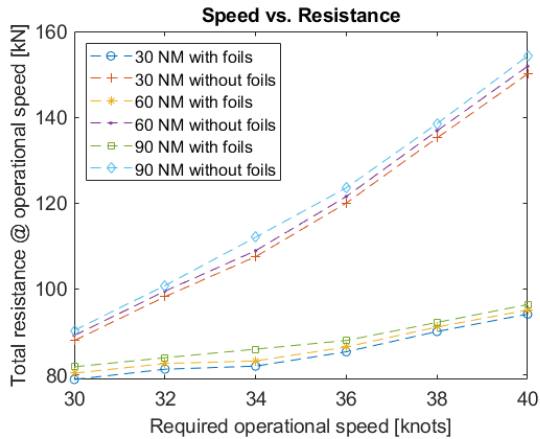
The results are in line with what can be expected. A higher operational speed requires a more powerful power plant, which increases the total used brake power. A more powerful power plant is also heavier as more fuel cells and larger electric motors are required. Therefore, the mass of the ferry increases. Moreover, a higher required range increases the required amount of hydrogen and hydrogen tanks, leading to a higher mass and brake power.

Figure 6.3 shows how the ferry's mass increases at higher required operational speeds. The added mass is mainly caused by fuel cell units added to the design. The zero-emission ferry is designed with symmetry in mind, so the number of required fuel cells is always an even number. In figure 6.3, the required number of fuel cells increases from 12 to 14 when going from 30 to 32 knots for the three tested ranges. Consequently, a sharper increase in the ferry's total mass is witnessed. Also, when looking at the 30 and 60 NM requirements, two additional fuel cells are required when going from 34 to

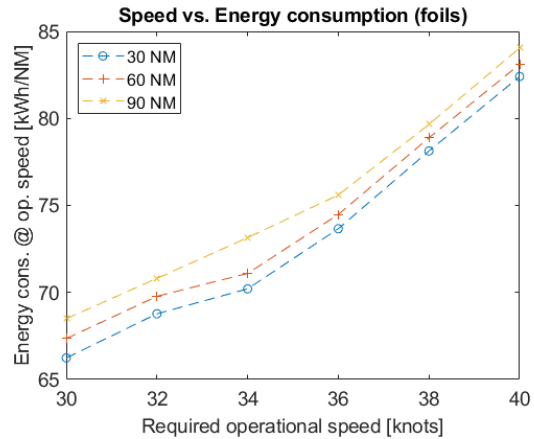
36 knots, but this is not yet required for the 90 NM requirement. This is why the lines of figure 6.3 do not follow the exact same pattern.

Figure 6.4 shows that a higher required speed does significantly increase the used brake power. The used brake power rises from around 2,000 kW at 30 knots to almost 3,400 kW at 40 knots. It is also concluded that increasing the required range has a much less significant impact on the used brake power. By increasing the required range, the most significant change is an increased number of required hydrogen and hydrogen tanks, causing only a slight increase in weight and therefore power.

Next, figures 6.5 and 6.6 show how the required operational speed and range affect the ferry's resistance and energy consumption.



**Figure 6.5:** The zero-emission ferry's total resistance as a function of its required operational speed

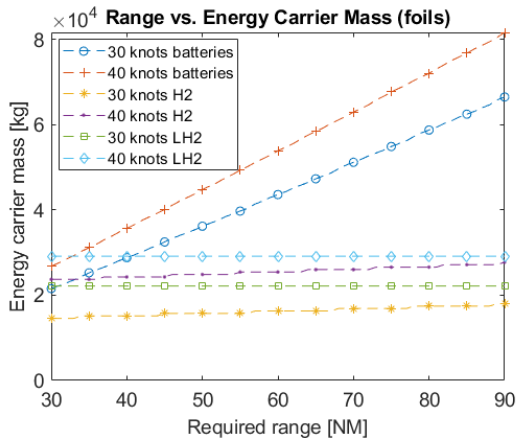


**Figure 6.6:** The zero-emission ferry's energy consumption as a function of its required operational speed

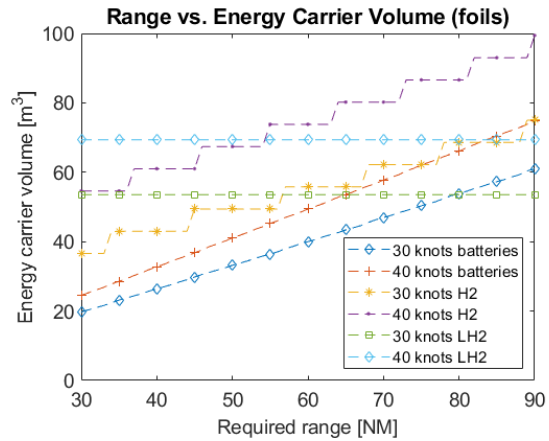
Figure 6.5 can be used to learn how the ferry's resistance changes by using hydrofoils or altering its range or speed. First of all, it is seen that a higher required range increases the ferry's resistance, as a higher range requirement results in a larger energy carrier system, which increases the ferry's weight and thus its resistance. However, this impact is relatively small, which was expected as the impact of increasing the required range on the brake power is also small, as was seen in figure 6.4. Next, it is concluded that a hydrofoil system lowers the ferry's resistance for the entire range of operational speeds. This difference is smallest at an operational speed of 30 knots and highest at 40 knots. In other words, the hydrofoil ferry's resistance increases relatively little when the operational speed is raised. This is one of the main reasons why some high-speed ships use hydrofoils.

Figure 6.6 shows the ferry's energy consumption as a function of the required speed. It shows similar characteristics as figure 6.4. As can be seen, the ferry's energy consumption ranges between roughly 66 kWh/NM at 30 knots and 84 kWh/NM at 40 knots. The energy consumption at 40 knots is slightly lower compared to the 150-passenger Electra hydrofoil ferry concept, which is expected to have an energy consumption of 90 kWh/NM at 40 knots [48]. On the other hand, the found energy consumption at 30 knots of 66 kWh/NM is significantly higher compared to the 150-passenger Beluga24 ferry concept, which promises a consumption of 30 kWh/NM at 30 knots [78].

The last two figures, figure 6.7 and 6.8, compare how the mass and volume of the three energy carrier options are affected by the speed and range requirements. The figures are created using a total ferry mass based on the mass of the compressed hydrogen energy carrier system for the listed range and speed requirements. In other words, the increased mass of the energy carrier system for higher ranges is not accounted for in the case of the battery- and LH<sub>2</sub>-powered ferries. As a result, it is important to note that, for example, the battery energy carrier mass would likely increase in a more exponential manner in reality. Still, the figures can be used to compare how the masses and volumes of the three energy carrier systems depend on the speed and range requirements.



**Figure 6.7:** The mass of the energy carrier system as a function of the required range



**Figure 6.8:** The volume of the energy carrier system as a function of the required range

Figure 6.7 shows the energy carrier system mass for a required range of 30 to 90 NM and a required speed of 30 or 40 knots. It shows that the compressed hydrogen energy carrier system is the lightest, especially at lower required speeds and ranges. As discussed in chapter 4.2, liquid hydrogen storage is most interesting for higher energy demands and larger storage tanks. The liquid hydrogen tank used in this analysis is rather large, and hydrogen itself is very light, so the mass of the liquid hydrogen energy carrier stays almost flat as the required range increases. Smaller liquid hydrogen tanks could be used too but may come with challenges such as a more significant energy loss due to the heat exchange and a more complex refueling system. Therefore, smaller liquid hydrogen tanks have not been considered in this thesis. At 40 knots and a required range of 90 NM, the mass of the compressed hydrogen system comes close to the mass of the liquid hydrogen system but does not transcend it. Last but not least, it can be seen that the mass of a battery system quickly increases at higher energy demands. Consequently, it can be concluded that a battery-powered ferry is not the most attractive for the studied range requirements if the goal is to minimize weight and, therefore, energy consumption.

At last, figure 6.8 is similar to figure 6.7 but compares the energy carrier's volume instead of its mass. It can be seen that the battery system scores much better on compactness than lightness as it is the most compact option below a required range of roughly 80 NM for a 30-knot ferry and around 83 NM for a 40-knot ferry. For higher ranges, it is observed that the liquid hydrogen system becomes the most compact. It can be seen that the volume of a compressed hydrogen energy carrier system is relatively high, especially for higher required ranges. So, although a compressed hydrogen system does have the advantage of low weight, it also shows a disadvantage in the form of a high volume.

### 6.3.3. Comparing a compressed hydrogen-, liquid hydrogen-, and battery-powered ferry

Chapter 6.3.1 and 6.3.2 inspected the best possible configuration for a specific range requirement. From the researched range requirements, the parametric model results led to the conclusion that a compressed hydrogen fuel cell system is the lightest and fits in the ferry. However, other energy carrier systems may be technically feasible too. They might not be the lightest but may have various technical or economic advantages compared to the compressed hydrogen configuration, which means it is important to study these configurations too. Therefore, this chapter will investigate the potential technical advantages of a compressed hydrogen-powered, liquid hydrogen-powered and battery-powered ferries.

First, a compressed hydrogen-powered ferry is studied. As illustrated by figures 6.7 and 6.8, the compressed hydrogen system is the lightest for the studied range requirements. Since a compressed hydrogen-powered ferry would have to be refueled more often compared to a liquid hydrogen-powered ferry, it would be advantageous to limit the required range to a value where the ferry could be refueled during the 30 minutes it spends in port. According to the Society of Automotive Engineers (SAE), compressed hydrogen tanks with a pressure of 350 bar can be refueled with a standard flow rate of 120 g/s [128]. Assuming time is needed to connect the ferry to a hydrogen refueling station and 20 minutes are available for refueling results in 144 kg of compressed hydrogen that could be refueled

during a stop. Using the parametric model, it was found that for a 30-knot ferry, a required range of 31 NM at most results in six required compressed hydrogen tanks, which would store 135 kg of hydrogen. Therefore, the range requirement of the compressed hydrogen-powered ferry is mainly limited by the refueling speed. A range requirement of 30 NM was chosen so that the compressed hydrogen-powered could be more easily compared with the battery-powered ferry, which will have the same speed and range requirements.

The second option is a liquid hydrogen-powered ferry. As found in chapter 4.2.4, a liquid hydrogen fuel cell system is most attractive when a relatively large hydrogen storage tank is used. This enables a better efficiency of the system due to a lower effective heat exchange, as the tank's surface-to-volume ratio is minimized. If the studied Gardner Cryogenics liquid hydrogen tank were installed on the zero-emission ferry, it could be attractive to fill it up as much as possible to increase the ferry's range and minimize the total required refueling procedures during a day of operation. Using the parametric model, it was found that a full LH2 tank would give a 30-knot zero-emission ferry a total range of 255 NM.

The final option is a battery-powered ferry. From figures 6.7 and 6.8, it can be concluded that a battery system is most attractive for lower range requirements as the system's mass and volume scale strongly when the range requirement is increased. Therefore, it is chosen to study a 30-knot battery-powered ferry with the lowest possible range requirement as determined in chapter 2.2, 30 NM.

The main specifications of the compressed hydrogen-, liquid hydrogen-, and battery-powered ferry are listed in table 6.1, in which the 'Speed' and 'Range' are input values for the parametric model. Besides the required speed and range inputs discussed above, all weight-saving measures have been enabled in the inputs, and the ship inputs and constants specific to the CC-200 were used, as listed in appendix C.1. The refueling time of the liquid hydrogen-powered ferry and CC-200 are not listed as they are not critical. At last, the mass and volume of the CC-200's energy carrier system are not listed due to the confidential nature of the information.

**Table 6.1:** Comparison of a compressed hydrogen-, liquid hydrogen-, and battery-powered ferry

	<b>CH2 + fuel cells</b>	<b>LH2 + fuel cells</b>	<b>Batteries</b>	<b>CC-200</b>
<i>Speed [knots]</i>	30	30	30	~30
<i>Range [NM]</i>	30	255	30	~420
Required refills per day [-]	9	1	9	1
Time in port [min]	30	30	30	30
Minimum refuel or recharge time [min]	20	N/A	18	N/A
Energy consumption [kWh/NM]	66	73	73	~80
Mass energy carrier system [t]	15	24	24	N/A
Volume energy carrier system [m <sup>3</sup> ]	37	58	22	N/A
Total mass [t]	120	131	131	~120

As found by the parametric model, all three ferry configurations comply with the minimum zero-emission ferry requirements and are thus technically feasible. From table 6.1, it can be concluded that the most technically-feasible ferry configuration depends on the preferences of the ferry's designer and operator, as each configuration has its (dis)advantages.

First, the compressed hydrogen-powered ferry is the lightest and therefore has the lowest energy consumption in kilowatt-hours per nautical mile. It has a range of 30 nautical miles, limited by the speed at which the hydrogen tanks can be refueled. Considering a single trip from Zhuhai to Shenzhen covers around 25 nautical miles, the compressed hydrogen tanks would be refueled every single-way trip, taking at least 20 minutes. The refueling procedure and logistics could be a disadvantage for the compressed hydrogen-powered ferry as a hydrogen refueling station will have to be built onshore at both ports, increasing costs.

The liquid hydrogen-powered ferry has a much higher range compared to the compressed hydrogen- and battery-powered ferry, being 255 NM. During an entire day of operation, the current CC-200 completes nine one-way trips on average and thus sails 225 NM [58]. Hence, the applied liquid hydrogen tank is sufficient to store enough liquid hydrogen needed for a whole day of operation. The liquid hydrogen-powered ferry can be operated by refueling it just once at the start of the day, which is a significant advantage compared to the compressed hydrogen- and battery-powered ferries. The refueling can be performed by a truck carrying a liquid hydrogen trailer, which would eliminate the need for

a hydrogen refueling station to be built onshore. The main downside of the liquid hydrogen-powered ferry is that a relatively large liquid hydrogen tank must be mounted on the top deck. Looking at the dimensions, the selected liquid hydrogen tank would fit on the top deck of the CC-200. However, additional structural reinforcements would be needed, which would increase the ferry's weight and therefore decrease its range. The mounting of the LH<sub>2</sub> tank may look similar to the LH<sub>2</sub> tank placement of the SF-BREEZE concept ferry, illustrated in figure 6.9 [147]. Additionally, the liquid hydrogen-powered ferry is the heaviest and therefore has the highest energy consumption.

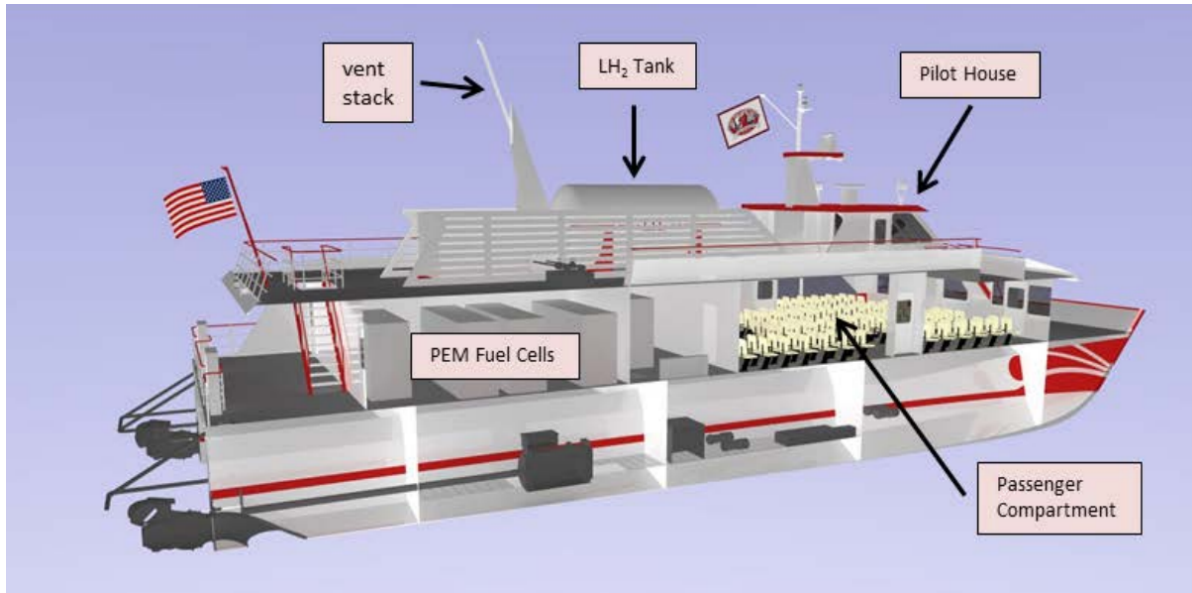


**Figure 6.9:** An engineering model of the SF-BREEZE, including the placement of its LH<sub>2</sub> tank [147]

At last, there is the option to use a battery-powered ferry. An advantage of the battery-powered ferry is that there is no requirement for the presence of a hydrogen supplier in the proximity of the ferry's port. However, there is a requirement for a suitable electricity grid and charging station. If enough power is available, the selected battery modules can be fully charged in 18 minutes. However, to minimize the load on the charging station, a time of 25 minutes is assumed for the charging procedure. Based on the ferry's energy consumption, it can be found that around 1,823 kWh of energy must be charged after a one-way trip. Together with the charging time, it would require a charging infrastructure that can charge at approximately 4.4 MW. In this thesis, it is assumed that this charging power is technically feasible, as other electric ferries like the MF Aurora (10.5 MW) and MS Color Hybrid (7 MW) charge at higher powers [86]. Besides, a company called Stemmman-Technik offers FerryCHARGER, which are various automated charging solutions for electric ferries with a charging power of up to 15 MW [56]. The FerryCHARGER, illustrated in figure 6.10, can connect to the ferry in 15 seconds, so the spare five minutes of non-charging time in port should be plenty to connect and disconnect the ferry between its trips [56].



Figure 6.10: The FerryCHARGER used to charge the electric, 400-passenger MF Suløy ferry [57]

Another advantage of the battery-powered ferry is that its required energy carrier volume ( $21.6 \text{ m}^3$ ) is much lower compared to both the compressed hydrogen ( $36.6 \text{ m}^3$ ) and liquid hydrogen ( $57.5 \text{ m}^3$ ) ferries. This frees up additional room inside the ferry, which could be used for various purposes, like increasing the passenger capacity or increasing the passenger's comfort by making the layout more spacious.

#### 6.3.4. The technical boundaries of a zero-emission ferry

In this subsection, the zero-emission ferry configurations found in chapter 6.3.3 are tested to find their technical boundaries. For operating speeds between 30 and 40 knots, the technical boundaries are found based on the following configurations:

- Optimized (hydrofoils and all weight-saving measures enabled)
- No foils (hydrofoils disabled)
- No WSM (all weight-saving measures disabled)
- No WSM + no foils (hydrofoils and all weight-saving measures disabled)

The technical boundaries of the ferries are assumed to be reached at one of the following limits:

- **Mass  $\geq 150$  tonnes.** If this limit is exceeded, it is assumed that the ferry becomes too heavy, as no hydrofoil lift and drag data are collected for a lift greater than 150 tonnes. It is chosen not to make this limit foil-specific to prevent a skewed comparison between a normal and hydrofoil ferry.
- **Total resistance  $\geq 105$  kN (foil-specific).** If this limit is exceeded, no data relevant to the propeller calculations was collected, which means results start becoming inaccurate. This limit is foil-specific as the ferry without hydrofoils uses a waterjet propulsion system.
- **Total brake power  $\geq 4,400$  kW.** Above this point, the most potent electric motors and gearboxes selected for the ferry are not powerful enough to comply with the ferry's power demand.
- **Energy carrier volume  $\geq 100 \text{ m}^3$ .** If this limit is exceeded, it is estimated that the energy carrier will not fit onboard the ferry.
- **Required charging power  $\geq 11$  MW (battery-specific).** This charging power is the limit of the Tower-type FerryCHARGER charging station [56]. The required charging power is based on a charging time of 25 minutes and a one-way sailing distance of 25 NM.
- **Hydrogen consumption per 25 NM  $\geq 180$  kg (CH<sub>2</sub>-specific).** This will exceed the maximum refill mass of the CH<sub>2</sub> tanks per trip of the CC-200, based on 25 minutes of refueling time and a standard flow rate of 120 g/s [128].

- **Required Gardner Cryogenics LH2 tanks  $\geq 2$  (LH2-specific).** It is assumed that only one of the selected LH2 tanks fits on the ferry's top deck.

#### Technical boundaries of the battery-powered ferry

The technical boundaries of the battery-powered ferry are illustrated in figure 6.11.

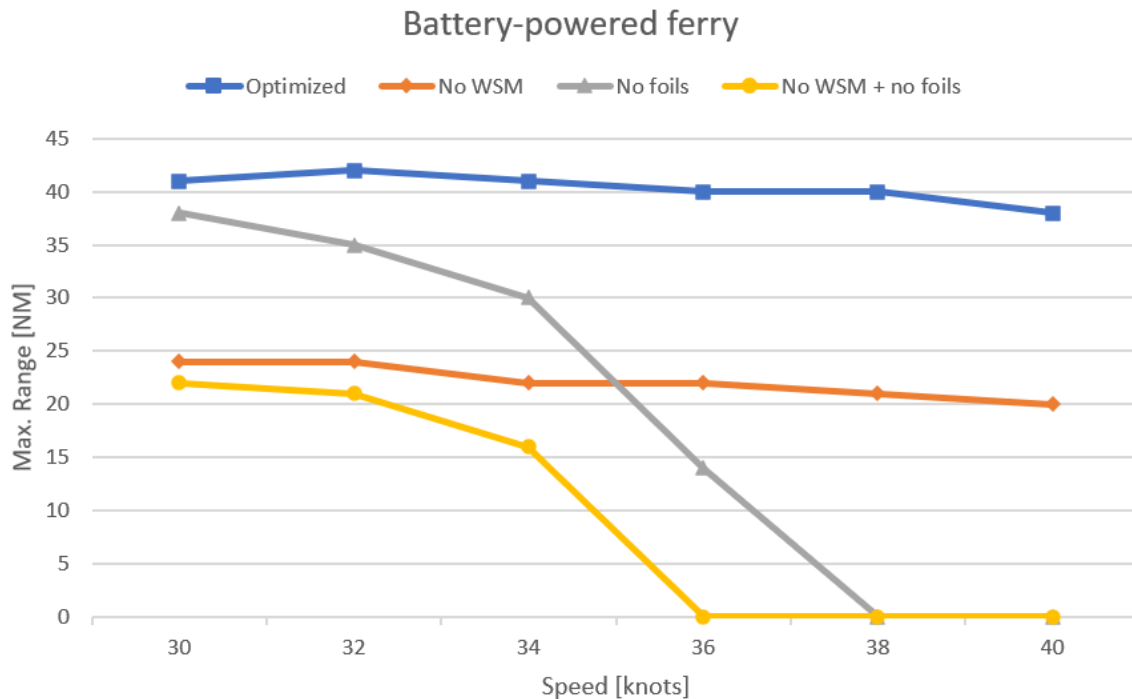


Figure 6.11: The technical boundaries of the battery-powered ferry

The technical boundaries were limited by the following constraints:

Table 6.2: Overview of the reached technical limits of the battery-powered ferry

Configuration	Speed [knots]	Reached limit
Optimized	30 - 40	Mass $\geq 150$ tonnes
No WSM	30 - 40	Mass $\geq 150$ tonnes
No foils	30 - 32	Mass $\geq 150$ tonnes
	34 - 40	Total brake power $\geq 4,400$ kW
No WSM + no foils	30 - 32	Mass $\geq 150$ tonnes
	34 - 40	Total brake power $\geq 4,400$ kW

Based on figure 6.11, the following conclusions can be made regarding the technical boundaries of the battery-powered ferry:

- The 30 NM range requirement can only be achieved for speeds up to 40 knots by the optimized configuration. The ferry without foils can only achieve the range requirement at a maximum speed of 34 knots. The other two configurations can not reach the range requirement.
- The speed of a hydrofoil ferry has a much less significant impact on its maximum range compared to a ferry without foils. This is mainly due to the ferry's resistance, which increases less significantly in case hydrofoils are used.

As a 30-knot, 30 NM, battery-powered ferry without hydrofoils is also technically feasible, it is compared to the same ferry with hydrofoils in table 6.3:

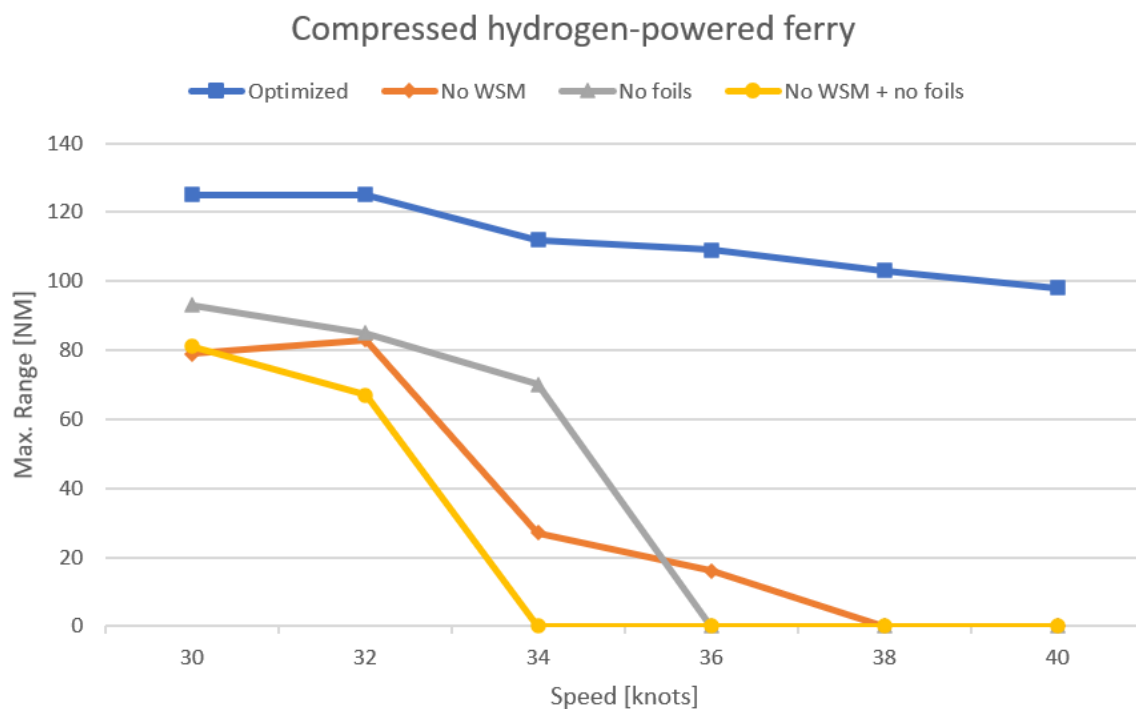
**Table 6.3:** The impact of hydrofoils on a 30-knot, 30 NM, battery-powered ferry

Ferry reqs.	Hydrofoils	Tot. req. P_B [MW]	Battery modules [-]	Energy cons. [kWh/NM]	Total mass [t]
30 knots, 30 NM	Yes	2.5	280	73	131
30 knots, 30 NM	No	3.2	354	92	130

From these specifications, it is seen that eliminating the hydrofoil system does not prevent it from being technically feasible, but it does increase the required brake power and energy consumption. For this reason, the propulsion and energy carrier system of the ferry without foils will be larger. To decide between these configurations, it is recommended to look at the economic feasibility. If the capital and operating expenses of the hydrofoil system are lower compared to the extra capital and operating expenses of the larger propulsion and energy carrier systems (compared to the systems of the hydrofoil ferry), then the hydrofoil ferry will be more attractive from an economic perspective, and vice versa.

#### Technical boundaries of the compressed hydrogen-powered ferry

The technical boundaries of the compressed hydrogen-powered ferry are illustrated in figure 6.12.

**Figure 6.12:** The technical boundaries of the compressed hydrogen-powered ferry

The technical boundaries were limited by the following constraints:

**Table 6.4:** Overview of the reached technical limits of the compressed hydrogen-powered ferry

Configuration	Speed [knots]	Reached limit
Optimized	30 - 40	Energy carrier volume $\geq 100 \text{ m}^3$
No WSM	30 - 40	Mass $\geq 150$ tonnes
No foils	30 - 34	Energy carrier volume $\geq 100 \text{ m}^3$
	36 - 40	Total brake power $\geq 4,400 \text{ kW}$
No WSM + no foils	30 - 32	Energy carrier volume $\geq 100 \text{ m}^3$
	34 - 40	Total brake power $\geq 4,400 \text{ kW}$

Based on figure 6.12, the following conclusions can be made regarding the technical boundaries of the compressed hydrogen-powered ferry:

- The 30 NM range requirement can only be achieved for speeds up to 40 knots by the optimized configuration. The ferry without weight-saving measures becomes too heavy at speeds at and above 34 knots and the ferry without hydrofoils requires too much brake power at and above 36 knots.
- The maximum range for the optimized configuration of the CH<sub>2</sub>-powered ferry is significantly higher compared to the battery-powered ferry. This maximum range is limited by the available room for the energy carrier system. However, it should also be noted that at higher range capabilities, the amount of time needed to fully refill the hydrogen tanks will increase significantly.
- If the maximum mass limit is eased, the ferry without weight-saving measures would likely also comply with the 30 NM range requirement at speeds of 30 to 40 knots.

At last, the same main conclusions can be made regarding the comparison of a 30-knot, 30 NM ferry with hydrofoils and the same ferry without hydrofoils as for the battery-powered ferry. This comparison for the compressed hydrogen-powered configurations is not made anymore in this section.

#### Technical boundaries of the liquid hydrogen-powered ferry

The technical boundaries of the liquid hydrogen-powered ferry are illustrated in figure 6.13.

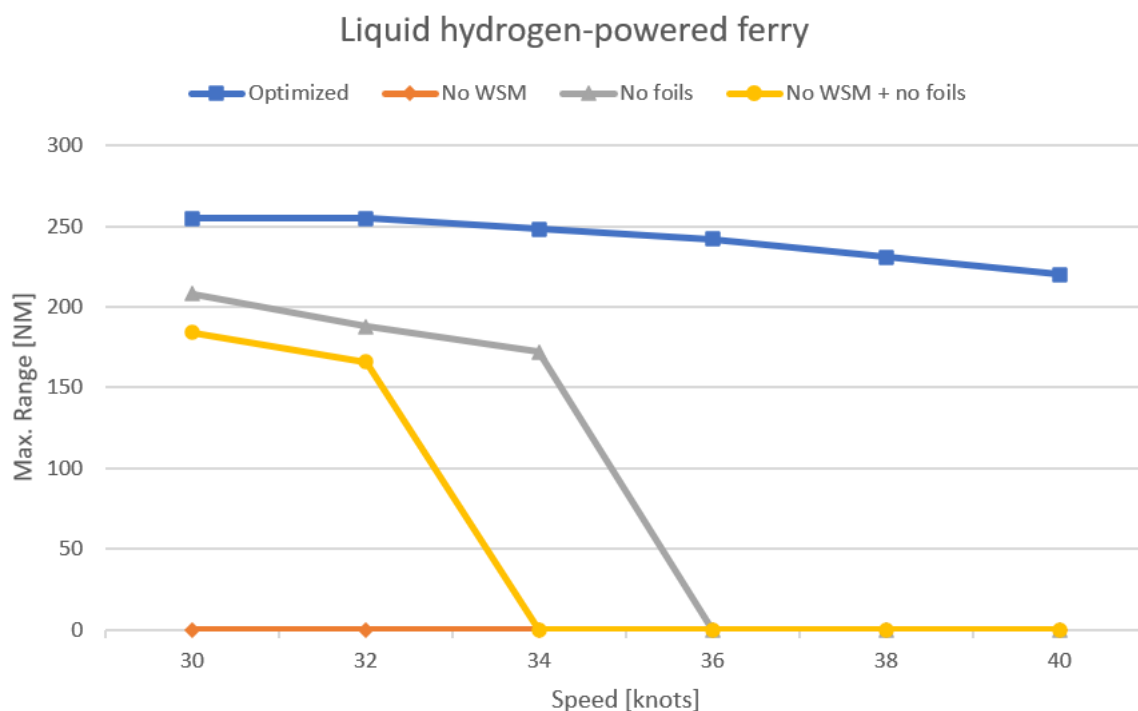


Figure 6.13: The technical boundaries of the liquid hydrogen-powered ferry

The technical boundaries were limited by the following constraints:

Table 6.5: Overview of the reached technical limits of the liquid hydrogen-powered ferry

Configuration	Speed [knots]	Reached limit
Optimized	30 - 40	Required Gardner Cryogenics LH2 tanks $\geq 2$
No WSM	30 - 40	Mass $\geq 150$ tonnes
No foils	30 - 34	Required Gardner Cryogenics LH2 tanks $\geq 2$
	36 - 40	Total brake power $\geq 4,400$ kW
No WSM + no foils	30 - 32	Required Gardner Cryogenics LH2 tanks $\geq 2$
	34 - 40	Total brake power $\geq 4,400$ kW

Based on figure 6.13, the following conclusions can be made regarding the technical boundaries of the liquid hydrogen-powered ferry:

- The 30 NM range requirement can only be achieved for speeds up to 40 knots by the optimized configuration. The ferry without weight-saving measures becomes too heavy at all speeds, and the ferry without hydrofoils requires too much brake power at and above 36 knots.
- In general, the maximum range of the liquid hydrogen-powered ferry is significantly higher compared to the compressed hydrogen- or battery-powered ferry. For the optimized configuration, the maximum range is limited by the hydrogen storage capacity of the selected liquid hydrogen tank.
- If the maximum mass limit is eased, the ferry without weight-saving measures would likely also comply with the 30 NM range requirement at speeds of 30 to 40 knots.

### 6.3.5. Parametric model sensitivity analysis

In this section, a sensitivity analysis is performed to assess the sensitivities of the developed parametric model. Four primary constraints have been identified and studied:

- **The hydrofoil chord.** Affects the lift/drag ratio of the hydrofoil system and, therefore, the ferry's resistance and power demand.
- **The hydrofoil system mass.** Affects the ferry's resistance and power demand.
- **The air resistance coefficient.** Affects the ferry's resistance and power demand.
- **The ferry's available energy carrier volume.** Affects the maximum energy storage capability of the used energy carrier and, therefore, the ferry's maximum range, mass, power demand, and energy demand.

#### Sensitivity of the hydrofoil chord

In chapter 3.2.2, the chord of the hydrofoil geometry was found using equation 3.3, which is based on the foil's structural strength and derived from a study by Hoerner et al. [79]. Using a yield stress of 276 MPa based on Aluminum 6061 (one of the most commonly used aluminum alloys globally), the minimum chord length was determined to be 0.68 meters. Then, the chord length of the foils was set to 0.80 meters for an additional margin of safety.

However, the hydrofoil system could also be constructed of state-of-the-art materials such as CFRP or a much stronger aluminum alloy like Aluminum 7068, which would lower the minimum chord length of the foils. Therefore, it is possible that the assumed chord length is unnecessarily high and can be shortened to improve performance. Aluminum 7068 is one of the strongest commercially available aluminum alloys and has a yield stress of 590 MPa [1]. Using this property in equation 3.3 yields a minimum chord length of around 0.38 meters. However, to also apply a margin of safety and prevent the foil's aspect ratio from becoming too high, a chord length of 0.60 meters is assumed for the comparison. Thus, the hydrofoil geometry as defined in chapter 3.2.2, but with a chord length of 0.60 meters, was modeled in Autowing to compare the resulting lift/drag ratios at a speed of 30 and 40 knots and at a similar generated lift. The results are listed in table 6.6:

**Table 6.6:** The impact of the hydrofoil chord on the lift-drag ratio

Speed [knots]	Chord [m]	AoA [deg]	Lift [t]	Drag [t]	Lift-drag [-]
30	0.80	2.5	108.5	6.14	17.7
30	0.60	4.0	106.6	5.70	18.7
30	0.80	4.0	132.6	8.06	16.4
30	0.60	6.0	132.0	7.88	16.8
40	0.80	0	115.8	6.70	17.3
40	0.60	1.0	117.8	6.02	19.6
40	0.80	0.5	130.2	7.45	17.5
40	0.60	1.5	129.5	6.61	19.6

From the results, it is seen that if a shorter chord of 0.60 meters would be possible, meaning a sufficient structural strength of the foils, it would likely improve the hydrofoil system's lift-drag ratio, especially at higher speeds. The smallest lift-drag ratio increase from the obtained data occurs at 30 knots at a lift of around 132 tonnes. It increases from 16.4 to 16.8, which is roughly 2.4 %. This increase

is studied in the parametric model for a 30-knot, 30 NM, battery-powered ferry sailing with hydrofoils and all weight-saving measures enabled.

Due to the improved lift-drag ratio, the ferry's total resistance, required brake power, and energy consumption would decrease by around 2.6, 2.5, and 2.5 %, respectively. From this finding, the conclusion can be made that the hydrofoil chord is an active constraint and is likely to alter the overall results in the tested conditions. Therefore, it could be interesting to perform a more detailed study into the optimal hydrofoil geometry as it could improve the technical boundaries of the zero-emission ferry.

#### Sensitivity of the hydrofoil system mass

In this thesis, the mass of the hydrofoil system was determined using equation 3.6, which led to an expected mass of six to eight tonnes. However, as was found in chapter 3.2.2, the hydrofoil system mass could increase to 12.5 tonnes in the worst-case scenario. Therefore, the sensitivity of increasing the hydrofoil system mass to 12.5 tonnes is studied in this subsection for a 30-knot, 30 NM, battery-powered ferry sailing with hydrofoils and all weight-saving measures enabled.

It is found that due to the increased hydrofoil system mass, the ferry's total mass increased by around 5.3 %. As a result, the ferry's total resistance and required brake power increased by roughly 7.0 and 6.9 %, respectively. Thus, the conclusion can be made that the total mass of the hydrofoil system or the ferry is an active constraint and should be determined as precisely as possible for accurate results.

#### Sensitivity of the air resistance coefficient

In the inputs of the parametric model listed in appendix C.1, an air resistance coefficient for the zero-emission ferry of 0.9 is assumed. G. Migeotte found that this air resistance coefficient usually lies between 0.6 and 0.9 for a catamaran in foilborne mode [115]. Therefore, this section studies the sensitivity of lowering the air resistance coefficient to 0.6 for a 30-knot, 30 NM, battery-powered ferry sailing with hydrofoils and all weight-saving measures enabled.

Due to the lowered air resistance coefficient, it is found that the ferry's total resistance and required brake power decreased by around 5.8 and 5.5 %, respectively. If a 40-knot ferry were investigated, the outcomes could decrease even more due to the typical exponential increase of wind resistance at higher speeds. Thus, it can be concluded that the air resistance coefficient is an active constraint in the model, and a study into the actual air resistance coefficient of the CC-200 would be interesting to improve the accuracy of the results.

#### Sensitivity of the available energy carrier volume

At last, the sensitivity of the available energy carrier volume is researched. In this thesis, an available energy carrier volume of 100  $m^3$  is assumed based on the CC-200's Rhino 3D model and the ferry's starboard and portside auxiliary, tank, void 1, and void 2 rooms. However, it is possible that this volume is overestimated or the required volume for the energy carrier systems is underestimated. Therefore, this subsection studies the effect of lowering the available energy carrier volume by 50 %, from 100  $m^3$  to 50  $m^3$ . The effect on the ferry's maximum range is studied for a 30-knot, battery-powered and compressed hydrogen-powered ferry using the limits determined in chapter 6.3.4. A liquid hydrogen-powered ferry is not studied as it is assumed that the liquid hydrogen tank would be placed on the top deck, which prevents volume inside the ferry from being critical. The results are listed in table 6.7:

**Table 6.7:** The impact of the available energy carrier volume on the zero-emission ferry's maximum range

Ferry	Max. $V_{ec}$ [ $m^3$ ]	Max. range [NM]	Reached limit
Battery-powered	100	41	Mass $\geq$ 150 tonnes
Battery-powered	50	41	Mass $\geq$ 150 tonnes
CH <sub>2</sub> -powered	100	125	Energy carrier volume $\geq$ 100
CH <sub>2</sub> -powered	50	56	Energy carrier volume $\geq$ 100

As can be seen, for the studied limits, the maximum available volume for the energy carrier is not an active constraint for the battery-powered ferry as it reaches the maximum mass limit at its highest possible range. However, the maximum available volume for the energy carrier is an active constraint for the battery-powered ferry, as lowering it by 50 % leads to a maximum range reduction of around 55 %, which is significant. Therefore, if one's goal is to maximize the range capability of a compressed hydrogen-powered ferry, it is beneficial to have a high volume available for the energy carrier.

## 6.4. Conclusion: the technical feasibility of a zero-emission ferry

Chapter 6 modeled the technical feasibility of a 200-passenger, 30- to 40-knot emission-free ferry. To achieve this goal, a parametric model was developed that requires a number of design inputs, ship inputs, and constants. The developed parametric model can calculate multiple specifications of the zero-emission ferry, including its weight, resistance, energy consumption, power demand, and energy demand. It can also select the best option from various energy carriers, propulsion systems, and whether or not to use hydrofoils. A flowchart of the developed parametric model is given in figure 6.1.

The parametric model was used in chapter 6.3 to find the most technically feasible configuration for the zero-emission ferry in terms of its energy carrier, weight-saving measures, the hydrofoil system, and propulsion system. Chapter 6.3.1 found that when the minimal speed and range requirements were applied, being 30 knots and 30 NM, a zero-emission ferry is technically feasible when it would apply the following:

- All identified weight-saving measures (chapter 3.1.2).
- A hydrofoil system (chapter 3.2).
- Two modified Hydromaster high-speed thrusters (chapter 5.2).
- Two Frame 450-9 electric motors manufactured by The Switch (chapter 5.2.3).
- Two ZF 5255 gearboxes (chapter 5.2.3).
- 12 PowerCell MS200 fuel cells (chapter 4.2).
- Six Quantum 936L compressed hydrogen tanks (chapter 4.2.4).

Once it was found that a zero-emission ferry with minimal design requirements was technically feasible, the impact of altering the required speed and range of a hydrofoil ferry was studied in chapter 6.3.2. During this investigation, a number of conclusions were made, including:

- At speeds of 30 to 40 knots and a range requirement of 30 to 90 NM, the compressed hydrogen energy carrier system was consistently chosen by the parametric model as it is the lightest and fits in the ferry.
- The operational speed has a relatively low impact on the ferry's total mass. At a required range of 30 NM, increasing the operational speed from 30 to 40 knots increases the ferry's total mass by around 13 % (figure 6.3).
- The operational speed has a relatively high impact on the ferry's used brake power. At a required range of 30 NM, increasing the operational speed from 30 to 40 knots increases the ferry's used brake power by around 65 % (figure 6.4).
- The hydrofoil system lowers the ferry's resistance for the entire array of tested speeds and required ranges. The most minor resistance difference between a hydrofoil and non-hydrofoil ferry occurs at the lowest speed (30 knots), while the difference becomes more considerable at higher operational speeds (figure 6.5).
- The expected energy consumption of the compressed hydrogen-powered CC-200 (84 kWh/NM at 40 knots) is slightly lower compared to the Electra hydrofoil ferry concept (90 kWh/NM at 40 knots, [48]) (figure 6.6).
- The mass of the battery energy carrier system increases more strongly for higher range requirements compared to the two hydrogen system options (figure 6.7).
- At lower range requirements, the battery energy carrier is the most compact. The liquid hydrogen system becomes the most compact after a required range of around 80 NM. A high energy carrier system volume is a disadvantage for the compressed hydrogen-powered ferry at higher required ranges (figure 6.8).

Next, chapter 6.3.3 compared a compressed hydrogen-, liquid hydrogen-, and battery-powered ferry and found that all meet the defined minimal requirements and are thus technically feasible. It also discusses the technical advantages and disadvantages of the three ferry configurations, resulting in the following conclusions:

- **Compressed hydrogen-powered ferry**
  - Advantage(s)

- \* The lightest and the lowest energy consumption in kWh/NM.
- \* The hydrogen tanks do not need a cooling system and can be operated at ambient temperatures.
- Disadvantage(s)
  - \* Requires two hydrogen refueling stations to be built at both ports.
  - \* The high-pressure compressed hydrogen tanks onboard the ferry may cause safety concerns.
- **Liquid hydrogen-powered ferry**
  - Advantage(s)
    - \* The highest total range of 255 NM.
    - \* Can sail based on the CC-200's operating profile for an entire day using a single fuel-up in the morning.
    - \* The ferry can be refueled by a liquid hydrogen trailer brought to the port by a truck.
  - Disadvantage(s)
    - \* A relatively large liquid hydrogen tank must be mounted on the top deck of the ferry, which will require additional structural reinforcements.
    - \* The heaviest ferry configuration, and a relatively large volume for the energy carrier system is required.
- **Battery-powered ferry**
  - Advantage(s)
    - \* There is no requirement for hydrogen that must be supplied at the port.
    - \* The required volume for the energy carrier is significantly lower compared to the hydrogen-powered ferries, freeing up additional room inside the ferry.
    - \* The battery system can be recharged in under 18 minutes if sufficient power is available.
  - Disadvantage(s)
    - \* A charging station with a power output of roughly 4.4 MW must be built at both ports.

Finally, the technical boundaries of the zero-emission ferry configurations were studied. The most important conclusions that resulted from this include:

- Using the identified weight-saving measures and hydrofoils, the 30 NM range requirement can be achieved by all three zero-emission ferry configurations sailing at an operating speed of up to 40 knots.
- In general, a zero-emission ferry without hydrofoils is technically feasible at an operating speed of 30 knots. However, when the speed is increased to 40 knots, the required brake power increases greatly, which puts the ferry's technical feasibility at risk.
- A 30-knot, 30 NM battery-powered ferry without hydrofoils is technically feasible but requires a significantly larger and more powerful energy carrier and propulsion system.
- For larger range requirements, the liquid hydrogen-powered ferry is likely to be the most technically-feasible configuration.

# 7

## Economic feasibility of a zero-emission ferry

Chapter 7 aims to answer the following sub-question:

*How economically feasible are the developed technically-feasible zero-emission ferry concepts?*

To assess the economic feasibility of the zero-emission ferries, this chapter aims to find the total cost of ownership per year for the current CC-200 and the three zero-emission ferry concepts, each using a different energy carrier. The total cost of ownership (TCO) of a passenger ferry is a combination of its capital expenditures (CAPEX) and operational expenditures (OPEX). Combining these allows the analysis of the average costs for the ferry's operator during one year of operation. If the yearly TCO of the zero-emission ferry is less or equal to the yearly TCO of the CC-200, it will be defined as economically feasible. It should be noted that the goal is to make a preliminary assessment of the zero-emission ferries' economic feasibility. Therefore, only the most considerable costs of the ferries were identified and studied.

### 7.1. Capital expenditures

This section investigates the CAPEX of the current CC-200, battery-powered, compressed hydrogen-powered, and liquid hydrogen-powered ferries.

Due to the confidential nature of information related to the CC-200's CAPEX, they are used as the reference, which means the CAPEX of the zero-emission ferries are expressed as a percentage of the CC-200's total CAPEX. Additionally, due to the uncertainty of the expenditures, the CAPEX values are rounded in whole percentages.

When switching from the CC-200 to a zero-emission ferry, the CAPEX:

- Decreases due to the removal of:
  - Any propulsion-related systems
  - The aluminum hull and superstructure
- Increases due to the addition of:
  - The weight-saving measures (e.g., a CFRP hull and superstructure)
  - The hydrofoil system
  - The thrusters, electric motors, and gearboxes
  - The energy carrier system
  - A hydrogen refueling or battery charging infrastructure

Resulting from discussions with Henk van Herwijnen, general manager at CoCo Yachts, it is estimated that the CC-200's propulsion-related systems sum to roughly 20 % of the ferry's total CAPEX, while the aluminum hull and superstructure amount to roughly 13 % of the ferry's total CAPEX.

The change in CAPEX when switching from the CC-200 to one of the zero-emission ferry concepts shown in table 6.1 is now studied, beginning with the battery-powered ferry.

### 7.1.1. CAPEX of the battery-powered ferry

In table 7.1, an estimation was made of the total CAPEX of the 30-knot, 30 NM, battery-powered ferry. The results have been obtained from various sources, including literature and information provided by CoCo Yachts and Hydromaster. For costs that are relatively uncertain, such as the hydrofoil or battery system, the CAPEX are listed as a range. A detailed explanation of the results is listed in appendix D.1.1.

**Table 7.1:** Estimated total CAPEX of the battery-powered ferry as a percentage of the CC-200's total CAPEX

<b>Component(s)</b>	<b>Estimated added CAPEX (% of CC-200's total CAPEX)</b>
CFRP hull and superstructure	41 % to 56 %
Hydrofoil system	11 % to 19 %
Hydromaster thrusters	15 %
Electric motors	5 %
Gearboxes	2 %
Battery system	25 % to 51 %
Onshore charging stations	42 % to 64 %
<b>Total:</b>	<b>141 % to 212 %</b>
<b>Component(s)</b>	<b>Estimated removed CAPEX (% of CC-200's total CAPEX)</b>
Diesel propulsion-related systems	20 %
Aluminum hull and superstructure	13 %
<b>Total:</b>	<b>33 %</b>
<b>Total CAPEX (battery) (% of the CC-200's total CAPEX)</b>	
<b>208 % to 279 %</b>	

It was assumed that the change in CAPEX of the zero-emission ferries can be estimated by subtracting the costs of the diesel propulsion-related systems as well as the aluminum hull and superstructure, and adding the costs of the new propulsion system components, CFRP hull and superstructure, and hydrofoil system. As a result, it was found that the CAPEX of the battery-powered ferry would be roughly 208 % to 279 % of the CC-200's CAPEX.

### 7.1.2. CAPEX of the compressed hydrogen-powered ferry

The CAPEX of the compressed hydrogen-powered ferry are based on the CAPEX of the battery-powered ferry. It was found that the cost of most components remains equal and that the most significant change results from the replacement of the battery system by the fuel cell system and compressed hydrogen tanks. An explanation of the obtained CAPEX is given in appendix D.1.2 and the results are listed in table 7.2:

**Table 7.2:** Estimated total CAPEX of the compressed hydrogen-powered ferry as a percentage of the CC-200's total CAPEX

<b>Component(s)</b>	<b>Estimated added CAPEX (% of CC-200's total CAPEX)</b>
CFRP hull and superstructure	41 % to 56 %
Hydrofoil system	11 % to 19 %
Hydromaster thrusters	15 %
Electric motors	4 %
Gearboxes	2 %
PowerCell MS200 fuel cells	55 % to 92 %
Quantum 936L tanks	1 %
CH <sub>2</sub> refueling stations	18 %
<b>Total:</b>	<b>147 % to 207 %</b>

<b>Component(s)</b>	<b>Estimated removed CAPEX (% of CC-200's total CAPEX)</b>
Diesel propulsion-related systems	20 %
Aluminum hull and superstructure	13 %
<b>Total:</b>	<b>33 %</b>

<b>Total CAPEX (CH<sub>2</sub>) (% of the CC-200's total CAPEX)</b>	
<b>214 % to 274 %</b>	

### 7.1.3. CAPEX of the liquid hydrogen-powered ferry

The CAPEX of the liquid hydrogen-powered ferry are based on the CAPEX of the compressed hydrogen-powered ferry. It was found that the cost of most components remains equal and that the most significant changes are a consequence of the liquid hydrogen storage. An explanation of the obtained CAPEX is given in appendix D.1.3 and the results are listed in table 7.3:

**Table 7.3:** Estimated total CAPEX of the liquid hydrogen-powered ferry as a percentage of the CC-200's total CAPEX

<b>Component(s)</b>	<b>Estimated added CAPEX (% of CC-200's total CAPEX)</b>
CFRP hull and superstructure	41 % to 56 %
Hydrofoil system	11 % to 19 %
Hydromaster thrusters	15 %
Electric motors	5 %
Gearboxes	2 %
Ballard FCwave fuel cells	65 % to 108 %
Gardner Cryogenics LH <sub>2</sub> tank	12 %
<b>Total:</b>	<b>151 % to 217 %</b>

<b>Component(s)</b>	<b>Estimated removed CAPEX (% of CC-200's total CAPEX)</b>
Diesel propulsion-related systems	20 %
Aluminum hull and superstructure	13 %
<b>Total:</b>	<b>33 %</b>

<b>Total CAPEX (LH<sub>2</sub>) (% of the CC-200's total CAPEX)</b>	
<b>218 % to 284 %</b>	

## 7.2. Operational expenditures

This section studies the OPEX of the current CC-200 and the battery-powered, compressed hydrogen-powered, and liquid hydrogen-powered ferries. In the calculations of this chapter, numbers entered within square brackets and separated with a "-" indicate a range of expected values.

### 7.2.1. OPEX of the Coastal Cruiser 200

First, the OPEX of the current CC-200 are studied, as they will serve as a benchmark for the zero-emission ferries. It was assumed that the main parts of the CC-200's OPEX are the costs for the crew,

fuel, and maintenance of the vessel. Additionally, it is the goal to also account for the indirect costs caused by the ICE emissions, so a possible  $CO_2$  tax is applied in the OPEX calculation.

### OPEX CC-200: operational

The CC-200 has a crew capacity of 12, and it was assumed that all 12 crew members are on board during the ferry's operating hours [73]. According to its operational profile, the CC-200 is operational for 1.5 hours per one-way trip, completes nine one-way trips on average per day (chapter 2.1), and does so for 350 days per year [58]. Together with an assumed average salary of € 20 to € 25 per hour, the yearly crew cost is calculated to be  $12 \cdot 1.5 \cdot 9 \cdot 350 \cdot [20 - 25] = € 1,134k$  to € 1,418k [12].

At operational speed, the diesel engines of the CC-200 consume 514 liters of fuel per hour [73]. The cost of MGO diesel fuel in China appears to be around \$ 1,175 to \$ 1,440 per tonne, or € 1.10 to € 1.35 per liter, considering price fluctuations [26] [167]. The CC-200 is in transit for around nine hours per day (one hour of transit time and nine one-way trips per day) and 350 days per year. As a result, the yearly fuel costs are calculated to be  $514 \cdot [1.10 - 1.35] \cdot 9 \cdot 350 = € 1,781k$  to € 2,186k.

To account for the indirect costs caused by the ICE emissions, a  $CO_2$  tax that could be applied to the diesel-driven CC-200 in the future has been added to the OPEX. The added  $CO_2$  tax is based on a national emissions trading system (ETS) designed to motivate companies and investors to contribute to the clean energy transition. China's ETS currently only covers the power generation sector and has put a price on carbon emissions of around € 6 per tonne of  $CO_2$  [157]. Meanwhile, the European Union's ETS only covers ships above 5,000 GT and reaches prices of roughly € 70 to € 100 per tonne of  $CO_2$ , as illustrated in figure 7.1, which is a significant difference [63]. To account for the indirect costs due to the ICE emissions as best as possible, it has been chosen to apply the European Union's carbon ETS prices to the current CC-200, as it is believed China's price is far too low. Additionally, a higher value for the carbon tax is set because the indirect costs caused by  $SO_X$  and  $NO_X$  emissions are not accounted for in these carbon ETS prices.



Figure 7.1: Price of the European Union's carbon permits [51]

MGO fuel has a density of 0.86 kg/l and around 3.206 kg of  $CO_2$  is produced per kg of used MGO fuel [93] [9]. Combined with the CC-200's fuel consumption of 514 l/hour, the yearly  $CO_2$  tax is assumed to be  $514 \cdot 0.86 \cdot 3.206 \cdot [0.070 - 0.100] \cdot 9 \cdot 350 = € 312k$  to € 446k.

### OPEX CC-200: maintenance

Resulting from conversations with Henk van Herwijnen, general manager at CoCo Yachts, the yearly maintenance costs of the CC-200 were estimated to be € 230k for the propulsion system-related maintenance (e.g., diesel engines and diesel generator sets) and € 160k for all other maintenance, based on an operational life of 25 years.

**OPEX CC-200: summary**

The main parts and results of the CC-200's yearly OPEX are summarized in table 7.4:

**Table 7.4:** Estimated yearly OPEX of the current CC-200

<b>Operational</b>	<b>Estimated expense (€/year)</b>
Crew	1,134k to 1,418k
Fuel	1,781k to 2,186k
CO2 tax	312k to 446k
<b>Maintenance</b>	
Propulsion system-related maintenance	230k
All other maintenance	160k
<b>Total OPEX (€/year)</b>	
<b>3,617k to 4,440k</b>	

**7.2.2. OPEX of the battery-powered ferry**

The main parts of the battery-powered ferry's OPEX are assumed to include the costs of the crew, electricity, propulsion system-related maintenance, and all other required maintenance.

**OPEX battery-powered ferry: operational**

The OPEX required for the crew was assumed to be equal to the CC-200. According to the parametric model, a 30-knot, 30 NM, battery-powered ferry would use around 1,823 kWh of energy per one-way trip. Large-scale industrial power rates in Guangzhou, located near the Pearl River Delta region, are around € 0.088/kWh for 35 kV and above [33]. Due to the fluctuation of electricity prices, a range of € 0.08/kWh to € 0.1/kWh was assumed in this thesis. Assuming the ferry completes nine one-way trips per day, 350 operational days per year, and a charging efficiency at high C-rates of 90 %, results in a yearly electricity cost of  $\frac{1,823}{0.9} \cdot [0.08 - 0.1] \cdot 9 \cdot 350 = € 510k$  to € 638k [103].

**OPEX battery-powered ferry: maintenance**

It is assumed that most propulsion system-related maintenance costs originate from the limited lifetime of the costly battery system, as the authors of SF-BREEZE found that the maintenance costs of electric motors are negligible [147]. At the used DSOC of 80 %, Xalt Energy indicated that the selected XMP 98P modules have a cycle life of more than 10,000 cycles at 1C charge-discharge [185]. However, the actual cycle life may be shorter in reality as the ferry would be charged at a C-rate of roughly 2.4, assuming a charging time of 25 minutes. Therefore, a battery system operational life of 2.5 to 3 years is assumed, which is equal to around 7,875 to 9,450 cycles. In appendix D.1.1, it was found that a new battery system would cost between € 1,641k and € 3,282k. This equals a yearly OPEX required for the eventual replacement of the battery system of  $\frac{[1,641 - 3,282]}{[3 - 2.5]} = € 547k$  to € 1,313k.

At last, the OPEX required for all other maintenance of the ferry were assumed to be equal to the CC-200.

**OPEX battery-powered ferry: summary**

The main parts and results of the battery-powered ferry's yearly OPEX are summarized in table 7.5:

**Table 7.5:** Estimated yearly OPEX of a battery-powered ferry

<b>Operational</b>	<b>Estimated expense (€/year)</b>
Crew	1,134k to 1,418k
Electricity	510k to 638k
<b>Maintenance</b>	
Propulsion-related maintenance	547k to 1,313k
All other maintenance	160k
<b>Total OPEX (% of CC-200)</b>	
<b>53 % to 98 %</b>	

### 7.2.3. OPEX of the compressed hydrogen-powered ferry

The main parts of the compressed hydrogen-powered ferry's OPEX are assumed to include the costs of the crew, hydrogen, propulsion system-related maintenance, and all other required maintenance.

#### OPEX compressed hydrogen-powered ferry: operational

The OPEX required for the crew were assumed to be equal to the CC-200. As discussed in chapter 4.2.3, grey hydrogen is currently produced in China for around \$6 to \$11 per kg. At the same time, China's goal is to produce green hydrogen for a cost lower than \$4.69 per kilogram by 2025. However, transport costs of the hydrogen must also be included, and for these reasons, this thesis assumes a total hydrogen cost of € 6/kg to € 9/kg for the OPEX calculations. According to the parametric model results, the compressed hydrogen-powered ferry will consume around 101 kg of hydrogen per one-way trip. Together with nine one-way trips per day for 350 days per year, it results in a yearly hydrogen cost of  $[6 - 9] \cdot 101 \cdot 9 \cdot 350 = € 1,909k$  to € 2,863k.

#### OPEX compressed hydrogen-powered ferry: maintenance

Like for the battery-powered ferry, it is assumed that the majority of the propulsion system-related maintenance costs originate from the limited lifetime of the costly fuel cell system. In chapter 4.2.2, the lifetime of PEM fuel cells was said to be 10,000 to 40,000 hours, after which a refurbishment is needed. In a study optimizing the design of the SF-BREEZE hydrogen-powered ferry, the lifetime for PEM fuel cells was said to be 10,000 to 15,000 hours [148]. In this thesis, a lifetime of 11,025 to 15,750 hours is assumed, which equals a refurbishment interval of 3.5 to 5 years.

From the parametric model results, it follows that the compressed hydrogen-powered ferry would require a power output of 2,285 kW. In turn, this leads to 12 installed PowerCell MS200 fuel cells, delivering 200 kW each, which equals a total installed power of 2,400 kW. The fuel cell refurbishment cost was set to € 900/kW, similar to the assumption of the SF-BREEZE optimization study [148]. Therefore, the cost that must be reserved for the fuel cell system refurbishment per year equals  $\frac{2,400 \cdot 900}{[5-3.5]} = € 432k$  to € 617k.

Lastly, the OPEX required for all other maintenance of the ferry were assumed to be equal to the CC-200.

#### OPEX compressed hydrogen-powered ferry: summary

The main parts and results of the compressed hydrogen-powered ferry's yearly OPEX are summarized in table 7.6:

**Table 7.6:** Estimated yearly OPEX of a compressed hydrogen-powered ferry

<b>Operational</b>	<b>Estimated expense (€/year)</b>
Crew	1,134k to 1,418k
Hydrogen	1,909k to 2,863k
<b>Maintenance</b>	
Propulsion-related maintenance	432k to 617k
All other maintenance	160k
<b>Total OPEX (% of CC-200)</b>	
<b>82 % to 140 %</b>	

#### 7.2.4. OPEX of the liquid hydrogen-powered ferry

For the OPEX calculation of the liquid hydrogen-powered ferry, it is assumed that all OPEX remain the same except for the hydrogen and propulsion-related maintenance cost.

First of all, the liquid hydrogen-powered ferry is heavier and consumes slightly more hydrogen compared to the compressed hydrogen-powered ferry. According to the parametric model results, the liquid hydrogen-powered ferry consumes around 118 kg of hydrogen per one-way trip. With nine one-way trips per day for 350 days per year, it results in a yearly hydrogen cost of  $[6 - 9] \cdot 118 \cdot 9 \cdot 350 = \text{€ } 2,230\text{k}$  to  $\text{€ } 3,345\text{k}$ .

Next, the liquid hydrogen-powered ferry is equipped with 14 fuel cells instead of 12, which results in an increase in yearly propulsion-related maintenance costs. These are estimated to be  $\frac{2,800 \cdot 900}{[5-3.5]} = \text{€ } 504\text{k}$  to  $\text{€ } 720\text{k}$ .

The main parts and results of the liquid hydrogen-powered ferry's yearly OPEX are summarized in table 7.7:

**Table 7.7:** Estimated yearly OPEX of a liquid hydrogen-powered ferry

<b>Operational</b>	<b>Estimated expense (€/year)</b>
Crew	1,134k to 1,418k
Hydrogen	2,230k to 3,345k
<b>Maintenance</b>	
Propulsion-related maintenance	504k to 720k
All other maintenance	160k
<b>Total OPEX (% of CC-200)</b>	
<b>91 % to 156 %</b>	

### 7.3. Total cost of ownership

When a ferry operator chooses between a diesel-driven ferry and various configurations of zero-emission ferries, it can be valuable to look at each ferry's total cost of ownership (TCO). The TCO combines the ferry's short-term price (CAPEX) and its long-term price (OPEX) and therefore represents the total costs for the ferry operator during the entire ownership. A ferry configuration with the lowest TCO will provide the best value for the operator in the long run.

In this section, the TCO of the CC-200, battery-powered, compressed hydrogen-powered, and liquid hydrogen-powered ferries is researched based on the previous CAPEX and OPEX results. The TCO of the CC-200 was calculated based on an operational life of 25 years. However, since the zero-emission ferries will apply a CFRP hull and superstructure, a slightly longer operational life of 30 years was assumed for the TCO calculations of the zero-emission ferries. To account for this difference in operational life, the total cost of ownership is calculated on a yearly basis using the following formula:

$$TCO_{yearly} = \frac{CAPEX}{Design\ life} + OPEX \quad (7.1)$$

With:

- $TCO_{yearly}$ , the yearly total cost of ownership [€/year]
- $CAPEX$ , the capital expenditures [€]
- $Design\ life$  [number of years]
- $OPEX$ , the operational expenditures [€/year]

The study's results on the yearly total cost of ownership are listed in table 7.8. Due to the confidential nature of the CC-200's CAPEX, the results of the zero-emission ferries' TCO are listed as a percentage of the CC-200's TCO.

**Table 7.8:** A comparison of the yearly TCO of the zero-emission ferries as a percentage of the CC-200's TCO

Ferry	$TCO_{yearly}$ (% of the CC-200's $TCO_{yearly}$ )
Battery-powered	60 % to 107 %
Compressed hydrogen-powered	87 % to 146 %
Liquid hydrogen-powered	96 % to 161 %

## 7.4. Conclusion: the economic feasibility of a zero-emission ferry

When assessing the economic feasibility of a zero-emission ferry, one should study its purchase price (CAPEX) and the costs associated with its operational activities (OPEX). In chapter 2.2, it was determined that in order for a zero-emission ferry to be economically feasible, its yearly total cost of ownership should not be higher than the CC-200's total cost of ownership, which is calculated to account for the indirect costs caused by its emissions.

In chapters 7.1 and 7.2, the CAPEX and OPEX of the CC-200 and the zero-emission ferry configurations (battery-powered, compressed hydrogen-powered, and liquid hydrogen-powered) found in table 6.3.3 were calculated. These were then combined to form the ferries' yearly total cost of ownership in chapter 7.3, which can be used to assess their economic feasibility. The main results of the study into the economic feasibility of the ferries are summarized in table 7.9:

**Table 7.9:** OPEX, CAPEX, and TCO of the CC-200 and the battery-, compressed hydrogen-, and liquid hydrogen-powered ferries

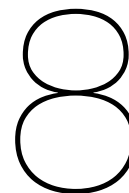
Ferry	CAPEX (% of CC-200)	OPEX (% of CC-200)	$TCO_{yearly}$ (% of CC-200)
Battery-powered	208 % to 279 %	53 % to 98 %	60 % to 107 %
CH <sub>2</sub> -powered	214 % to 274 %	82 % to 140 %	87 % to 146 %
LH <sub>2</sub> -powered	218 % to 284 %	91 % to 156 %	96 % to 161 %

From this table, it is seen that the CAPEX ranges of the zero-emission ferries are very close to each other. Therefore, the main costs that influence the difference in the yearly TCO are the OPEX. On average, the OPEX of the battery-powered ferry is considerably lower compared to the OPEX of the CC-200 or the hydrogen-powered ferries. This is mainly due to the lower cost of electricity compared to diesel fuel or hydrogen.

It can be concluded that according to the definition of "economic feasibility" in this thesis, all three zero-emission ferry configurations could be economically feasible as their yearly TCO may be lower than the CC-200's yearly TCO. At the same time, all zero-emission ferries could not be economically feasible, as their yearly TCO may also be higher compared to the CC-200's yearly TCO. Still, by looking at the range of the yearly TCO's of the zero-emission ferries, it is seen that on average, the range is lowest for the battery-powered ferry and highest for the liquid hydrogen-powered ferry. Thus, it can be concluded that out of the three configurations, the battery-powered ferry is most likely to be economically feasible, while the liquid hydrogen-powered ferry is least likely to be economically feasible.

In the worst-case scenario, the battery-powered ferry would cost almost three times as much as the CC-200 to purchase but would still have a lower OPEX. Therefore, its yearly TCO would be 7 % higher compared to the CC-200's yearly TCO, which is still very close to economic feasibility.

At last, it can be noted that a large part of the hydrogen-powered ferries' OPEX are formed from the cost of hydrogen, which was assumed to be between € 6/kg and € 9/kg in this thesis. If China achieves its goal of producing green hydrogen at a cost lower than \$ 4.69/kg by 2025, it will significantly increase the likelihood that a fast, hydrogen-powered, zero-emission ferry is economically feasible.



# Conclusion and recommendations

In this chapter, the thesis is finalized by providing a synthesis of key findings in the conclusion (chapter 8.1), an overview of recommended new areas for future research in the recommendations (chapter 8.2), and thoughts about individual experiences through a personal reflection (chapter 8.3).

## 8.1. Conclusion

$CO_2$ ,  $NO_x$ ,  $SO_x$ , and particulate matter emitted by traditional, diesel-driven vessels are a cause of multiple social, environmental, health, economic, and ethical concerns. Like many other ferries, a 200-passenger, 30-knot ferry called the CC-200 is a source of these ICE emissions. To negate the CC-200's contribution to the total ICE emissions, a zero-emission version of the ferry could be developed, built, and operated. However, is this technically and economically feasible? To study this, the following main research question was answered in this thesis:

**How technically and economically feasible is a 200-passenger, 30- to 40-knot emission-free ferry operating on the Zhuhai-Shenzhen route in the Pearl River Delta?**

First, a 200-passenger ferry based on the CC-200 was studied that used the following:

- Weight-saving measures.
  - Using fiber-reinforced composites for the hull and superstructure.
  - Removing unnecessary items (e.g., thermal and noise insulation).
  - Reducing the mass of currently-equipped items (e.g., seats, glass windows).
- A hydrofoil system.
- A propulsion system consisting of thrusters, gearboxes, and electric motors.

It was concluded that it is **technically feasible** to operate a 200-passenger, 30-knot emission-free ferry on the Zhuhai-Shenzhen route using one of the three identified zero-emission energy carriers, showing the following advantages and disadvantages:

- Compressed hydrogen in combination with PEM fuel cells.
  - **Advantages**
    - \* The lightest and most energy-efficient ferry.
    - \* No cooling system is needed for the hydrogen tanks.
  - **Disadvantages**
    - \* The hydrogen tanks would require a refuel after every one-way trip.
    - \* The hydrogen tanks may cause safety concerns due to their high operating pressures.
- Liquid hydrogen in combination with PEM fuel cells.

– **Advantages**

- \* Has the energy storage capability to operate for an entire day using a single fuel-up in the morning.
- \* The hydrogen tank can be refueled by a truck carrying a liquid hydrogen trailer.

– **Disadvantages**

- \* Structural reinforcements are needed for the placement of the hydrogen tank.
- \* The heaviest ferry configuration.

- NMC Li-ion battery modules.

– **Advantages**

- \* There is no requirement for a hydrogen supplier in the proximity of the port.
- \* Requires a low volume for the energy carrier.

– **Disadvantage**

- \* A charging station with a power output of roughly 4.4 MW must be built at both ports.

Meanwhile, it is **economically feasible** to operate a 200-passenger, 30-knot emission-free ferry on the Zhuhai-Shenzhen route using all three above-mentioned energy carrier configurations in the **best-case** economic scenario, but not in the **worst-case** economic scenario.

Thus, in the best-case economic scenario, it is **both technically and economically feasible** to operate a 200-passenger, 30-knot emission-free ferry on the Zhuhai-Shenzhen route using one of the following zero-emission energy carriers:

- Compressed hydrogen in combination with PEM fuel cells.
- Liquid hydrogen in combination with PEM fuel cells.
- NMC Li-ion battery modules.

For this statement, it should be noted that economic feasibility can not be guaranteed, and both the worst- and best-case economic scenarios are unlikely to occur. However, it can be stated that the operation of a 200-passenger, 30-knot emission-free ferry on the Zhuhai-Shenzhen route powered by NMC Li-ion battery modules has **the highest probability of being both technically and economically feasible**, mainly due to the lower operating cost of using electricity instead of hydrogen or diesel fuel.

This answer clearly illustrates the technical and economic feasibility of a 30-knot, emission-free ferry using hydrofoils and weight-saving measures, but therefore also raises the question of the technical boundaries of the ferry when the operating speeds are increased towards 40 knots, or the hydrofoils or weight-saving measures are eliminated. By researching this question, the following main conclusions about a zero-emission ferry sailing on the Zhuhai-Shenzhen route were made:

- A compressed hydrogen-, liquid hydrogen-, or battery-powered ferry is technically feasible at **operating speeds up to 40 knots** when all identified weight-saving measures and hydrofoils are applied.
- A compressed hydrogen-, liquid hydrogen-, and battery-powered ferry with an operating speed of 30 knots sailing **without hydrofoils** is likely to be technically feasible. However, the technical feasibility is quickly put at risk when the required operating speed is increased towards 40 knots.
- A 30-knot, battery-powered ferry **without hydrofoils** is technically feasible. However, it requires a significantly larger and more powerful energy carrier and propulsion system compared to the same ferry with a hydrofoil system.
- When the identified weight-saving measures are not applied, the maximum range of the zero-emission ferry decreases. A 30-knot, hydrofoil, compressed hydrogen-, liquid hydrogen-, or battery-powered ferry **without weight-saving measures** is likely to be technically feasible. However, no definite conclusion could be made here due to the limitations of the developed parametric model.

To sum up, the main research question can be answered in short by the following:

The operation of a 200-passenger, 30- to 40-knot emission-free ferry on the Zhuhai-Shenzhen route is technically feasible when implementing a CH<sub>2</sub>-, LH<sub>2</sub>-, or battery-based energy carrier system in combination with thrusters and hydrofoils. For these configurations at 30 knots, economic feasibility may or may not be achieved, depending on the exact costs. However, the 30-knot, battery-powered ferry has the highest chance of being both technically and economically feasible.

### 8.1.1. Contributions

In chapter 1, the social, environmental, health, and economic problems related to ICE emissions were discussed. By concluding that the operation of a 200-passenger, 30-knot, emission-free ferry on the Zhuhai-Shenzhen route is technically feasible and could be economically feasible, more zero-emission ferries instead of diesel-driven ferries may be built in the future. In that case, ICE emissions, and therefore the issues related to them, will be reduced, leading to a social contribution of this thesis.

This research also brought a scientific contribution by providing an up-to-date study on the technical and economic feasibility of a zero-emission ferry that distinguishes itself by having a significantly higher passenger capacity and operating speed compared to all currently operating and the majority of concept zero-emission ferries. Due to the positive results regarding the ferry's technical feasibility, a contribution to the industry is provided as the obtained knowledge can contribute to a consideration of a zero-emission propulsion system when a new ferry is designed, helping the industry reduce its carbon footprint.

## 8.2. Recommendations

Based on the conclusions of this thesis, several recommendations can be given that will allow future studies to build on, confirm, or enrich the results presented in this report. These recommendations are discussed in this section.

### 8.2.1. Hydrofoil system

First, several recommendations can be suggested related to the ferry's hydrofoil system. These are summarized below.

- **Stability and safety.** To better understand the implications of applying a hydrofoil system on a fast ferry, future studies can research the impact of such a system on the ferry's stability and safety. As mentioned before, a fully-submerged foil system will likely need an active control system to provide sufficient stability for the vessel. Also, the ferry's new center of gravity should be accounted for in the stability analysis.
- **Geometry.** To optimize results, further research is needed to determine the best geometry for the hydrofoil system. Various foil parameters can be altered, such as the chord, span, and taper. Also, it is recommended to perform a more in-depth structural analysis of the hydrofoil system. At last, the performance of other configurations like surface-piercing, aircraft, or canard foils can be investigated.
- **Cavitation and ventilation.** Based on the results of other studies, cavitation and ventilation are unlikely to occur at the operating speeds studied in this thesis. However, it is recommended that future studies work on an analysis to confirm this, as these phenomena will likely affect the foil's performance if they do occur.

### 8.2.2. Low-emission, carbon-neutral, and future emission-free energy carriers

This thesis studied a zero-emission ferry, defined as a vessel that uses an energy carrier system that operates with absolutely zero or only  $H_2O$  emissions. Also, the selected zero-emission energy carrier had to be available now or in the coming five years. Because of these constraints, several promising low-emission, carbon-neutral, and future emission-free energy carriers could not be studied.

To better understand the impact of these constraints on the ferry's technical and economic feasibility, future studies could research low-emission or carbon-neutral energy carriers. Examples include hydrogen in combination with internal combustion engines (releases  $NO_X$ ), (green) ammonia (releases  $NO_X$ ), (green) methanol (releases  $CO_2$  and  $NO_X$ ), and renewable methane (releases  $CO_2$  and  $NO_X$ ).

Studies into future emission-free energy carriers can also be interesting. Examples include future flow batteries, supercapacitors, solid-state batteries, and graphene batteries.

### 8.2.3. Validation

To confirm the results of this thesis, it is recommended to further validate a number of outcomes. The main recommended areas of validation are summarized below:

- **Weight and weight-saving measures.** Future studies could work on an improved weight estimate for the zero-emission ferry. For instance, a battery-powered ferry will likely require significantly more converters and cables compared to the CC-200, but this was not studied in detail. The same applies to the additional weight due to structural reinforcements required for the LH2 ferry's hydrogen tank. Besides, a number of assumptions were made to determine the saved weight as a result of the identified weight-saving measures. Some of these assumptions can be seen as relatively uncertain. Examples include the weight saving as a result of using CFRP for the hull and superstructure and switching from a water- to air-based cooling system. Future studies could confirm and validate these assumptions to address this uncertainty.
- **Hydrofoil system.** It is recommended to validate the hydrofoil lift and drag data obtained from Autowing. It is expected that a more accurate performance analysis can be made using computational fluid dynamics (CFD) or physical model tests.
- **Propulsion system.** In this thesis, it was assumed that a high-speed thruster would be compatible with the designed hydrofoil system. To better understand the limits of this compatibility, especially at higher speeds and brake powers, it is recommended for future studies to validate and study the design of the selected thruster propulsion system coupled with the hydrofoil system.
- **Economic feasibility.** During the economic feasibility analysis, several assumptions of costs related to the zero-emission ferries were made. This was done as the exact costs of many components of the ferry are not publicly available. Therefore, it is recommended for future studies to validate these costs by contacting the relevant manufacturers. Doing this will also decrease the uncertainty in the economic feasibility results.

### 8.2.4. Economic feasibility

Another recommendation for future studies is to build on the economic feasibility analysis. In this thesis, only the most considerable costs of the ferry have been taken into account. However, when all remaining costs were too accounted for, the results would differ. An example is the insurance cost, which could be higher for a zero-emission ferry as emission-free propulsion systems have a much shorter proven track record compared to diesel propulsion systems. Other examples include the cost of licensing, converters, electric cables, sensor and security systems, port fees, and depreciation.

Furthermore, the economic feasibility analysis of this thesis did not take into account how the expenses of a (zero-emission) ferry are expected to change over time. If the price of components of zero-emission power plants, hydrogen, or electricity lowers in the future, a zero-emission ferry will become more attractive from an economic perspective. If an in-depth study shows that a zero-emission ferry is not economically feasible, one could investigate if government financing is available to achieve economic feasibility.

Future studies could also extend the economic feasibility analysis by studying other ferry configurations. For instance, a CH2 ferry with sufficient hydrogen storage to complete one round trip eliminates the need for a second hydrogen refueling station. Other ideas could be to study technically-feasible ferries designed for an operating speed of 40 knots or ferries sailing without hydrofoils.

### 8.2.5. Larger ferries

Based on the conclusions of this thesis, a 200-passenger, 30- to 40-knot, zero-emission ferry is technically feasible. Using this thesis' obtained knowledge based on the latest technology and the developed parametric model, it would be interesting to return to the thesis performed by Moreno Francis in 2019 to investigate how the conclusions on the technical and economic feasibility of the Coastal Cruiser 300 would change [58]. For instance, Francis concluded that a 300-passenger, battery-powered ferry of the Coastal Cruiser series was not technically feasible in 2019, but this study concluded that a 200-passenger variant is technically feasible [58]. Where is this technically-feasible passenger capacity limit placed today?

### 8.2.6. System interfaces

The final recommendation is to perform a more in-depth study of the ferry's system interfaces. The requirements, design, and costs of the harbor infrastructure, such as a hydrogen refueling or battery charging station, could be studied in more detail during future studies. Also, the system constraints, such as rules and regulations regarding zero-emission ferries may be studied.

At last, a recommendation is to zoom out and investigate the well-to-wake emissions instead of only the tank-to-wake emissions studied in this thesis. The production and transportation of electricity or hydrogen can also be a source of greenhouse gases or other harmful substances. Therefore, a well-to-wake emission analysis is required to analyze the entire industrial chain related to the operation of a fast ferry.

## 8.3. Personal reflection

My life as a university student in Delft started in 2017 when I enrolled in the study program BSc in Mechanical Engineering. It required hard work, but I completed the study nominally and got my BSc degree after three years. The Mechanical Engineering courses were mostly very interesting, but the overall program was very broad. Therefore, it was time to choose a field to focus on for my MSc degree. Ultimately, I chose to pursue my interest in the maritime industry and started with the Master's program in Marine Technology. I did not experience a difficult transition in terms of teaching materials from the switch from Mechanical Engineering to Marine Technology, as the courses of Mechanical Engineering provided an excellent basis for the Marine Technology Master courses. Unfortunately, I started at the beginning of the pandemic, which eventually led to me performing a majority of my Master's study online, from home. Although I had few problems following lectures online and saved a lot of travel time, I did miss the real-life interaction with other students and teachers.

In cooperation with CoCo Yachts, I started working on this thesis in November 2021. Luckily, everything during the duration of my thesis went smoothly and without any major hurdles. A contributing factor to this is that I enjoyed working on this topic, which, in my opinion, turned out to be very interesting. I think it is an important topic related to the time we are living in, and I expect zero-emission ferries to become more and more dominant in the future. Although the commute to CoCo Yachts' office was a bit far, I enjoyed working at CoCo Yachts whenever possible due to the friendly colleagues, excellent working space, and because there was always someone willing to help with any of my questions. In the end, I gained a deep understanding and knowledge of the challenges of designing zero-emission vessels, and I am satisfied with my results.

# References

- [1] *7068 Alloy | Properties, Price & Application | Material Properties*. 2022. URL: <https://material-properties.org/7068-alloy-properties-application-price/>.
- [2] *A flawed wonder material - Green Light*. Apr. 2019. URL: <https://greenlight.nl/carbon-fibre/?lang=en>.
- [3] Fredrik G. Aarskog et al. "Concept risk assessment of a hydrogen driven high speed passenger ferry". In: *International Journal of Hydrogen Energy* (Jan. 2020). ISSN: 0360-3199. DOI: 10.1016/J.IJHYDENE.2019.05.128. URL: <https://www.sciencedirect.com/science/article/pii/S0360319919319846>.
- [4] *Airfoil Tools*. 2022. URL: <http://airfoiltools.com/>.
- [5] Aníbal de Almeida et al. *VSDs for Electric Motor Systems*. June 2022.
- [6] *Alternative fuel: G-Stor™ H2 – carbon composite type 3 cylinders | Luxfer Gas Cylinders*. 2022. URL: <https://www.luxfercylinders.com/products/marine/g-stor-h2-hydrogen-cylinders>.
- [7] *Aluminium vs carbon fiber– comparison of materials*. Oct. 2015. URL: <http://www.dexcraft.com/articles/carbon-fiber-composites/aluminium-vs-carbon-fiber-comparison-of-materials/>.
- [8] *Ampere Electric-Powered Ferry*. Nov. 2021. URL: <https://www.ship-technology.com/projects/norled-zero-cat-electric-powered-ferry/>.
- [9] Anish. *A Guide To Marine Gas Oil and LSFO Used On Ships*. Dec. 2020. URL: <https://www.marineinsight.com/guidelines/a-guide-to-marine-gas-oil-and-lsfo-used-on-ships/>.
- [10] *ASM Material Data Sheet Aluminum 6061-T6*. 2022. URL: <https://asm.matweb.com/search/SpecificMaterial.asp?bassnum=ma6061t6>.
- [11] *Autowing - Lehrstuhl für Modellierung und Simulation - Universität Rostock*. 2022. URL: <https://www.lemos.uni-rostock.de/lehre/sonstiges/downloads/autowing/>.
- [12] *Average Salary in Shenzhen 2022 - The Complete Guide*. 2022. URL: <http://www.salaryexplorer.com/salary-survey.php?loc=3023&loctype=3>.
- [13] Will Ayers and Elliott Bay. *Comparative Payback of Lithium-Ion Batteries for Pacific NW Ferries*. 2016. URL: [https://www.ebdg.com/wp-ebdg-content/uploads/2017/02/Payback\\_Lithium-Ion\\_NWFerries\\_paper.pdf](https://www.ebdg.com/wp-ebdg-content/uploads/2017/02/Payback_Lithium-Ion_NWFerries_paper.pdf).
- [14] *Azipod electric propulsion | ABB Marine & Ports*. 2022. URL: <https://new.abb.com/marine/systems-and-solutions/azipod#large>.
- [15] Lars Baetcke and Martin Kaltschmitt. "Hydrogen Storage for Mobile Application: Technologies and Their Assessment". In: *Hydrogen Supply Chain: Design, Deployment and Operation* (Aug. 2018), pp. 167–206. DOI: 10.1016/B978-0-12-811197-0.00005-1. URL: <https://www.sciencedirect.com/science/article/pii/B9780128111970000051>.
- [16] "Basic principles of ship propulsion". In: *MAN Energy Solutions* (Oct. 2018). URL: [https://www.man-es.com/docs/default-source/marine/tools/basic-principles-of-ship-propulsion\\_web\\_links.pdf?sfvrsn=12d1b862\\_10](https://www.man-es.com/docs/default-source/marine/tools/basic-principles-of-ship-propulsion_web_links.pdf?sfvrsn=12d1b862_10).
- [17] *BB Green prototype*. 2022. URL: <https://www.bbgreen.eu/>.
- [18] Valentin Beggi, Louise Loisel, and Xuan-Truong Nguyen. "Microgrid in USTH campus : Architecture and Power Management Strategies". PhD thesis. July 2018. DOI: 10.13140/RG.2.2.25145.42085.

- [19] Eric Besnard et al. "HYDROFOIL DESIGN AND OPTIMIZATION FOR FAST SHIPS". In: *ASME International Congress and Exhibition* (Nov. 1998). URL: <https://citeseerx.ist.psu.edu/viewdoc/download?doi=10.1.1.537.6282&rep=rep1&type=pdf>.
- [20] Lindert van Biert, Kamil Mrozewski, and Pieter 't Hart. *Public final report: Inventory of the application of Fuel Cells in the MARitime sector (FCMAR) Project data*. Jan. 2021. URL: <https://www.koersenvaart.nl/files/MIIP%5C%20007-2020%5C%20FCMAR%5C%2003022021.pdf>.
- [21] Nick Blenkey. *Sea Change ferry completes landmark hydrogen fueling - Marine Log*. Nov. 2021. URL: <https://www.marinelog.com/passenger/ferries/sea-change-ferry-completes-landmark-hydrogen-fueling/>.
- [22] *Boundary Layer Technologies reveals concept design of zero emission electric hydrofoil ferry | Shippax*. Oct. 2021. URL: <https://www.shippax.com/en/press-releases/boundary-layer-technologies-reveals-concept-design-of-zero-emission-electric-hydrofoil-ferry.aspx>.
- [23] Paul Breeze. "Marine Power Generation Technologies". In: *Power Generation Technologies* (2014), pp. 287–311. DOI: 10.1016/B978-0-08-098330-1.00014-4. URL: <https://www.sciencedirect.com/topics/engineering/hydrofoil>.
- [24] T. M. Buermann, P. Leehey, and J. J. Stilwell. "An Appraisal of Hydrofoil Supported Craft". In: *The Society of Naval Architects and Marine Engineers* (Nov. 1953). URL: <http://www.foils.org/wp-content/uploads/2018/01/SNAMEtransactionsVol61-1953.pdf>.
- [25] Mariska Buitendijk. *Repeat Order for Three Coastal Cruisers 200: SWZ: Maritime*. Feb. 2014. URL: <https://swzmaritime.nl/news/2014/02/12/repeat-order-for-three-coastal-cruisers-200/>.
- [26] *Bunker Prices - Ship & Bunker*. 2022. URL: <https://shipandbunker.com/prices/cn-china>.
- [27] Molly Burgess. *Safety, quality, and performance | Features | gasworld*. June 2021. URL: <https://www.gasworld.com/safety-quality-and-performance/2020970.article>.
- [28] Magnus Burman et al. "Comparative Life Cycle Assessment of the hull of a high-speed craft:" in: *SAGE Publications* 230.2 (Apr. 2015), pp. 378–387. ISSN: 20413084. DOI: 10.1177/1475090215580050. URL: <https://journals.sagepub.com/doi/abs/10.1177/1475090215580050>.
- [29] Jeff Butler. *This new high speed ferry is an electric hydrofoil catamaran*. Aug. 2021. URL: <https://plugboats.com/new-high-speed-ferry-electric-hydrofoil-catamaran/>.
- [30] Gerry Byrne, Tim Persoons, and William Kingston. "Experimental validation of lift and drag forces on an asymmetrical hydrofoil for seafloor anchoring applications". In: *Journal of Ocean and Climate* (Oct. 2018). URL: <https://journals.sagepub.com/doi/pdf/10.1177/1759313118811979>.
- [31] Huicui Chen, Pucheng Pei, and Mancun Song. "Lifetime prediction and the economic lifetime of Proton Exchange Membrane fuel cells". In: *Applied Energy* 142 (Mar. 2015), pp. 154–163. ISSN: 0306-2619. DOI: 10.1016/J.APENERGY.2014.12.062. URL: <https://www.sciencedirect.com/science/article/pii/S0306261914013191>.
- [32] Yuqing Chen et al. "A review of lithium-ion battery safety concerns: The issues, strategies, and testing standards". In: *Journal of Energy Chemistry* 59 (Aug. 2021), pp. 83–99. ISSN: 2095-4956. DOI: 10.1016/J.JECHEM.2020.10.017.
- [33] *China Electricity Price: 36 City | CEIC*. 2022. URL: <https://www.ceicdata.com/en/china/electricity-price-36-city>.
- [34] Meta Christina, Borgen Dam, and Niels Brehm Nielsen. *Sustainability of Carbon Ferries*. Aug. 2013. URL: [http://carbonferries.weebly.com/uploads/1/2/6/2/12627010/sustainability\\_of\\_carbon\\_ferries.pdf](http://carbonferries.weebly.com/uploads/1/2/6/2/12627010/sustainability_of_carbon_ferries.pdf).
- [35] B. R. Clayton and R. E. D. Bishop. *Mechanics of Marine Vehicles*. Bristol: Gulf Publishing Company, 1982.
- [36] *COBRA Compact Battery Rack - Becker Marine Systems*. 2022. URL: <https://www.becker-marine-systems.com/products/product-detail/becker-cobra-compact-battery-rack.html>.

- [37] Wesley Cole and A Will Frazier. "Cost Projections for Utility-Scale Battery Storage". In: *National Renewable Energy Laboratory* (June 2019). URL: <https://www.nrel.gov/docs/fy19osti/73222.pdf>.
- [38] *Composite Technology for Work Boats - Can Composites Pay Their Way?* Apr. 2015.
- [39] *Computergestuurde draagvleugelboot P-30 wordt onderdeel van OV in Stockholm • AT-Aandrijftechniek*. Apr. 2021. URL: <https://www.at-aandrijftechniek.nl/algemeen/computergestuurde-draagvleugelboot-p-30-wordt-onderdeel-van-ov-in-stockholm/68142/>.
- [40] *Copper vs. Aluminum Conductors | Anixter*. 2022. URL: [https://www.anixter.com/en\\_us/resources/literature/wire-wisdom/copper-vs-aluminum-conductors.html#](https://www.anixter.com/en_us/resources/literature/wire-wisdom/copper-vs-aluminum-conductors.html#).
- [41] Ben Craig. *The Future of Batteries in the Marine Sector: What Lies Beyond the Horizon?* 2020. URL: <https://www.southampton.ac.uk/~assets/doc/The%5C%20Future%5C%20of%5C%20Batteries%5C%20in%5C%20the%5C%20Marine%5C%20Sector.pdf>.
- [42] P. R. Crewe. "The hydrofoil bots; its history and future prospects". In: *The institution of naval architects, Quarterly Transactions* (Oct. 1958). URL: <http://www.foils.org/wp-content/uploads/2018/01/INATransactions1958Oct.pdf>.
- [43] *Critical raw materials*. 2022. URL: [https://ec.europa.eu/growth/sectors/raw-materials/areas-specific-interest/critical-raw-materials\\_en](https://ec.europa.eu/growth/sectors/raw-materials/areas-specific-interest/critical-raw-materials_en).
- [44] *Cruise News - Maritime News // Cruiseshipportal*. Nov. 2018. URL: <https://www.cruiseshipportal.com/news/cruise-news-maritime-news/the-worlds-first-electric-car-mf-ampere-has-now-gone-a-distance-equivalent-to-six-times-around-th/>.
- [45] *Designer's Guide MJP CSU*. July 2016.
- [46] "DETERMINING ELECTRIC MOTOR LOAD AND EFFICIENCY". In: *Motor Challenge - U.S. Department of Energy* (Apr. 2014). URL: <https://www.energy.gov/sites/prod/files/2014/04/f15/10097517.pdf>.
- [47] Brent Deverman. *Shekou and Zhuhai Jiuzhou Ferry Schedules*. Sept. 2021. URL: <https://www.nowshenzhen.com/ferry/shekou-zhuhai-jiuzhou-port/>.
- [48] *Electra*. 2022. URL: <https://www.boundarylayer.tech/electra>.
- [49] *Electrifying city transports – safety first when going from fossil fuels to batteries*. Nov. 2021. URL: <https://echandia.se/insights/article/electrifying-city-transport-safety-first-when-going-from-fossil-fuels-to-batteries/>.
- [50] *Energy Storage Solutions - Corvus Energy*. 2022. URL: <https://corvusenergy.com/products/energy-storage-solutions/>.
- [51] *EU Carbon Permits - 2022 Data - 2005-2021 Historical - 2023 Forecast - Price - Quote*. URL: <https://tradingeconomics.com/commodity/carbon>.
- [52] Odd M. Faltinsen. *Hydrodynamics of High-Speed Marine Vehicles*. Cambridge University Press, 2005.
- [53] *Fast Ferry 4212*. 2022. URL: <https://res.cloudinary.com/damen-shipyards2/catalogue/ferries/fast-ferry/product-sheet-damen-fast-ferry-4212.pdf>.
- [54] *Fast ferry: Coastal Cruiser Series*. 2022. URL: <https://www.cocoyachts.com/boats/coastal-cruiser/>.
- [55] *Ferry lines Shenzhen, time tables and distances*. Gorinchem, 2019.
- [56] *FerryCHARGER*. 2022. URL: [https://www.stemmann.com/documents/catalogues/FerryCHARGER\\_Solutions.pdf](https://www.stemmann.com/documents/catalogues/FerryCHARGER_Solutions.pdf).
- [57] *Fjord1, Corvus, and VesselMan collaborate on "Smart Maintenance" project – VPO*. Mar. 2022. URL: <https://vpoglobal.com/2022/03/02/fjord1-corvus-and-vesselman-collaborate-on-smart-maintenance-project/>.
- [58] Moreno Francis. *Feasibility Study of a Fast Electric Passenger Ferry*. Aug. 2019. URL: <http://resolver.tudelft.nl/uuid:cf138038-adc9-41b6-a08f-3f2e9359a3fc>.

- [59] Nathaniel Frithiof. *Five lessons to learn on hydrogen as ship fuel*. July 2021. URL: <https://www.dnv.com/expert-story/maritime-impact/Five-lessons-to-learn-on-hydrogen-as-ship-fuel.html>.
- [60] *Fuel Cell | Cummins Inc.* 2021. URL: <https://www.cummins.com/new-power/technology/fuel-cell>.
- [61] "Fuel Cells". In: *U.S. Department of Energy* (Nov. 2015). URL: [https://www.energy.gov/sites/prod/files/2015/11/f27/fcto\\_fuel\\_cells\\_fact\\_sheet.pdf](https://www.energy.gov/sites/prod/files/2015/11/f27/fcto_fuel_cells_fact_sheet.pdf).
- [62] *Fuel Cells | Fuji Electric Global*. 2022. URL: <https://www.fujielectric.com/products/fuelcell/>.
- [63] Isabelle Gerretsen. *EU carbon tax puts a price on shipping emissions*. Feb. 2022. URL: <https://chinadialogue.net/en/transport/eu-carbon-tax-puts-a-price-on-shipping-emissions/>.
- [64] David L Greene. *Status and Prospects of the Global Automotive Fuel Cell Industry and Plans for Deployment of Fuel Cell Vehicles and Hydrogen Refueling Infrastructure Prepared by*. July 2013. URL: <http://www.osti.gov/contact.html>.
- [65] Jasper Grevink. *MT44006 2021-2-CPP complete*. Delft, 2021.
- [66] Jasper Grevink. *MT44006 2021-6-Waterjets*. Delft, 2021.
- [67] Katherine de Guia. *Cummins fuel cells powering North America's first commercial zero emissions ferry*. Feb. 2021. URL: <https://www.cummins.com/news/2021/02/09/cummins-fuel-cells-powering-north-americas-first-commercial-zero-emissions-ferry>.
- [68] Måns Håkansson, Erland Johnson, and Jonas W. Ringsberg. "Cost and weight of composite ship structures: A parametric study based on Det Norske Veritas rules". In: *Proceedings of the Institution of Mechanical Engineers Part M: Journal of Engineering for the Maritime Environment* 232.3 (Aug. 2018), pp. 331–350. ISSN: 20413084. DOI: 10.1177/1475090217693419. URL: [https://www.researchgate.net/publication/315649927\\_Cost\\_and\\_weight\\_of\\_composite\\_ship\\_structures\\_A\\_parametric\\_study\\_based\\_on\\_Det\\_Norske\\_Veritas\\_rules](https://www.researchgate.net/publication/315649927_Cost_and_weight_of_composite_ship_structures_A_parametric_study_based_on_Det_Norske_Veritas_rules).
- [69] Casey M Harwood. *Hydrodynamic Design of a Foil System for a High-Speed Catamaran*. June 2011. URL: <https://www.researchgate.net/publication/293654137>.
- [70] Henrik Helgesen, Sondre Henningsgard, and Andrea Aarseth Langli. "BATTERY SYSTEMS FOR MARITIME APPLICATIONS-TECHNOLOGY, SUSTAINABILITY AND SAFETY STUDY ON ELECTRICAL ENERGY STORAGE FOR SHIPS". In: *EMSA European Maritime Safety Agency DNV GL* (May 2020). URL: <https://ktn-csbs-media.s3-eu-west-1.amazonaws.com/62714fed-93be-4ee3-82d4-3195419cc09b/studyelectricalenergystorageforships.pdf>.
- [71] *Help for Autowing*. 2022. URL: [https://www.lemos.uni-rostock.de/storages/uni-rostock/Alle\\_MSF/Lemos/Lehre/Downloads/CFD/AUTOWING\\_Help\\_for\\_Autowing.pdf](https://www.lemos.uni-rostock.de/storages/uni-rostock/Alle_MSF/Lemos/Lehre/Downloads/CFD/AUTOWING_Help_for_Autowing.pdf).
- [72] Tommy Hertzberg. *LASS, Lightweight Construction Applications at Sea*. Aug. 2016. URL: [http://e-lass.eu.loopiadns.com/media/2016/08/LASS-SP\\_Report\\_2009\\_13.pdf](http://e-lass.eu.loopiadns.com/media/2016/08/LASS-SP_Report_2009_13.pdf).
- [73] Henk van Herwijnen. *Technical Specification Coastal Cruiser 199.docx*. Tech. rep. Gorinchem: CoCo Yachts, Mar. 2017.
- [74] Henk van Herwijnen. *160801\_Weight Calculation\_CC199\_Rev.xlsx*. 2018.
- [75] Gerben Hieminga. *High gas prices triple the cost of hydrogen production | Article | ING Think*. Oct. 2021. URL: <https://think.ing.com/articles/hold-1of4-high-gas-prices-triples-the-cost-of-hydrogen-production/>.
- [76] *High speed passenger ferry Coastal Cruiser 200 sold to Shenzhen Pengxing Shipping Co*. URL: <https://www.cocoyachts.com/news/coastal-cruiser-200-sold-shenzhen-pengxing-shipping-co/>.
- [77] *High Speed Thrusters*. 2022. URL: <https://hydromasterpropulsion.com/product/high-speed-thrusters/>.

- [78] *High-speed emission free catamaran – BELUGA24*. Aug. 2021. URL: <https://www.shippax.com/en/press-releases/high-speed-emission-free-catamaran-beluga24.aspx>.
- [79] S. F. Hoerner et al. "Hydrofoil handbook Volume 1: Design of hydrofoil craft". In: *Hydrofoil research project for office of naval research navy department, Washington* (1954).
- [80] *Hydrogen – Natural Gas & Hydrogen tanks & cylinders, fuel systems and virtual pipeline trailers*. 2022. URL: <https://www.qtw.com/product/hydrogen/>.
- [81] *Hydrogen Cylinder General Specifications*. Sept. 2021. URL: [https://www.energy.ca.gov/almanac/transportation\\_data/gge.html](https://www.energy.ca.gov/almanac/transportation_data/gge.html).
- [82] *Hydrogen Tank : Doosan Mobility Innovation*. 2022. URL: <https://www.doosanmobility.com/en/products/hydrogen-tank/>.
- [83] *IMO Marine Engine Regulations*. 2022. URL: <https://dieselnet.com/standards/inter/imo.php>.
- [84] Jaya Verma and Deepak Kumar. "Recent developments in energy storage systems for marine environment". In: *Materials Advances* 2.21 (Nov. 2021), pp. 6800–6815. ISSN: 26335409. DOI: 10.1039/D1MA00746G. URL: <https://pubs.rsc.org/en/content/articlehtml/2021/ma/d1ma00746g> <https://pubs.rsc.org/en/content/articlelanding/2021/ma/d1ma00746g>.
- [85] Teo Karayannis, Apostolos Papanikolaou, and AF Molland. *The introduction of high-speed ferries into the Eastern Mediterranean*. Jan. 2000. URL: [https://www.researchgate.net/publication/310504172\\_The\\_introduction\\_of\\_high-speed\\_ferries\\_into\\_the\\_Eastern\\_Mediterranean](https://www.researchgate.net/publication/310504172_The_introduction_of_high-speed_ferries_into_the_Eastern_Mediterranean).
- [86] Siamak Karimi, Mehdi Zadeh, and Jon Are Suul. *Shore charging for plug-in battery-powered ships: power system architecture, infrastructure and control*. Tech. rep. URL: [https://ntnuopen.ntnu.no/ntnu-xmlui/bitstream/handle/11250/2736779/IEEE\\_EM\\_Shore\\_to\\_ship\\_charging\\_Submission.pdf?sequence=2](https://ntnuopen.ntnu.no/ntnu-xmlui/bitstream/handle/11250/2736779/IEEE_EM_Shore_to_ship_charging_Submission.pdf?sequence=2).
- [87] H. van Keimpema and E. Ulijn. *PropCalc*. Delft.
- [88] H. Klein Woud and D. Stapersma. *Selected Chapters of Design of Auxiliary Systems, Shafting and Flexible Mounting*. Delft: TU Delft, 2016.
- [89] N. V. Kornev. "The Computational Vortex Element Method and its application to the ship hydro-aerodynamics". PhD thesis. Marine Technical University St.Petersburg, 1998.
- [90] N. V. Kornev and A. E. Taranov. *Investigation of the Vortex-Wave Wake behind a Hydrofoil*.
- [91] Nikolai Kornev et al. "Design of Hydrofoil Assisted Catamarans using a Non-Linear Vortex Lattice Method". In: *Journal of Marine Engineering* (2005). URL: <https://marine-eng.ir/article-1-13-en.pdf>.
- [92] Christian Krajewski. *HMCS Bras d'Or FHE400*. July 1997. URL: <http://www.shipspotting.com/gallery/photo.php?lid=2556304>.
- [93] Gustav Krantz. *CO2 and sulphur emissions from the shipping industry*. Tech. rep. Oct. 2016. URL: <https://www.egcsa.com/wp-content/uploads/CO2-and-sulphur-emissions-from-the-shipping-industry.pdf>.
- [94] Jean Kumagai. *Lithium-Ion Battery Recycling Finally Takes Off in North America and Europe - IEEE Spectrum*. Jan. 2021. URL: <https://spectrum.ieee.org/lithiumion-battery-recycling-finally-takes-off-in-north-america-and-europe>.
- [95] Juri Kuzjatkin. "Structural Weight Optimisation of a Carbon Fibre Ferry". PhD thesis. KTH Royal Institute of Technology, Aug. 2014.
- [96] *Launching ARGO: a zero emissions hydrofoil containership that will replace air freight starting Q3 2024*. Mar. 2022. URL: <https://workboat365.com/commercial-marine-news/ship-boat-building/launching-argo-a-zero-emissions-hydrofoil-containership-that-will-replace-air-freight-starting-q3-2024/>.
- [97] Rebecca Lindsey. *Climate Change: Atmospheric Carbon Dioxide*. Aug. 2020. URL: <https://www.climate.gov/news-features/understanding-climate/climate-change-atmospheric-carbon-dioxide>.

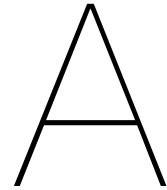
- [98] *Lithium Manganese Oxide (LMO) Battery*. 2022. URL: [https://www.greenway-battery.com/news/Lithium-Manganese-Oxide-\(LMO\)-Battery---LiMn2O4-Manufacturer-101.html](https://www.greenway-battery.com/news/Lithium-Manganese-Oxide-(LMO)-Battery---LiMn2O4-Manufacturer-101.html).
- [99] *Lithium marine batteries*. 2022. URL: <https://www.super-b.com/en/lithium-marine-batteries>.
- [100] *Lithium mining: What you should know about the contentious issue*. Mar. 2020. URL: <https://www.volkswagenag.com/en/news/stories/2020/03/lithium-mining-what-you-should-know-about-the-contentious-issue.html#>.
- [101] *Lithium-Ion Battery 12V - 150Ah - 1.92kWh - PowerBrick+ / LiFePO4*. 2022. URL: <https://www.powertechsystems.eu/home/products/12v-lithium-battery-pack-powerbrick/150ah-12v-lithium-ion-battery-pack-powerbrick/>.
- [102] Gui Lohmann and Jakob Trischler. "The Failure of Fast Ferry Catamaran Operations in New Zealand and Hawaii". In: *Journal of Transportation Technologies* 02.02 (2012), pp. 102–112. DOI: 10.4236/jtts.2012.22012. URL: [https://www.researchgate.net/publication/232608083\\_The\\_Failure\\_of\\_Fast\\_Ferry\\_Catamaran\\_Operations\\_in\\_New\\_Zealand\\_and\\_Hawaii](https://www.researchgate.net/publication/232608083_The_Failure_of_Fast_Ferry_Catamaran_Operations_in_New_Zealand_and_Hawaii).
- [103] J.Y. Looijenga. "The feasibility of zero-emission ferries in the Wadden Sea". PhD thesis. Delft: TU Delft, Feb. 2020.
- [104] Howard Loveday. "The design of a hydrofoil system for sailing catamarans". PhD thesis. University of Stellenbosch, Mar. 2006. URL: <https://scholar.sun.ac.za/handle/10019.1/1982>.
- [105] Xingcheng Lu et al. "Estimation of health and economic costs of air pollution over the Pearl River Delta region in China". In: *Science of The Total Environment* 566-567 (2016), pp. 134–143. DOI: 10.1016/j.scitotenv.2016.05.060. URL: <https://www.sciencedirect.com/science/article/abs/pii/S0048969716309913#f0020>.
- [106] *Manufacturing Cost Analysis of 100 and 250 kW Fuel Cell Systems for Primary Power and Combined Heat and Power Applications*. Tech. rep. Columbus: U.S. Department of Energy, 2017. URL: [https://www.energy.gov/sites/prod/files/2018/02/f49/fcto\\_battelle\\_mfg\\_cost\\_analysis\\_100\\_250kw\\_pp\\_chp\\_fc\\_systems\\_jan2017.pdf](https://www.energy.gov/sites/prod/files/2018/02/f49/fcto_battelle_mfg_cost_analysis_100_250kw_pp_chp_fc_systems_jan2017.pdf).
- [107] Xiaoli Mao et al. *Costs and benefits of a Pearl River Delta Emission Control Area*. July 2019. URL: [https://theicct.org/sites/default/files/publications/ICCT\\_pearl\\_river\\_delta\\_eca\\_20190718.pdf](https://theicct.org/sites/default/files/publications/ICCT_pearl_river_delta_eca_20190718.pdf).
- [108] *Marine MegaWatt Solutions - PowerCellution*. 2022. URL: <https://powercellution.com/marine-megawatt-solutions>.
- [109] *Marine Modules - Fuel Cell Power Products | Ballard Power*. 2022. URL: <https://www.ballard.com/fuel-cell-solutions/fuel-cell-power-products/marine-modules>.
- [110] *Marine Seats For Passenger With Various Types | YSmachines*. 2022. URL: <https://www.ysmarines.com/products/collections/passengerseat.html>.
- [111] Tiffany Means. *Greenhouse gases: Causes, sources and environmental effects*. June 2021. URL: <https://www.livescience.com/37821-greenhouse-gases.html>.
- [112] Jacob Meijer. "Production of composite ship hulls". PhD thesis. Delft: TU Delft, Jan. 2015.
- [113] Ajay Menon. *Understanding Water Jet Propulsion - Working Principle, Design And Advantages*. Sept. 2021. URL: <https://www.marineinsight.com/naval-architecture/understanding-water-jet-propulsion-working-principle-design-and-advantages/>.
- [114] John R. Meyer. *SHIPS THAT FLY..... A STORY OF THE MODERN HYDROFOIL*. Hydrofoil Technology Inc., 1990. URL: <http://www.foils.org/wp-content/uploads/2018/01/ShipsThatFly.pdf>.
- [115] Günther Migeotte. "Design and Optimization of Hydrofoil-Assisted Catamarans". PhD thesis. Stellenbosch: University of Stellenbosch, Mar. 2002.
- [116] Keh-Sik Min, Seon-Hyung Kang, and Oi-Hyun Kim. "Conceptual Design of Very Large-Size Super-High-Speed Foil Catamaran Containership". In: *Practical Design of Ships and Other Floating Structures* 1 (2001), pp. 105–111. DOI: 10.1016/B978-008043950-1/50014-4. URL: <https://www.sciencedirect.com/science/article/pii/B9780080439501500144>.

- [117] *MobyFly | Our Boats*. 2022. URL: <https://mobyfly.com/our-boats/>.
- [118] Anthony F. Molland and Stephen R. Turnock. *Marine Rudders, Hydrofoils and Control Surfaces: Principles, Data, Design*. Ed. by Carrie Bolger. 2nd ed. Butterworth-Heinemann, Nov. 2021.
- [119] Kasper T. Møller et al. "Hydrogen - A sustainable energy carrier". In: *Progress in Natural Science: Materials International* 27.1 (Feb. 2017), pp. 34–40. ISSN: 1002-0071. DOI: 10.1016/J.PNSC.2016.12.014. URL: <https://www.sciencedirect.com/science/article/pii/S1002007116303240>.
- [120] Ryno Moolman et al. "Comparative Evaluation of a Hydrofoil-Assisted Trimaran". In: *R & D Journal* (2006). URL: <https://icarusmarine.com/wp-content/uploads/2018/02/Moolman-et-al.-2006-Comparitive-Evaluation-of-a-hydrofoil-assisted-Trimaran.pdf>.
- [121] *MS Medstraum*. July 2021. URL: <https://corvusenergy.com/projects/medstraum/>.
- [122] *NACA63-615*. 2022. URL: [http://bigfoil.com/2b18d983-f953-42ef-bf58-24e14f938d64\\_info.php](http://bigfoil.com/2b18d983-f953-42ef-bf58-24e14f938d64_info.php).
- [123] Narve Mjøs, Gerd Petra Haugom, and Ben Gully. "DNV GL Handbook for Maritime and Offshore Battery Systems". In: *DNV GL* (Dec. 2016).
- [124] Thomas Nemeth et al. "Lithium titanate oxide battery cells for high-power automotive applications – Electro-thermal properties, aging behavior and cost considerations". In: *Journal of Energy Storage* 31 (Oct. 2020), p. 101656. ISSN: 2352-152X. DOI: 10.1016/J.EST.2020.101656.
- [125] MI News Network. *The World's Fastest Ship – Built in Tasmania is Christened by Argentina's President*. Oct. 2019. URL: <https://www.marineinsight.com/shipping-news/worlds-fastest-ship-built-tasmania-christened-argentinas-president/>.
- [126] Michael Nicholas. "Estimating electric vehicle charging infrastructure costs across major U.S. metropolitan areas". 2019. URL: [https://theicct.org/sites/default/files/publications/ICCT\\_EV\\_Charging\\_Cost\\_20190813.pdf](https://theicct.org/sites/default/files/publications/ICCT_EV_Charging_Cost_20190813.pdf).
- [127] Daekyun Oh, Seungho Jung, and Sookhyun Jeong. "Effect of a Lightweight Hull Material and an Electric Propulsion System on Weight Reduction: Application to a 45ft CFRP Electric Yacht". In: *Journal of the Korean Society of Marine Environment & Safety* 24.6 (Oct. 2018), pp. 818–824. DOI: 10.7837/kosomes.2018.24.6.818. URL: <https://doi.org/10.7837/kosomes.2018.24.6.818>.
- [128] *Overview Hydrogen Refuelling For Heavy Duty Vehicles*. Aug. 2021. URL: [https://h2-mobility.de/wp-content/uploads/sites/2/2021/08/H2-MOBILITY\\_Overview-Hydrogen-Refuelling-For-Heavy-Duty-Vehicles\\_2021-08-10.pdf](https://h2-mobility.de/wp-content/uploads/sites/2/2021/08/H2-MOBILITY_Overview-Hydrogen-Refuelling-For-Heavy-Duty-Vehicles_2021-08-10.pdf).
- [129] *Overview of Greenhouse Gases*. 2022. URL: <https://www.epa.gov/ghgemissions/overview-greenhouse-gases>.
- [130] *Passenger Hydrofoil with Fully-Submerged Foils: Kawasaki's JETFOIL*. July 2020. URL: <https://answers.khi.co.jp/en/mobility/20200731e-02/>.
- [131] *Pearl River Delta: China's Biggest Economic Hub*. Nov. 2017. URL: <https://www.webuildvalue.com/en/reportage/pearl-river-delta-infrastructure-for-china-megacity.html>.
- [132] *PEM-FCS Stack Technology | Nedstack*. 2022. URL: <https://nedstack.com/en/pem-fcs-stack-technology>.
- [133] *PemGen MT-FCPI-500 | Nedstack*. 2022. URL: <https://nedstack.com/en/pemgen-solutions/maritime-power-installations/pemgen-mt-fcpi-500>.
- [134] *Permanent-magnet based technology - The Switch*. 2022. URL: <https://theswitch.com/industry/combined-heat-and-power/permanent-magnet-based-technology/>.
- [135] "Perspectives for the Use of Hydrogen as Fuel in Inland Shipping". In: *MariGreen* (Oct. 2018). URL: <https://cdn.hexagongroup.com/uploads/2019/11/Hydrogen-Feasibility-Study-MariGreen.pdf>.
- [136] Magdalena Petrova. *How cobalt-free batteries will bring down the cost of EVs*. Nov. 2021. URL: <https://www.cnbc.com/video/2021/11/17/how-cobalt-free-batteries-will-bring-down-the-cost-of-evs.html>.

- [137] Minh Triet Pham, Khanh Hieu Ngo, and Tat Hien Le. "Optimal Selection of Marine Propellers Based on Wageningen B-Series". In: *Applied Mechanics and Materials* 889 (Mar. 2019), pp. 455–460. DOI: 10.4028/WWW.SCIENTIFIC.NET/AMM.889.455. URL: [https://www.researchgate.net/publication/331518402\\_Optimal\\_Selection\\_of\\_Marine\\_Propellers\\_Based\\_on\\_Wageningen\\_B-Series](https://www.researchgate.net/publication/331518402_Optimal_Selection_of_Marine_Propellers_Based_on_Wageningen_B-Series).
- [138] *Photos: World's First Zero-Emission Hydrogen Fuel Cell Ferry Hits The Water*. Sept. 2021. URL: <https://www.marineinsight.com/shipping-news/photos-worlds-first-zero-emission-hydrogen-fuel-cell-ferry-hits-the-water/>.
- [139] *Platform-based ferry product family - NAVAIS*. 2021. URL: <https://www.navais.eu/workspaces/platform-based-ferry-product-family>.
- [140] *PMM 450 1.6 MW*. 2016. URL: <http://theswitch.com/wp-content/uploads/2016/08/450.pdf>.
- [141] *PMM 500 3.1 MW*. 2016. URL: <https://1r7x2o2d2jd315najr469y1c-wpengine.netdna-ssl.com/wp-content/uploads/2016/08/500-3.1-mw.pdf>.
- [142] Nicolas Pocard. *Fuel Cell Price to Drop 70-80% as Production Volume Scales*. Jan. 2020. URL: <https://blog.ballard.com/fuel-cell-price-drop>.
- [143] *Polycarbonate Windows for Your Race Car (Lexan)*. Sept. 2016. URL: <http://timeattackbuilders.com/2016/09/29/polycarbonate-race-car-windows/>.
- [144] Hartmut Popp et al. *Lifetime analysis of four different lithium ion batteries for (plug – in) electric vehicle*. Apr. 2014.
- [145] Antonio Posa, Riccardo Broglia, and Elias Balaras. "The wake structure of a propeller operating upstream of a hydrofoil". In: *Journal of Fluid Mechanics* 904 (Dec. 2020), A12. ISSN: 0022-1120. DOI: 10.1017/jfm.2020.680.
- [146] *PowerCellution Marine System 200*. 2021. URL: <https://www.datocms-assets.com/36080/1637225345-marine-system-200-v-221.pdf>.
- [147] Joseph W. Pratt and Leonard E. Klebanoff. *Feasibility of the SF-BREEZE: a Zero-Emission, Hydrogen Fuel Cell, High-Speed Passenger Ferry*. Sept. 2016. URL: <https://www.maritime.dot.gov/sites/marad.dot.gov/files/docs/innovation/meta/9841/sf-breeze-ferry-feasibility-study-report-sandia-national-laboratory-2.pdf>.
- [148] Joseph W. Pratt and Leonard E. Klebanoff. *Optimization of Zero Emission Hydrogen Fuel Cell Ferry Design, With Comparisons to the SF-BREEZE*. Tech. rep. Sandia National Laboratories, Jan. 2018. URL: <https://www.osti.gov/servlets/purl/1513454>.
- [149] Naida Hakirevic Prevljak. *Construction starts on world's 1st zero-emission fast ferry*. June 2021. URL: <https://www.offshore-energy.biz/construction-starts-worlds-1st-zero-emission-fast-ferry/>.
- [150] *Product Overview Marine Propulsion Systems*. 2018. URL: [https://www.zf.com/products/media/industrial/marine/brochures\\_1/ZF\\_Product\\_Overview\\_2018.pdf](https://www.zf.com/products/media/industrial/marine/brochures_1/ZF_Product_Overview_2018.pdf).
- [151] *Product Selection Guide 2022*. 2022. URL: [https://www.zf.com/products/media/industrial/marine/brochures\\_1/Product\\_Selection\\_Guide.pdf](https://www.zf.com/products/media/industrial/marine/brochures_1/Product_Selection_Guide.pdf).
- [152] *PROJECTS*. 2022. URL: <https://ggzeromarine.com/projects/>.
- [153] *Public transport - Candela*. 2021. URL: <https://candela.com/public-transport/>.
- [154] *Reducing emissions from the shipping sector*. 2021. URL: [https://ec.europa.eu/clima/eu-action/transport-emissions/reducing-emissions-shipping-sector\\_en](https://ec.europa.eu/clima/eu-action/transport-emissions/reducing-emissions-shipping-sector_en).
- [155] *RESISTANCE AND POWERING OF SHIPS*. 2021. URL: [https://www.usna.edu/NAOE/\\_files/documents/Courses/EN400/02.07%20Chapter%207.pdf](https://www.usna.edu/NAOE/_files/documents/Courses/EN400/02.07%20Chapter%207.pdf).
- [156] Etienne Rivard, Michel Trudeau, and Karim Zaghbi. *Hydrogen Storage for Mobility: A Review*. June 2019. DOI: 10.3390/ma12121973.
- [157] Renato Roldao. *China's ETS: Carbon trading the Chinese way*. Jan. 2022. URL: <https://www.energymonitor.ai/policy/carbon-markets/carbon-trading-the-chinese-way>.

- [158] *Rolls-Royce provides power and propulsion to third fast ferry for Zhuhai High Speed Ferry Company*. Oct. 2016. URL: <https://www.rolls-royce.com/media/press-releases/2016/10-11-2016-rr-provides-power-and-propulsion-to-third-fast-ferry.aspx>.
- [159] Dricus De Rooij. *LCO Batteries*. July 2021. URL: <https://sinovoltaics.com/learning-center/storage/lco-batteries/>.
- [160] Felice Rubino et al. "Marine Application of Fiber Reinforced Composites: A Review". In: *Journal of Marine Science and Engineering 2020, Vol. 8, Page 26* 8.1 (Jan. 2020), p. 26. ISSN: 20771312. DOI: 10.3390/JMSE8010026. URL: <https://www.mdpi.com/2077-1312/8/1/26/htm%20https://www.mdpi.com/2077-1312/8/1/26>.
- [161] A. Rufolo. "Foil Weight Saving and Hydrofoil Performance". In: *Naval Engineers Journal* 78.5 (1966), pp. 905–913.
- [162] Christian Ruoff. *Charged EVs | Seaworthy EVs: Leclanché designs and manufactures Li-ion cells and systems - Charged EVs*. Dec. 2016. URL: <https://chargedevs.com/features/seaworthy-evs-leclanche-designs-and-manufactures-li-ion-cells-and-systems/>.
- [163] Jon Anders Ryste, Martin Wold, and Terje Sverud. *Comparison of Alternative Marine Fuels*. Tech. rep. DNV-GL, Sept. 2019. URL: [https://sea-lng.org/wp-content/uploads/2020/04/Alternative-Marine-Fuels-Study\\_final\\_report\\_25.09.19.pdf](https://sea-lng.org/wp-content/uploads/2020/04/Alternative-Marine-Fuels-Study_final_report_25.09.19.pdf).
- [164] Naohiro Saito. *The economic analysis of commercial ships with hydrogen fuel cell through case studies*. Apr. 2018. URL: [https://commons.wmu.se/cgi/viewcontent.cgi?article=1617&context=all\\_dissertations](https://commons.wmu.se/cgi/viewcontent.cgi?article=1617&context=all_dissertations).
- [165] Mike Schuler. *Over 80 Injured as High-Speed Hydrofoil Ferry Hits Whale in Japan*. Apr. 2019. URL: <https://gcaptain.com/high-speed-hydrofoil-ferry-hits-whale-in-japan/>.
- [166] *Seawater - Properties*. 2022. URL: [https://www.engineeringtoolbox.com/sea-water-properties-d\\_840.html](https://www.engineeringtoolbox.com/sea-water-properties-d_840.html).
- [167] *Shanghai Bunker Fuel Prices Today, IFO 380, IFO 180, MGO Prices per Ton*. 2022. URL: <https://www.oilmonster.com/bunker-fuel-prices/far-east-and-south-pacific/shanghai/78>.
- [168] *Shenzhen Shekou to Zhuhai*. 2021. URL: <https://www.rome2rio.com/map/Shenzhen-Shekou/Zhuhai>.
- [169] *SIEMENS 1LE1503 IE3 serie - ElectroProject*. 2022. URL: <https://shop.electroproject.nl/1le1503-3ab53-4aa4-200kw-elektromotor-88447448.html>.
- [170] Srijna Singh et al. "Numerical simulation of Vortex-shedding from NACA4418 hydrofoil". In: *Vibroengineering PROCEDIA* (Dec. 2018), pp. 125–130. ISSN: 2345-0533. DOI: 10.21595/VP.2018.20396. URL: <https://www.extrica.com/article/20396>.
- [171] Alex Smith. *Worlds first zero-emission fast ferry to be named Medstraum*. Feb. 2021. URL: <https://www.cruiseandferry.net/articles/worlds-first-zero-emission-fast-ferry-to-be-named-medstraum-1>.
- [172] Daniele Stampatori, Pier Paolo Raimondi, and Michel Noussan. "Li-Ion Batteries: A Review of a Key Technology for Transport Decarbonization". In: *Energies 2020, Vol. 13, Page 2638* 13.10 (May 2020). ISSN: 19961073. DOI: 10.3390/EN13102638. URL: <https://www.mdpi.com/1996-1073/13/10/2638/htm%20https://www.mdpi.com/1996-1073/13/10/2638>.
- [173] *Technology & Products - PureCell Model 400 - M400 Hydrogen*. 2022. URL: <https://www.doosanfuelcell.com/en/prod/prod-0102/>.
- [174] *The Beluga24*. 2022. URL: <https://www.greencityferries.com/>.
- [175] Matthew Tremblay. *Feasibility of Hydrogen-Powered High Speed Ferry Proven*. July 2017. URL: <https://www.maritime-executive.com/features/feasibility-of-hydrogen-powered-high-speed-ferry-proven>.
- [176] *Underlying mathematical methods used in the Software family Autowing*. 2022. URL: [https://www.lemos.uni-rostock.de/storages/uni-rostock/Alle\\_MSF/Lemos/Lehre/Downloads/CFD/MATH\\_Math.models\\_in\\_Autowing.pdf](https://www.lemos.uni-rostock.de/storages/uni-rostock/Alle_MSF/Lemos/Lehre/Downloads/CFD/MATH_Math.models_in_Autowing.pdf).

- [177] Laurens Van Hoecke et al. "Challenges in the use of hydrogen for maritime applications". In: *Energy & Environmental Science* 14.2 (Feb. 2021), pp. 815–843. ISSN: 17545706. DOI: 10.1039/D0EE01545H. URL: <https://pubs.rsc.org/en/content/articlehtml/2021/ee/d0ee01545h>; <https://pubs.rsc.org/en/content/articlelanding/2021/ee/d0ee01545h>.
- [178] Yixu Wang and Hsiao Ying Shadow Huang. "Comparison of lithium-ion battery cathode materials and the internal stress development". In: *ASME 2011 International Mechanical Engineering Congress and Exposition, IMECE 2011 4.PARTS A AND B* (2011), pp. 1685–1694. DOI: 10.1115/IMECE2011-65663. URL: [https://www.researchgate.net/publication/267594447\\_Comparison\\_of\\_Lithium-Ion\\_Battery\\_Cathode\\_Materials\\_and\\_the\\_Internal\\_Stress\\_Development](https://www.researchgate.net/publication/267594447_Comparison_of_Lithium-Ion_Battery_Cathode_Materials_and_the_Internal_Stress_Development).
- [179] *Waterjets; Overview of Different Systems*. Gorinchem, 2019.
- [180] Savannah Weeda. *PEM fuel cells: the future is now - Offshore Energy*. June 2021. URL: <https://www.offshore-energy.biz/pem-fuel-cells-the-future-is-now/>.
- [181] Kazimierz Witkowski. "Research of the Effectiveness of Selected Methods of Reducing Toxic Exhaust Emissions of Marine Diesel Engines". In: *Journal of Marine Science and Engineering* 8.6 (2020). DOI: 10.3390/jmse8060452. URL: <https://www.mdpi.com/2077-1312/8/6/452/pdf#>.
- [182] *Worlds first zero-emission hydrogen fuel cell ferry launched*. Sept. 2021. URL: <https://safet-y4sea.com/worlds-first-zero-emission-hydrogen-fuel-cell-ferry-launched/>.
- [183] Peng Wu and Richard Bucknall. "Marine propulsion using battery power". PhD thesis. University College London, 2016.
- [184] *www.barcaferry.com*. 2021. URL: [http://www.barcaferry.com/photo/turbojet/ps30/turbojet\\_ps30.htm](http://www.barcaferry.com/photo/turbojet/ps30/turbojet_ps30.htm).
- [185] *XMP 98P High Power*. Jan. 2022. URL: <https://indd.adobe.com/view/c0c507f9-ce02-466c-a2e3-87b8909d3566>.
- [186] *XPAND XMP and XMOD – XALT Energy*. 2022. URL: <https://www.xaltenergy.com/xpand-xmp-and-xmod/>.
- [187] Chang Yang. "Policies, regulatory framework and enforcement for air quality management: The case of China". In: *OECD Environment Working Papers* (May 2020). DOI: 10.1787/7d1d1a82-en. URL: [https://www.oecd.org/officialdocuments/publicdisplaydocumentpdf/?cote=ENV/WKP\(2020\)4&docLanguage=En](https://www.oecd.org/officialdocuments/publicdisplaydocumentpdf/?cote=ENV/WKP(2020)4&docLanguage=En).
- [188] Ivy Yin. *China's hydrogen fuel price to be competitive against petroleum by 2030: Sinopec Marketing | S&P Global Platts*. Nov. 2021. URL: <https://www.spglobal.com/platts/en/market-insights/latest-news/energy-transition/110921-chinas-hydrogen-fuel-price-to-be-competitive-against-petroleum-by-2030-sinopec-marketing>.
- [189] Liang Yun and Alan Bliault. *High Performance Marine Vessels*. Springer, 2012.
- [190] Ghassan Zubi et al. "The lithium-ion battery: State of the art and future perspectives". In: *Renewable and Sustainable Energy Reviews* 89 (June 2018), pp. 292–308. ISSN: 1364-0321. DOI: 10.1016/J.RSER.2018.03.002.



# Hydrofoils: calculations and results

## A.1. The chord length of the hydrofoils

One of the design choices of the hydrofoil system's geometry is the chord length. For a high lift/drag ratio, it should be as low as possible, but it is limited by the structural strength. Therefore, a MATLAB script was written to determine the minimum chord length that used expressions developed by Hoerner et al. [79]:

```
1  %%% hydrofoil_structural_calcs.m
2  %%%
3  %%% created by Patryk Doornebos, February 2022
4  %%% last updated May 2022
5  %%%
6  close all
7  clear
8  clc
9
10
11 sigma = 276; %MPa, yield strength of foil material, Aluminum 6061
12 f = 1.15; %-, safety factor
13
14 M_ferry = 150000; %kg, mass of zero-emission ferry
15 F_L = 0.5*M_ferry * 9.81; %N, lift force of one-out-of-two hydrofoils
16
17 b = 6; %m, length between struts of foils
18 s = 9; %m, span of foils
19
20 t_c_ratio = 0.15; %-, thickness ratio of NACA63-615 foil
21
22
23 %Based on equation C.10-C.13 of Moreno, 2019
24 c_min = ((0.96/b)*(sqrt(sigma*1e6/f))*((t_c_ratio)/sqrt(F_L/s)))^(-3/2); %Minimum chord ...
    length (structural, to support mass of ferry)
25
26 %Design choice: make aft struts thicker too for possible propulsion forces or room for ...
    waterjet intake
27
28 c_foils = 0.8; %m, minimum chord length (plus extra margin) of foils based on ...
    structural considerations
29
30 %Aft foils: NACA 0024
31 c_strut_aft = c_foils;
32 t_strut_aft = 0.24 * c_strut_aft;
33
34 %Forward foils: NACA 0009
35 c_strut_for = c_foils;
36 t_strut_for = 0.09 * c_strut_for;
37
38 submergence = 2 * c_foils; %m, hydrofoil submergence, deep enough to avoid most free ...
```

```

surface effects (x2 instead of 1.5)
39 length_struts = submergence + 1; %m, length of the struts, assuming vessel sails lm ...
   above water surface in foilborne condition

```

## A.2. Autowing: working principles and methods

Autowing uses a Cartesian coordinate system, with the x-axis pointing forward to the direction of the hydrofoil's forward velocity, the y-axis pointing straight upwards, and the z-axis pointing at an angle of 90 degrees of the x- and y-axis, as illustrated in figure 3.13.

Autowing mainly relies on vortex lattice theory, which is well known for modeling flow around lifting surfaces. More specifically, the nonlinear vortex lattice method is used. A lifting surface generates a continuous vortex sheet in its downstream wake. The vortex lattice method uses a set of discrete vortices to model this vortex sheet. The distribution of the vortex sheet of unknown vector density  $\vec{\gamma}$  on the free surface wave, calculated by the dynamic free surface boundary condition for steady flow conditions (equation A.1), is used to simulate nonlinear free surface waves [176].

$$VW_x - \frac{1}{2}|\vec{W}|^2 - gy = 0 \quad (\text{A.1})$$

Where:

- $V$ , the forward speed.
- $\vec{W}$ , the velocity under the free surface.
- $g$ , gravity constant.
- $y$ , the wave elevation.

The vector density  $\vec{\gamma}$  can be decomposed into a sum of two components,  $\gamma_\zeta$ , perpendicular to the x-axis, and  $\gamma_\xi$ , perpendicular to  $\gamma_\zeta$ . Both are tangential to the free surface. With some transformations and knowing that  $\vec{\gamma}$  is the vortex sheet intensity per unit area, equation A.2 can be formed [115].

$$\gamma_\zeta = \left| \vec{W}_0 \right|^2 + (\vec{n} \times \vec{\gamma}) \vec{W}_0 + \frac{1}{4}|\gamma|^2 + 2\frac{y}{F_n^2} - 2W_{0x} \quad (\text{A.2})$$

Where:

- $\vec{W}_0$ , the forward speed on the free surface (i.e. the vortex sheet).
- $\vec{n}$ , an unit vector normal to the vortex sheet.
- $F_n$ , the Froude number

This equation is then combined with the divergence-free condition  $\nabla \times \vec{\gamma} = 0$ , the kinematic condition on the free surface, and conditions at infinity like the radiation condition ( $\vec{\gamma} = 0$  at infinity) to obtain a closed system of equations for the vector density [176] [115]. Therefore, equation A.2 represents the basic equation of implementing the vortex lattice method for fully solving the nonlinear dynamic free surface boundary condition. By obtaining the distribution of vortices on the surface of the mean line for each hydrofoil, Autowing acquires the force acting on each hydrofoil. The algorithm does so by obtaining the force coefficient ( $\vec{C}$ ), given in equation A.3:

$$\vec{C} = \frac{2B^2}{S} \int_S \left( \vec{W}_0 - V \right) \times \vec{\gamma} \, d\tilde{S} \quad (\text{A.3})$$

Where:

- $B$ , a characteristic length.
- $S$ , a surface over which the force coefficient is calculated.
- $\tilde{S}$ , non-dimensional area ( $\tilde{S} = S/B^2$ ).

It should be mentioned that the entire working principle and list of used equations of Autowing are a number of times more extensive and complex than this overview. Therefore, further details of the algorithm are covered by various studies and documentation, such as [176] [115] [89] [90].

### A.3. Autowing lift and drag data with corresponding curve-fitted mass-resistance equations

Using the modelled hydrofoil geometry illustrated in figure 3.13, lift and drag data has been obtained for various sailing speeds and angles of attack using Autowing. The angles of attack have been varied with the goal of achieving lift values of 100 to 150 tonnes, which is the expected range of the zero-emission ferry's mass. Furthermore, the calculations, each taking around 10 minutes of computing time, used the following inputs:

- Configuration, as discussed in chapter 3.2.2 and illustrated in figure 3.13. Using NACA 63-615, NACA 0015, and NACA 0024 foils. Table A.1 lists the main specifications of the defined hydrofoil configuration.
- Speed, based on the operational speed, ranging from 30 to 40 knots. A step size of 2 knots was chosen for the computational experiments.
- Angle of attack, varying from 0 to 4 degrees.
- Roughness, assumed equal to 40 microns for fresh paint [71]
- Coefficient of kinematic viscosity, assumed equal to  $1.063 \text{ mm}^2/\text{s}$  [166]
- Temperature, assumed equal to 20 degrees Celcius
- Number of iterations, set equal to 20 to reach a converging solution for an acceptable computing time

**Table A.1:** Specifications of the defined hydrofoil system geometry

	<b>Number of foils [-]</b>	<b>Span [m]</b>	<b>Chord [m]</b>	<b>Profile [-]</b>	<b>Angle of attack [deg]</b>
Lifting foils	2	9	0.8	NACA 63-615	Variable
Forward support struts	2	2.6	0.8	NACA 0015	0
Aft support struts	2	2.6	0.8	NACA 0024	0

The acquired data is shown in table A.2:

**Table A.2:** Lift and drag data results from experiments using Autowing (appendix)

Speed [knots]	Angle of attack [deg]	Lift [t]	Drag [t]	Lift/drag [-]
30	4	132.6	-8.06	16.44
30	3.5	124.7	-7.38	16.89
30	3	116.6	-6.74	17.31
30	2.5	108.5	-6.14	17.67
30	2	100.3	-5.58	17.97
32	4	150.1	-9.28	16.17
32	3	131.9	-7.77	16.97
32	2.5	122.7	-7.08	17.32
32	2	113.4	-6.44	17.60
32	1.5	104.1	-5.85	17.80
34	2.5	137.8	-8.01	17.20
34	2	127.4	-7.28	17.49
34	1.5	116.9	-6.61	17.69
34	1	106.3	-5.98	17.76
36	2	142.1	-8.17	17.39
36	1.5	130.4	-7.41	17.59
36	1	118.6	-6.71	17.68
36	0.5	106.3	-6.04	17.59
38	1	131.6	-7.47	17.61
38	0.5	117.9	-6.72	17.52
38	0	104.9	-6.06	17.32
40	0.5	130.2	-7.45	17.48
40	0.25	122.7	-7.06	17.38
40	0	115.8	-6.70	17.28

Quadratic regression was used on the lift and drag data from table A.2 to obtain equations that estimate the resistance of the hydrofoils based on the ferry's mass. The obtained equations are listed below, for various sailing speeds:

$$30 \text{ knots: } R_{foils} = 0.000369325 \cdot M_{Ferry}^2 - 0.00923751 \cdot M_{Ferry} + 2.79409 \quad (\text{A.4})$$

$$32 \text{ knots: } R_{foils} = 0.00030512 \cdot M_{Ferry}^2 - 0.0029254 \cdot M_{Ferry} + 2.84703 \quad (\text{A.5})$$

$$34 \text{ knots: } R_{foils} = 0.00025522 \cdot M_{Ferry}^2 + 0.00203548 \cdot M_{Ferry} + 2.88229 \quad (\text{A.6})$$

$$36 \text{ knots: } R_{foils} = 0.000219345 \cdot M_{Ferry}^2 + 0.00487874 \cdot M_{Ferry} + 3.04589 \quad (\text{A.7})$$

$$38 \text{ knots: } R_{foils} = 0.000147621 \cdot M_{Ferry}^2 + 0.0179634 \cdot M_{Ferry} + 2.55171 \quad (\text{A.8})$$

$$40 \text{ knots: } R_{foils} = 0.000019212 \cdot M_{Ferry}^2 + 0.0471586 \cdot M_{Ferry} + 0.984514 \quad (\text{A.9})$$

## A.4. Validating the hydrofoil system mass

In this section, the estimated hydrofoil mass given in chapter 3.2.2 is validated by calculating the total volume of the foils, which multiplied by the density gives an estimate for the hydrofoil system mass. The cross-sectional areas of the wing profiles have been obtained from Autowing.

The hydrofoil system masses resulting from the validation are given in table A.3. The results show a hydrofoil system mass of 4.30 tonnes for aluminum, 12.5 tonnes for steel, and 2.80 tonnes for CFRP. It should be noted that it was assumed that CFRP would offer a 35% weight saving compared to aluminum, like for the switch from an aluminum to a CFRP hull as discussed in chapter 3.1.2.

**Table A.3:** Calculations of the hydrofoil system mass by volume (chapter 3.2)

<b>Foil [-]</b>	<b>Cross-sectional area [m<sup>2</sup>]</b>	<b>Span [m]</b>	<b>Number of foils [-]</b>	<b>Volume [m<sup>3</sup>]</b>
NACA 66-209	0.03937	9	2	0.7089
NACA 0024	0.1046	2.6	2	0.5439
NACA 0015	0.06539	2.6	2	0.3400
<b>Total</b>	N/A	N/A	6	1.5926

	<b>Density [kg/m<sup>3</sup>]</b>	<b>Mass foils [t]</b>
Aluminum	2,700	<b>4.30</b>
Steel	7,850	<b>12.5</b>
CFRP	1,755	<b>2.80</b>

# B

## Propulsion system: calculations and results

### B.1. The efficiency of waterjets integrated with a hydrofoil system

In this section, the efficiency of a waterjet propulsion system integrated with a hydrofoil system is estimated for a 30-knot ferry. This is done by estimating the required power to pump the seawater through the hydrofoil struts. In combination with the known efficiency of the waterjet used in the CC-200, an estimate can be given for the waterjet efficiency for the zero-emission hydrofoil CC-200.

First of all, the total resistance for the foiling, zero-emission CC-200 at 30 knots is estimated, with a significant margin of safety, to be roughly 80 kN, based on results from the parametric model covered in chapter 6 and hydrofoil drag results of table A.3. The strut span is 2.6 m, while the chord of the struts is 0.8 m, as discussed in chapter 3.2.2. Like the CC-200, the zero-emission ferry would have two waterjets, so the required thrust per jet is 40 kN. The inlet speed of the waterjet intake is assumed to be equal to the ship speed of 30 knots (15.43 m/s). The two 3,000 kW MJP 650 waterjets used in the CC-200 have an inlet diameter of 0.65 m, which is assumed equal to the diameter of the pipe in the struts [45]. The generated thrust of a waterjet can be calculated using equation B.1:

$$T_{waterjet} = \rho_{sw} \cdot Q \cdot V_{flow} \quad (B.1)$$

Meanwhile, the increased flow velocity can be calculated using equation B.2:

$$V_{flow} = \frac{Q}{(\pi/4) \cdot D_{inlet}^2} \quad (B.2)$$

Using these equations, it was found that a volume flow ( $Q$ ) of  $3.60 \text{ m}^3/\text{s}$  results in an increased flow velocity ( $V_{flow}$ ) of 10.85 m/s and roughly the required thrust ( $T_{waterjet}$ ) of 40 kN. The volume flow ( $Q$ ) of  $3.60 \text{ m}^3/\text{s}$  equals to a mass flow of roughly 221 tons per minute, which is a bit higher than the 180 tons per minute of the Jetfoil hydrofoil ferry illustrated in figure 3.2 [130]. If the mass flow would be too high, it could be reduced by using an intake pipe with a reduced diameter and an increased flow velocity.

The pressure loss due to the strut height can be calculated using equation B.3:

$$\Delta p_{loss,height} = \rho_{sw} \cdot g \cdot \Delta z = 1,025 \text{ [kg/m}^3] \cdot 9.81 \text{ [m/s}^2] \cdot 2.6 \text{ [m]} = 26.14 \text{ [kPa]} \quad (B.3)$$

Additionally, the pressure loss due to the two 90-degree bends can be calculated using equation B.4 and a bend resistance factor of 0.4, obtained from [88].

$$\Delta p_{loss,bend} = \zeta \cdot 0.5 \cdot \rho_{sw} \cdot V_{flow}^2 = 0.4 \text{ [-]} \cdot 0.5 \text{ [-]} \cdot 1,025 \text{ [kg/m}^3] \cdot 10.85^2 \text{ [m}^2/\text{s}^2] = 24.13 \text{ [kPa]} \quad (B.4)$$

The total pressure loss per waterjet can now be obtained by summing two times the pressure loss for one bend and the pressure loss due to the height, resulting in 74.40 kPa. The additional required

power for the waterjet due to this pressure loss is the calculated by multiplying the pressure loss by the volume flow, resulting in 267.8 kW. For two waterjets, this results in a total additional required power of 535.7 kW.

At 30 knots, the two diesel engines of the CC-200 output roughly 2,050 kW [73]. Using equation B.5, it has been estimated that around 26.1% additional power is required to overcome the losses due to the hydrofoil system:

$$P_{additional} = \frac{P_{nominal} + P_{extra}}{P_{nominal}} = \frac{2050 [kW] + 535.7 [kW]}{2050 [kW]} = 1.261 [-] \quad (B.5)$$

The waterjet efficiency on the CC-200 is around 68% [179]. However, due to the additional power, the efficiency on a hydrofoil ferry will drop to around 53.9%, as shown by equation B.6:

$$\eta_{waterjet,hydrofoils} = \frac{\eta_{waterjet,nominal}}{P_{additional}} = \frac{68\%}{1.261} = 53.9\% \quad (B.6)$$

While the waterjet efficiency has dropped quite significantly already, it is expected that this is still an optimistic estimate. The estimated resistance of 80 kN used in the calculation is based on the hydrofoil geometry discussed in chapter 3.2.2. However, the aft struts in that geometry have a thickness lower than the required inlet diameter of 0.65 m. In other words, they would have to be made thicker, which would increase the resistance of the ferry. Additionally, the weight of the seawater in the struts should be considered in the design too. Using the inlet diameter, strut height, and the density of seawater, it was determined that the weight of the water in one strut would be around 884 kg, which also increases the ferry's resistance.

## B.2. Results: propeller open water characteristics

The PropCalc tool was used to obtain propeller open water characteristics based on inputs described in chapter 5.2.1 relevant to the zero-emission CC-200. For each situation, PropCalc requires three main inputs, also discussed in chapter 5.2.1. The velocity, which was varied between 30 and 40 knots as per the research question of this thesis. The propeller diameter, which was set to 1.6 meters. Lastly, the total thrust, which was assumed equal to the total resistance, and for which a range was estimated based on the parametric model discussed in chapter 6 and the hydrofoil drag results from chapter 3.2. For the foilborne condition, the total resistance was estimated to be in the range of 65 to 100 kN, depending on the velocity. The resistances were tested in steps of 5 kN. The obtained data is listed in table B.1:

**Table B.1:** PropCalc results: propeller open water characteristics based on the defined inputs and tested range of velocities and thrusts (chapter 5.2.1)

V [knots]	R [kN] (=T [kN])	n_prop [RPM]	K_T [-]	K_Q [-]	
30		65	450.5	0.086	0.0248
		70	454.1	0.091	0.0258
		75	457.7	0.096	0.0269
		80	461.2	0.101	0.0278
		85	464.7	0.106	0.0288
		90	468.1	0.11	0.0297
32		70	477.8	0.082	0.024
		75	481.3	0.087	0.025
		80	484.7	0.091	0.0259
		85	488	0.096	0.0268
		90	491.3	0.1	0.0277
34		70	501.7	0.075	0.0225
		75	505.1	0.079	0.0234
		80	508.3	0.083	0.0242
		85	511.6	0.087	0.025
		90	514.8	0.091	0.0259
36		75	529.1	0.072	0.0219
		80	532.2	0.076	0.0227
		85	535.4	0.08	0.0235
		90	538.5	0.083	0.0243
		95	541.5	0.087	0.025
38		75	553.2	0.066	0.0207
		80	556.3	0.069	0.0214
		85	559.3	0.073	0.0221
		90	562.3	0.076	0.0228
		95	565.3	0.08	0.0235
40		80	580.5	0.064	0.0202
		85	583.4	0.067	0.0209
		90	586.4	0.07	0.0216
		95	589.2	0.073	0.0222
		100	592	0.076	0.0229

### B.3. Overview: specifications of electric motors and gearboxes

In table B.2, the most important technical specifications of the electric motors that may be used for the zero-emission ferry are listed:

**Table B.2:** The technical specifications of a selection of electric motors from The Switch [140] [141]

E-motor	Max. cont. torque [kNm]	Speed range [RPM]	Output power [kW]	Efficiency [%]	Total weight [kg]
Frame 450-6	5.3	0 ... 2,000	810	97.2	3,360
Frame 450-7	6.1	0 ... 2,000	930	97.3	3,620
Frame 450-8	7	0 ... 2,000	1,070	97.3	3,880
Frame 450-9	7.9	0 ... 2,000	1,210	97.4	4,140
Frame 450-10	8.8	0 ... 2,000	1,350	97.4	4,400
Frame 450-11	9.6	0 ... 2,000	1,470	97.5	4,660
Frame 450-12	10.5	0 ... 2,000	1,610	97.5	4,920
Frame 500-11	12.2	0 ... 2,000	1,860	97.3	6,070
Frame 500-13	14.4	0 ... 2,000	2,200	97.4	6,630

It is important to note that the output power (equal to the rotational speed times the torque) is based on 1,500 RPM. Also, the given total weight includes the weight of the machine as well as the rotor.

The dimensions of the above-mentioned electric motors can be seen in table B.3:

**Table B.3:** The dimensions of a selection of electric motors from The Switch [140] [141]

<b>E-motor</b>	<b>Length [m]</b>	<b>Width [m]</b>	<b>Height [m]</b>
Frame 450-6	1.628	1.01	1.588
Frame 450-7	1.688	1.01	1.588
Frame 450-8	1.748	1.01	1.588
Frame 450-9	1.808	1.01	1.588
Frame 450-10	1.868	1.01	1.588
Frame 450-11	1.928	1.01	1.588
Frame 450-12	1.988	1.01	1.588
Frame 500-11	2.09	1.11	1.779
Frame 500-13	2.27	1.11	1.779

In table B.4, the most important technical specifications of the gearboxes that may be used for the zero-emission ferry are listed:

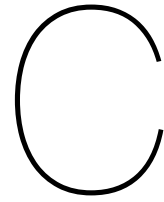
**Table B.4:** The technical specifications of a selection of gearboxes from ZF [151]

<b>Gearbox</b>	<b>Ratio (min, max) [-]</b>	<b>Power factor [kW/RPM]</b>	<b>Max. P_B @1,500 RPM [kW]</b>	<b>Weight [kg]</b>
ZF 3355	2.647 ... 4.727	0.5508	826.2	670
ZF 5000	1.256 ... 2.963	0.6670	1,000	740
ZF 5050	1.256 ... 2.963	0.7466	1,120	740
ZF 5255 A	2.588 ... 3.692	0.8906	1,336	870
ZF 7600	1.545 ... 3.174	1.0577	1,586	970
ZF 7640	3.308 ... 4.238	1.2356	1,853	1,325
ZF 7645	3.308 ... 4.238	1.3131	1,970	1,325
ZF 9050	1.186 ... 3.448	1.4660	2,199	1,400

The dimensions of the selection of gearboxes are listed in table B.5:

**Table B.5:** The dimensions of a selection of gearboxes from ZF [151]

<b>Gearbox</b>	<b>Length [m]</b>	<b>Width [m]</b>	<b>Height [m]</b>
ZF 3355	0.670	0.750	1.067
ZF 5000	0.956	0.850	0.960
ZF 5050	0.956	0.850	0.960
ZF 5255 A	0.956	0.890	1.106
ZF 7600	1.039	1.000	1.042
ZF 7640	1.011	1.000	1.236
ZF 7645	1.011	1.000	1.236
ZF 9050	1.177	1.090	1.205



# Parametric model

## C.1. Parametric model: inputs

All inputs used in the parametric model, including design inputs, ship inputs, and constants, are listed below.

- Design inputs
  - **Design velocity [knots]**. The ferry's design velocity, valid values are 30, 32, 34, 36, 38, and 40, as per the available hydrofoil resistance data and the research question of this thesis.
  - **Required range [NM]**. The ferry's required range in nautical miles.
  - **Use of composites [-]**. Choice to enable a weight saving by use of composites.
  - **Remove unnecessary items [-]**. Choice to enable a weight saving by removing unnecessary items.
  - **Reduce weight of items [-]**. Choice to enable a weight saving by reducing weight of currently equipped items.
- Ship inputs
  - **Maximum mass of the CC-200 [kg]**. The maximum mass of the CC-200.
  - **CC-200 propulsion-related systems mass [kg]**. The mass of the CC-200's diesel engine and propulsion-related systems.
  - **Weight saving due to use of composites [kg]**. The weight saving due to the use of composites.
  - **Weight saving due to the removal of unnecessary items [kg]**. The weight saving due to the removal of unnecessary items.
  - **Weight saving due to a reduction in weight of items [kg]**. The weight saving due to a reduction in weight of currently-equipped items.
  - **Air resistance coefficient [-]**. The air resistance coefficient for catamarans in foilborne mode, assumed to be 0.9. Normally lies between 0.6 and 0.9 [115].
  - **Waterline length CC-200 [m]**. The waterline length of the CC-200.
  - **Foilborne frontal area [ $m^2$ ]**. The frontal area of the CC-200, estimated using the Rhino 3D model of the CC-200, including the tunnel area as a measure of safety in case of unfavorable wind angles.
  - **Planing frontal area [ $m^2$ ]**. The frontal area of the CC-200 in planing mode, estimated to be roughly 85% of the foilborne frontal area.
  - **Available volume energy carrier [ $m^3$ ]**. The available volume in the ferry for the energy carrier, assumed to be  $100 m^3$  for both the starboard and portside auxiliary, tank, void 1, and void 2 rooms.
  - **Hotel load [kW]**. The hotel load of the CC-200 during its operation, assumed to be 50 kW.
- Constants
  - **Air density [ $kg/m^3$ ]**. The air density at sea level, approximately  $1.225 kg/m^3$ .

- **Seawater density** [ $kg/m^3$ ]. The seawater density, approximately  $1,025 kg/m^3$ .
- **Seawater viscosity** [ $m^2/s$ ]. The viscosity of the seawater, approximately  $1.2E-6 m^2/s$ .
- **Gravitational constant** [ $m/s^2$ ]. The gravitational acceleration, approximately  $9.81 m/s^2$ .

## C.2. Parametric model: pseudocode

In this section, a pseudocode of the developed parametric model is given, making it easier to obtain a clear understanding of the algorithm.

According to the flow chart illustrated in figure 6.1, the parametric model uses three loop structures (FOR-END statements), which are elaborated in the list below.

- **Main loop: 20 iterations.** The main loop of the parametric model is placed at the very beginning and at the very end of the model and is set to 20 iterations. The main function of this loop is to input the correct mass of the zero-emission energy carrier, propulsion system, and hydrofoil system into the model's weight calculation block, which calculates the expected weight of the zero-emission ferry. As the masses of the ferry's energy carrier and propulsion system are based on commercially-available components with known weights, they are not continuous. Therefore, the mass of the ferry has a relatively low sensitivity, meaning that when the energy or power demand increases just a little, the mass of the ferry can remain equal. Thus, relatively little main loop iterations are needed. It was found that in most cases, the results of the parametric model converged almost completely (>99.9 %) after just four iterations. However, as the model runs in a very short time (+- one second), the number of iterations was set to 20 to further increase the likelihood of a converged result.
- **Hydrofoil mass loop: 20 iterations.** The second loop occurs at the start of the model. It calculates the expected mass of the hydrofoil system based on equation 3.6 and adds it to the expected mass of the zero-emission ferry to obtain the ferry's total mass, including hydrofoils. It was found that in most cases, the results of the ferry's mass including hydrofoils converged almost completely (>99.9 %) after five iterations. However, as the model runs in just a second, the number of iterations was set to 20 to further increase the likelihood of a converged result.
- **Power demand and propulsion system selection loop: 5 iterations.** The third loop is placed roughly halfway the model. This loop only starts altering the results when the calculated required brake power is on the limit of changing to a stronger electric motor and gearbox. For example, if the required brake power per motor is 810 kW, the model selects a particular electric motor and gearbox. However, if the required brake power per motor is 811 kW, the model selects an electric motor and gearbox that are somewhat stronger and therefore heavier, which may require an increase in brake power again. As the ranges of the brake power are relatively wide (e.g., between 810 and 930 kW), this loop rarely affects the result and therefore does not need many iterations. If it does affect the results, they will converge very quickly, so it has been chosen to use five iterations.

This parametric model will assess the technical feasibility of a zero-emission ferry based on a set of design inputs, with the most important ones being the required operational speed and range.

FOR 20 iterations

**Weight calculation**

Calculate the weight saving due to the weight-saving measures

Calculate the ferry's mass excluding foils

FOR 20 iterations

    Calculate the ferry's mass including foils based on the mass excluding foils

END FOR

**Hydrofoil model (part 1)**

*Foilborne phase:*

IF speed is 30 knots

    Find the hydrofoil drag based on the determined ferry mass and 30 knots

ELSE IF speed is 32 knots

    Find the hydrofoil drag based on the determined ferry mass and 32 knots

ELSE IF speed is 34 knots

    Find the hydrofoil drag based on the determined ferry mass and 34 knots

ELSE IF speed is 36 knots

    Find the hydrofoil drag based on the determined ferry mass and 36 knots

ELSE IF speed is 38 knots

    Find the hydrofoil drag based on the determined ferry mass and 38 knots

ELSE IF speed is 40 knots

    Find the hydrofoil drag based on the determined ferry mass and 40 knots

ELSE

    Find the hydrofoil drag based on an assumed lift/drag coefficient of 16 and give an error message that the results may be inaccurate

END IF

IF the ferry's mass including foils is below 100 or above 150 tonnes

    Give an error message because the mass lies outside of the tested range of values

END IF

Calculate the air resistance of the ferry in foilborne mode

Sum the air resistance of the ferry in foilborne mode with the hydrofoil resistance at operational speed

*Resistance hump:*

Calculate the displacement volume of the zero-emission ferry

Estimate the resistance hump speed

Calculate the air resistance of the ferry at the resistance hump speed

IF the hump speed is between 9.8 and 10.9 knots

    Set the corresponding hydrofoil drag and lift values, estimated using Autowing.

ELSE IF the hump speed is between 10.9 and 12.8 knots

    Set the corresponding hydrofoil drag and lift values, estimated using Autowing.

ELSE

    Display an error message that the hump speed lies outside of the tested values

END IF

Calculate the frictional resistance coefficient at the resistance hump

Calculate the residual resistance coefficient at the resistance hump

Calculate the wetted surface area at the resistance hump

Calculate the hull resistance at the resistance hump using the frictional and residual resistance coefficients

Calculate the total resistance at the resistance hump by summing the air, foil, and hull resistances and adding a 25% margin

**Ferry resistance without foils**

Calculate the frictional resistance coefficient at the operational speed  
 Calculate the residual resistance coefficient at the operational speed  
 Calculate the wetted surface area at the operational speed  
 Calculate the hull resistance at the operational speed using the frictional and residual resistance coefficients  
 Calculate the air resistance at the operational speed  
 Sum the hull resistance and the air resistance at the operational speed to find the total resistance for the zero-emission ferry without foils

**Hydrofoil model (part 2)**

IF the hydrofoil system lowers the ferry's resistance at the operational speed and the hump resistance is greater than the hydrofoil ferry's resistance at the operational speed  
 A hydrofoil system is applied and a note is printed that the maximum resistance lies at the resistance hump  
 ELSE IF the hydrofoil system lowers the ferry's resistance at the operational speed and the hump resistance is lower than the hydrofoil ferry's resistance at the operational speed  
 A hydrofoil system is applied and a note is printed that the maximum resistance lies at the operational speed  
 ELSE  
 A hydrofoil system is not applied as it increases the resistance of the ferry at the operational speed  
 END IF

**Power demand and propulsion system selection**

FOR 5 iterations

IF hydrofoils are applied, the input speed is 30 knots, and the resistance is 60-95 kN  
 Select a thruster as the propulsion system and find the propeller's open water characteristics  
 ELSE IF hydrofoils are applied, the input speed is 30 knots, and the resistance is not 60-95 kN  
 Select a thruster as the propulsion system, find the propeller's open water characteristics, and print a potential error message that results may be inaccurate  
 ELSE IF hydrofoils are applied, the input speed is 32 knots, and the resistance is 65-95 kN  
 Select a thruster as the propulsion system and find the propeller's open water characteristics  
 ELSE IF hydrofoils are applied, the input speed is 32 knots, and the resistance is not 65-95 kN  
 Select a thruster as the propulsion system, find the propeller's open water characteristics, and print a potential error message that results may be inaccurate  
 ELSE IF hydrofoils are applied, the input speed is 34 knots, and the resistance is 65-95 kN  
 Select a thruster as the propulsion system and find the propeller's open water characteristics  
 ELSE IF hydrofoils are applied, the input speed is 34 knots, and the resistance is not 65-95 kN  
 Select a thruster as the propulsion system, find the propeller's open water characteristics, and print a potential error message that results may be inaccurate  
 ELSE IF hydrofoils are applied, the input speed is 36 knots, and the resistance is 70-100 kN  
 Select a thruster as the propulsion system and find the propeller's open water characteristics  
 ELSE IF hydrofoils are applied, the input speed is 36 knots, and the resistance is not 70-100 kN  
 Select a thruster as the propulsion system, find the propeller's open water characteristics, and print a potential error message that results may be inaccurate  
 ELSE IF hydrofoils are applied, the input speed is 38 knots, and the resistance is 70-100 kN  
 Select a thruster as the propulsion system and find the propeller's open water characteristics  
 ELSE IF hydrofoils are applied, the input speed is 38 knots, and the resistance is not 70-100 kN  
 Select a thruster as the propulsion system, find the propeller's open water characteristics, and print a potential error message that results may be inaccurate  
 ELSE IF hydrofoils are applied, the input speed is 40 knots, and the resistance is 75-105 kN  
 Select a thruster as the propulsion system and find the propeller's open water characteristics  
 ELSE IF hydrofoils are applied, the input speed is 40 knots, and the resistance is not 70-100 kN  
 Select a thruster as the propulsion system, find the propeller's open water characteristics, and print a potential error message that results may be inaccurate  
 ELSE IF hydrofoils are not applied  
 Select a waterjet as the propulsion system and find the required brake power based on an assumed efficiency of 68%

```

ELSE
    Display an error that no propulsion system could be selected
END IF

IF a thruster is selected as the propulsion system
    Use the determined propeller open water characteristics and drivetrain efficiencies to calculate the required brake power
END IF

IF a thruster is selected and the required brake power is below 810 kW
    Select Frame 450-6 e-motor and ZF 3355 gearbox
ELSE IF a thruster is selected and the required brake power is between 810 and 930 kW
    Select Frame 450-7 e-motor and ZF 5000 gearbox
ELSE IF a thruster is selected and the required brake power is between 930 and 1,070 kW
    Select Frame 450-8 e-motor and ZF 5050 gearbox
ELSE IF a thruster is selected and the required brake power is between 1,070 and 1,210 kW
    Select Frame 450-9 e-motor and ZF 5255 gearbox
ELSE IF a thruster is selected and the required brake power is between 1,210 and 1,350 kW
    Select Frame 450-10 e-motor and ZF 7600 gearbox
ELSE IF a thruster is selected and the required brake power is between 1,350 and 1,470 kW
    Select Frame 450-11 e-motor and ZF 7600 gearbox
ELSE IF a thruster is selected and the required brake power is between 1,470 and 1,610 kW
    Select Frame 450-12 e-motor and ZF 7640 gearbox
ELSE IF a thruster is selected and the required brake power is between 1,610 and 1,860 kW
    Select Frame 500-11 e-motor and ZF 7645 gearbox
ELSE IF a thruster is selected and the required brake power is between 1,860 and 2,200 kW
    Select Frame 500-13 e-motor and ZF 9050 gearbox
ELSE
    Print an error that no electric motor or gearbox has been selected because the required brake power is too high
END IF

IF the maximum torque of the electric motor or the gearbox is lower than the required torque
    Print an error that the gearbox or electric motor can not handle the required torque
END IF

IF a thruster is selected
    Calculate the total weight of the selected propulsion system
ELSE
    Assume a propulsion system weight of 20,000 kg (not expected to happen)
END IF

END FOR

```

### **Energy demand and energy carrier selection**

```

Calculate the sailing time based on the input 'Range' and operational speed
Calculate the total energy demand of the ferry by multiplying the total brake power by the sailing time

```

```

Calculate the energy consumption of the zero-emission ferry in kWh/NM

```

#### *Batteries:*

```

Calculate the number of required battery modules

```

```

IF the number of required battery modules is odd
    Make the number of required battery modules even for a symmetrical design
END IF

```

```

Calculate the total mass and volume and maximum output power of the battery system

```

```

IF the maximum power output of the battery system is lower than the total required brake power
    Print an error that the battery system can not provide the required brake power
END IF

```

Calculate the required charge time of the battery system based on DSOC

*Fuel cell + liquid hydrogen storage:*

Calculate the number of fuel cell units needed to deliver the required power

IF the number of required fuel cell modules is odd

    Make the number of required fuel cell modules even for a symmetrical design

END IF

Calculate the total mass and volume of the required fuel cells

Calculate the required mass and volume of LH2

IF the required mass or volume of LH2 is larger than the LH2 tank capacity

    Print an error that a larger or multiple LH2 tanks are needed

END IF

Calculate the total mass and volume of the LH2 tank and fuel cells

Calculate the range of the ferry when a full LH2 tank would be used

*Fuel cell + compressed hydrogen storage:*

Calculate the number of fuel cell units needed to deliver the required power

IF the number of required fuel cell modules is odd

    Make the number of required fuel cell modules even for a symmetrical design

END IF

Calculate the total mass and volume of the required fuel cells

Calculate the required number of compressed H2 tanks

IF the number of required CH2 tanks is odd

    Make the number of required CH2 tanks even for a symmetrical design

END IF

Calculate the total mass and volume of the compressed H2 tanks and fuel cells

**Energy carrier results:**

IF the total mass of the battery energy carrier is the lowest

    Set the battery energy carrier to be the lightest option

ELSE IF the total mass of the LH2 tank + fuel cell is the lowest

    Set the LH2 fuel cell energy carrier to be the lightest option

ELSE IF the total mass of the compressed H2 tank + fuel cell is the lowest

    Set the compressed H2 fuel cell energy carrier to be the lightest option

ELSE

    Print an error: fault in comparing the total masses of the energy carriers

END IF

IF the total volume of the battery energy carrier is the lowest

    Set the battery energy carrier to be the most compact option

ELSE IF the total volume of the LH2 tank + fuel cell is the lowest

    Set the LH2 fuel cell energy carrier to be the most compact option

ELSE IF the total volume of the compressed H2 tank + fuel cell is the lowest

    Set the compressed H2 fuel cell energy carrier to be the most compact option

ELSE

    Print an error: fault in comparing the total volumes of the energy carriers

END IF

IF the battery energy carrier is the lightest and most compact

    Select the battery system as the energy carrier for the zero-emission ferry

ELSE IF the LH2 fuel cell energy carrier is the lightest and most compact

    Select the LH2 fuel cell system as the energy carrier for the zero-emission ferry

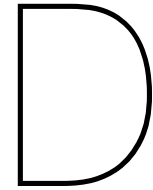
ELSE IF the compressed H2 fuel cell energy carrier is the lightest and most compact

    Select the compressed H2 fuel cell system as the energy carrier for the zero-emission ferry

```
IF the battery system is the lightest and fits in the ferry
  Select the battery system as the energy carrier for the zero-emission ferry
ELSE IF the LH2 fuel cell system is the lightest and fits in the ferry
  Select the LH2 fuel cell system as the energy carrier for the zero-emission ferry
ELSE IF the compressed H2 fuel cell system is the lightest and fits in the ferry
  Select the compressed H2 fuel cell system as the energy carrier for the zero-emission ferry
ELSE IF the battery system is the most compact and fits in the ferry
  Select the battery system as the energy carrier for the zero-emission ferry
ELSE IF the LH2 fuel cell system is the most compact and fits in the ferry
  Select the LH2 fuel cell system as the energy carrier for the zero-emission ferry
ELSE IF the compressed H2 fuel cell system is the most compact and fits in the ferry
  Select the compressed H2 fuel cell system as the energy carrier for the zero-emission ferry
ELSE
  Print an error: no energy carrier has been selected, likely caused by a too small available volume
in the ferry for the given requirements
END IF

IF the battery energy carrier is selected
  Set the ferry's energy carrier mass equal to the battery system mass
ELSE IF the LH2 fuel cell energy carrier is selected
  Set the ferry's energy carrier mass equal to the LH2 fuel cell system mass
ELSE IF the compressed H2 fuel cell energy carrier is selected
  Set the ferry's energy carrier mass equal to the compressed H2 fuel cell system mass
ELSE
  Print an error: the energy carrier has not been selected
END IF

END FOR
```



# Economic feasibility

This appendix contains calculations related to the CC-200's and zero-emission ferry's economic feasibility. Due to the confidential nature of information related to the CC-200's mass and costs, a number of specific values related to this study could not be mentioned. Therefore, some CAPEX are expressed as a percentage of the CC-200's total CAPEX. Additionally, due to the uncertainty of the capital expenditures, they are rounded in whole percentages of the CC-200's CAPEX.

## D.1. CAPEX calculations

In this section, the CAPEX calculations for the zero-emission ferries are listed. The resulting CAPEX are compared to the known total CAPEX of the CC-200.

### D.1.1. CAPEX of the battery-powered ferry

In this section, the CAPEX of a 30-knot, 30 NM, battery-powered ferry is investigated.

The first thing that increases the CAPEX of the battery-powered ferry is the weight-saving measures. The most significant change here comes from the switch from an aluminum hull to a CFRP hull. The costs of a composite ship hull is estimated at roughly € 123/kg to € 166/kg [38] [112]. When combined with the expected mass of the CFRP hull, it results in a cost of 41 % to 56 % of the CC-200's total CAPEX.

The cost from other weight-saving measures, such as the removal and reduction in weight of certain items, have been assumed negligible as eliminating items will decrease the CAPEX, and replacing items may either compensate for this decrease or lower the CAPEX even further.

Next, the costs of the hydrofoil system must be estimated. Unfortunately, no estimations for these costs could be found in literature. Therefore, it has been assumed that the cost of the hydrofoil system would be between € 110/kg and € 180/kg, similar to the cost of the CFRP hull and superstructure, but with a higher uncertainty. Together with the expected hydrofoil weight, the hydrofoil system is assumed to cost between 11 % and 19 % of the CC-200's total CAPEX.

The CAPEX of the thrusters have been estimated by contacting Hydromaster Propulsion Systems, the manufacturer of the chosen high-speed thrusters. Jan Terlouw, working at Hydromaster, gave an estimation for a set of Z-drive thrusters that would comply with the required brake power of the 30-knot zero-emission ferry concepts. The set of Z-drive thrusters is expected to cost around € 950k.

Electric motors are estimated to cost € 115/kW [5] [169]. A power output of 2,515 kW is required for the battery-powered ferry. Therefore, two Frame 450-10 electric motors have been chosen by the parametric model, which have a combined power output of 2,700 kW. As a result, the electric motors are expected to cost around € 311k.

The costs of the required gearboxes are assumed to be equal to the cost of the gearboxes used in the CC-200, as the brake power of the prime movers is roughly equal. Therefore, the total cost of the battery-powered ferry's two gearboxes is set to 2 % of the CC-200's total CAPEX.

The last cost that is considered is the cost for the battery system. The exact cost of a Li-ion battery system is hard to estimate, as a range of 200 to 1,400 \$/kWh is found from various studies [37] [163] [183]. To make this range slightly smaller and considering a low production volume due to the

innovative nature of the project, a range of € 600/kWh to € 1,200/kWh is assumed for this study. From the parametric model results shown in table 6.1, it is found that the required energy demand for the battery-powered ferry configuration is 2,188 kWh. Together with the assumed DSOC, this results in an installed battery system capacity of 2,735 kWh based on 280 XMP 98P battery modules, which is expected to cost € 1,641k to € 3,282k.

At last, two battery charging stations are taken into account for the battery-powered ferry's CAPEX. As no information could be obtained on the cost of a product similar to the FerryCHARGER illustrated in figure 6.10, the cost of the battery charging stations will be based on charging stations for electric vehicles. A study found that a fast, 350 kW DC charger would cost \$ 140k [126]. Considering the battery-powered ferry would require around 4.4 MW of charging power, it is assumed that it could be charged with a charging station that is cost-equivalent to 13 of the 350 kW DC chargers, which would then cost  $\$140k \cdot 13 = \$ 1,820k$ . The two charging stations for the battery-powered ferry are then assumed to cost \$ 3,640k, or around € 3,450k. Assuming a 20% higher and lower margin, this equals a cost of € 2,760k to € 4,140k.

### D.1.2. CAPEX of the compressed hydrogen-powered ferry

The CAPEX of the 30-knot, 30 NM, compressed hydrogen-powered ferry are based on the CAPEX of the battery-powered ferry. It is assumed that all components of the calculation remain the same, except for the following:

- The cost of the battery system is replaced by the cost of the PowerCell MS200 fuel cells and the compressed hydrogen tanks.
- The cost of the charging station is replaced by the cost of a hydrogen refueling station.
- The cost of the electric motors may slightly decrease, due to a lower required brake power of the ferry.

As was found in chapter 4.2.2, the cost of a fuel cell system strongly depends on the production volume. In this thesis, it has been assumed that the required fuel cells will be manufactured at low production volumes. Therefore, the costs of fuel cells was set at a range of € 1,500/kW to € 2,500/kW, comparable to other studies that estimate fuel cell costs for low production volumes [147] [106]. From the parametric model results listed in table 6.1, it follows that the compressed hydrogen-powered ferry would require a power output of 2,285 kW. In turn, this leads to 12 installed PowerCell MS200 fuel cells, delivering 200 kW each, which sums up to a total installed power of 2,400 kW. This results in an expected fuel cell system cost of € 3,600k to € 6,000k.

The cost of the compressed hydrogen tanks must be added. For the 30 NM compressed hydrogen-powered ferry, six Quantum 936L compressed hydrogen tanks would be required, which store 22.5 kg of hydrogen each. This results in a total of 135 kg of hydrogen stored. The cost of compressed hydrogen tanks is approximately \$ 15/kWh, which together with hydrogen's gravimetric density of 33.33 kWh/kg results in approximately \$ 500/kg, or € 468/kg [156]. An additional 30 % has been assumed for the rack, connections, and safety system on a system level, resulting in around € 600/kg. Therefore, the compressed hydrogen tanks are estimated to cost roughly € 81k.

The hydrogen refueling station for the compressed hydrogen-powered ferry is assumed to be based on the cost of the ferry's compressed hydrogen tanks. Assuming two compressed hydrogen refueling stations are built at both ports, which each have a storage capability of roughly one day of operation, it would require the equivalent of  $2 \cdot 6 \cdot 9 = 108$  Quantum 936L compressed hydrogen tanks. This is 18 times as much as mounted on the compressed hydrogen-powered ferry, so the CAPEX for the hydrogen refueling station is assumed to be roughly  $18 \cdot 81\% = € 1,458k$ . The Sea Change, a hydrogen-powered ferry, proves that the refueling of compressed hydrogen does not need to be complex or expensive, as it can be refilled with 242 kg of compressed hydrogen by a small truck that brings it to the port [21].

At last, electric motors are estimated to cost € 115/kW [5] [169]. A power output of 2,285 kW is required for the compressed hydrogen-powered ferry, as seen in table 6.1. Therefore, two Frame 450-9 electric motors have been chosen by the parametric model, which have a combined power output of 2,420 kW. As a result, the electric motors are expected to cost around € 278k.

### D.1.3. CAPEX liquid hydrogen-powered ferry

The CAPEX of the 30-knot, 255 NM, liquid hydrogen-powered ferry are based on the CAPEX of the compressed hydrogen-powered ferry. It is assumed that all components of the calculation remain the

same, except for the following:

- The cost of the hydrogen refueling station is removed, as it is assumed that hydrogen is brought to the port by a hydrogen refueling truck.
- The cost of the energy carrier system may change due to a lower or higher power demand and a liquid hydrogen tank instead of compressed hydrogen tanks.
- The cost of the electric motors may change, due to a lower or higher required brake power of the ferry.

Like for the compressed hydrogen-powered ferry, the cost for the fuel cells is assumed to be € 1,500/kW to € 2,500/kW. From the parametric model results listed in table 6.1, it follows that the liquid hydrogen-powered ferry would require a power output of 2,524 kW. In turn, this leads to 14 installed Ballard FCwave fuel cells, delivering 200 kW each, which sums up to a total installed power of 2,800 kW. This results in an expected fuel cell system cost of € 4,200k to € 7,000k.

Now, the cost of the liquid hydrogen tank must be added. For the 255 NM liquid hydrogen-powered ferry, a Garder Cryogenics liquid hydrogen tank which holds 1,200 kg of hydrogen has been selected. This tank was also used by the authors of the SF-BREEZE feasibility study, who estimated its cost to be \$ 850k, which equals to approximately € 795k [147].

At last, electric motors are estimated to cost € 115/kW [5] [169]. Two Frame 450-10 electric motors have been chosen by the parametric model, which have a combined power output of 2,700 kW. As a result, the electric motors are expected to cost around € 311k.